VECTORED THRUST CONTROL

Brian John Horais

NAVAL POSTGRADUATE SCHOOL
Monterey, California

THESIS

VECTORED THRUST CONTROL

by

Brian John Horais

Thesis Advisor: G. J. Hokenson

December 1972

Approved for public release; distribution unlimited.

Vectored Thrust Control

by

Brian John Horais
Ensign, United States Navy
B.S.A.E., United States Naval Academy, 1971

Submitted in partial fulfillment of the
requirements for the degree of

MASTER OF SCIENCE IN AERONAUTICAL ENGINEERING

from the

NAVAL POSTGRADUATE SCHOOL
December 1972

ABSTRACT

Supersonic two-dimensional flow from a nozzle with the exit plane inclined to the central axis of the nozzle will be turned if the exit pressure of the nozzle is not matched to the external pressure. The direction and magnitude of the flow deflection angle and the resulting deflection force is a function of the exit pressure of the nozzle, the exit Mach number and the amount the exit plane is inclined to the central axis of the nozzle. A study of the deflection forces and deflection angles generated for a Mach number range of 1.2 to 2.4 and for a wide range of exit pressures is presented in this paper.

TABLE OF CONTENTS

LIST OF TABLES

LIST OF DRAWINGS

I. INTRODUCTION

The static pressure at the exit of a supersonic nozzle can be greater than, equal to or less than the external static pressure. When the pressure at the exit is less than the external pressure (overexpanded flow), the static pressure of the flow is increased to the external pressure by passing through oblique shock waves that originate at or near the corners of the nozzle exit. (See Figure I-c). These shock waves reflect from the free boundary of the jet as expansion waves, and a series of interacting expansion waves and compression waves develops downstream in the flow. This expansion and compression wave generation soon dies out due to turbulent mixing at the free boundary.

When the exit static pressure is equal to the external static pressure, parallel (matched) flow results.

For the case when the exit static pressure is greater than the external static pressure (underexpanded flow), the flow pressure is reduced to the external pressure by passing through expansion waves originating at or near the corners of the nozzle exit. These expansion waves are reflected from the free boundaries as compression waves, and a series of compression and expansion waves results downstream. (See Figure I-a). These waves are also dissipated by turbulent mixing at the free boundary.

For the case when the nozzle exit is not perpendicular to the flow direction, the interaction of waves for the over and underexpanded cases is not symmetric about the central axis of the nozzle

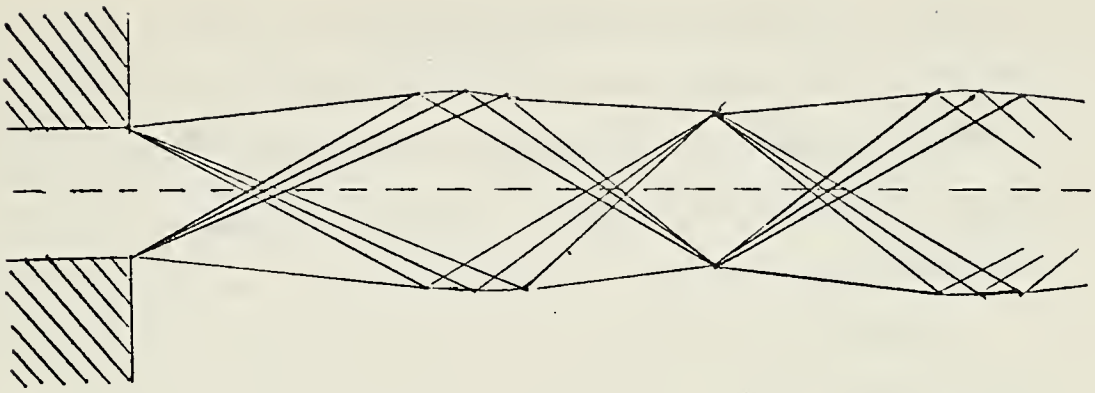

Figure I-a. Underexpanded - Symmetric Exit Plane

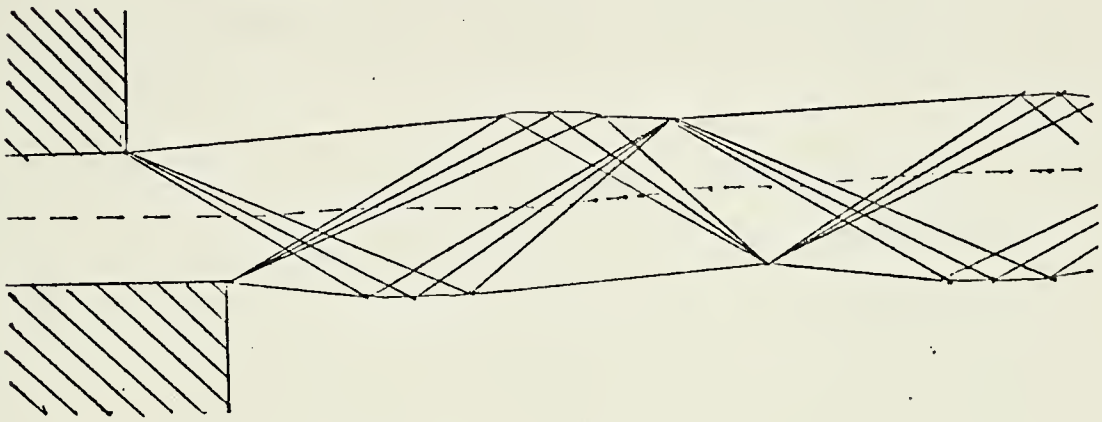

Figure I-b. Underexpanded - Asymmetric Exit Plane

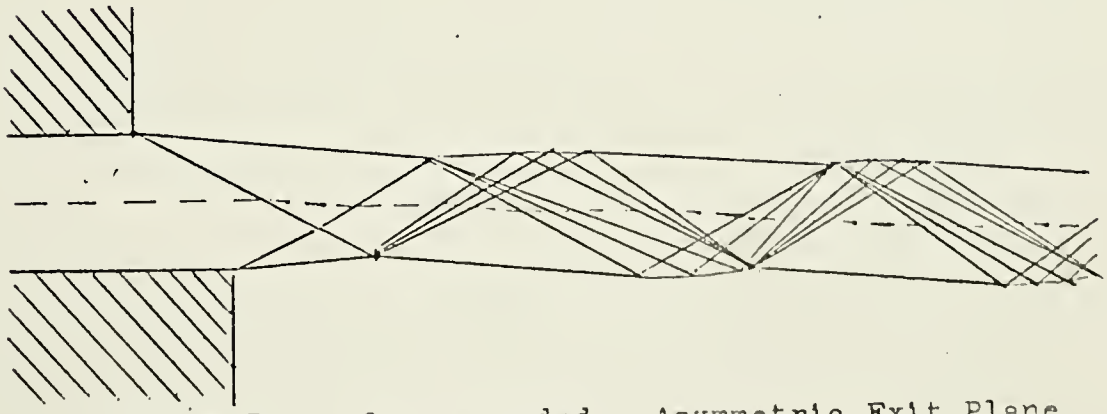

Figure I-c. Overexpanded - Asymmetric Exit Plane

and the flow is turned as indicated in Figures I-b and I-c. This turning of the flow resulting from both an asymmetric exit plane and exit pressures not matched to the external static pressure results in deflection forces on the nozzle. The direction of the flow depends upon the orientation of the exit plane and the exit static pressure.

The purpose of this study was to investigate the effects of varying pressures, Mach numbers and exit plane configurations on the flow deflection force and flow turning angle. To accomplish this a two dimensional supersonic free jet with a Mach number range of 1.2 to 2.4 and pressure range of 20 psig to 220 psig was used.

II. DESCRIPTION OF APPARATUS

A. BLOWDOWN FREE JET

Supersonic flow was achieved through use of an Amrad Model W-4 Flow Converter, consisting of a plenum chamber and a variable throat area ratio supersonic nozzle (See Figure A-1). The variable nozzle was a semi-flexible type developed by Amrad Corporation and provided a continuous Mach number range from 1.0 to 3.5. Plenum chamber pressures were limited to 500 psig, above which pressure (at high Mach numbers and overexpanded flow) the flow would unstart, due to shock induced separation at the nozzle walls, resulting in distortion of the semi-flexible nozzle.

The nozzle exit was rectangular in shape: 0.250 inches wide and 0.385 inches high. Mach numbers were varied by setting a counter which was physically geared to the flexible throat. Reliable Mach numbers below 1.2 were beyond the capabilities of the test apparatus. Variations in pressure and Mach number were determined by Flow Converter settings. A pressure gage was provided with the Flow Converter (See Figure A-1), for setting plenum pressures.

B. TWO-DIMENSIONAL ASYMMETRIC NOZZLE EXIT

Two-dimensional flow was achieved by mounting two parallel clear Plexiglass plates at the nozzle exit, 0.25 inches apart and flush with the vertical walls of the nozzle (See Figure A-2). The length of the lower horizontal surface of the nozzle exit was varied by mounting machined aluminum blocks flush with the lower edge of the

nozzle exit. Slots were machined in the Plexiglass walls to hold the aluminum blocks and the block used during a particular run was clamped externally (See Figure A-2). The aluminum blocks were machined in one eighth inch increments from one eighth inch to two inches (See Figure A-3).

C. FLOW VISUALIZATION

To study the effects of the variables on the flow in the nozzle exit plane it was necessary to devise an adequate flow visualization process. The initial method made use of the schlieren system provided with the Amrad Supersonic Demonstrator. This system was modified to include a traversing apparatus which would permit movement of the field of view in the flow plane (See Figure A-4). Visual results from the schlieren system provided an inadequate representation of the flow and, as a result, another visualization method was attempted.

The second flow visualization process employed a solution of oil and ultraviolet light sensitive particles. This solution was painted on the interior walls of the Plexiglass plates and illuminated with ultraviolet light. When the supersonic jet was in operation, the ultraviolet particles flowed downstream along the flow streamlines. This method provided a detailed visualization of the flow but the light intensity provided by the ultraviolet lighting was insufficient to allow reasonable camera exposure times when photographic data were taken.

The third flow visualization process which was used was similar to the second in that a solution was pointed on the interior walls of the clear Plexiglass plates. The solution used was lampblack and oil

mixed to the consistency of a thin paste. When the blowdown jet was in operation, the lampblack-in-oil solution provided a distinct representation of the flow stream-lines (See Figure A-5). The contrast of the fine black lines was increased by backlighting the flow field with white light. The backlighting consisted of a transluscent white Plexiglass sheet behind which a light bulb was mounted (See Figure A-6). This method provided sufficient light for photographic data of the flow fields to be taken. Photographs were taken with a 35mm camera mounted on a tripod at the level of the flow streamlines and located sufficiently close to record the data with a large field of view.

D. BALANCE STAND

To facilitate direct measurement of the deflection and lift forces generated by turning the mean flow, the entire test apparatus was mounted on a spring balance stand designed for this experiment. The balance stand was calibrated in ounces at one foot of moment arm. A typical set of calibration curves is included in Appendix B. To eliminate any moments generated by the reaction force of the jet, parallel to the central axis of the nozzle, the hinge point of the balance stand coincided with the centerline of the nozzle. Details of the balance stand construction are shown in Figures A-6 and A-7. In order to provide sufficient flexibility in the system, the pressure lines leading to the plenum chamber were changed to flexible rubber hoses which were suspended from the ceiling to provide free movement of the test apparatus on the balance stand (See Figure A-8).

For increasing plenum pressures one might expect the flexible pressure lines to become more rigid and generate an upward movement of the balance stand (See Figure A-8 for flexible hose mounting details). To investigate this posible source of error in balance stand deflection, several runs of the apparatus were made with a symmetric nozzle. The resulting deflections were negligible when compared with the corresponding forces generated by an asymmetric nozzle.

III. EXPERIMENTAL PROCEDURE

During the course of the experimental runs the effects of pressure, Mach number and block length variations on the mean flow angular deflection and deflection side force were studied. The various block lengths, as described in the DESCRIPTION OF APPARATUS section, were used to produce the asymmetric exit plane configurations (See Figure III-a).

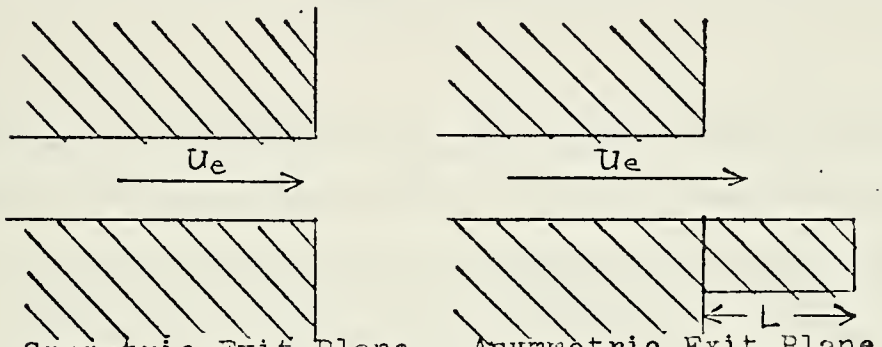

Figure III- a

Measurements of all five quantities mentioned above were made for each of the approximately 200 runs performed.

Determination of the block lengths to be used was made by limiting the field of study to simple undisturbed flow over the entire block length. Simple flow, in the sense used in this paper, is that flow in which the Mach line from the upper corner of the exit plane of the nozzle does not "strike" the block surface. A representation of simple and non-simple flow, as used in this paper, is given in Figure III-b.

The boundary between simple and non-simple flow is that condition where the characteristic from the upper corner of the nozzle exit

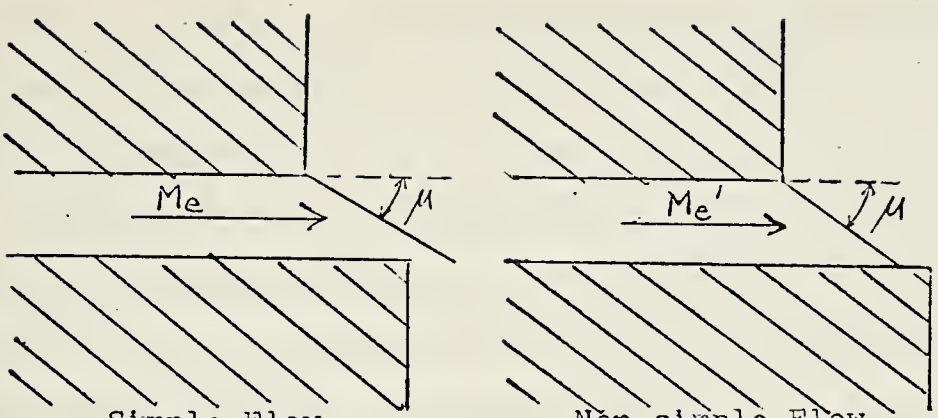

Figure III-b

intersects the downstream corner of the block. This determined the maximum block length that could be used for a given Mach number. A plot of exit Mach number versus the maximum block length for simple flow over the entire plate is given in Appendix B. The blocks were machined in one-eighth inch increments. The block lengths used for the various Mach numbers are given in Table III-a.

TABLE III-a MACH NUMBER VERSUS BLOCK LENGTH

Mach Number	Block Lengths (inches)
1.2	1/8 to 1/4
1.4	1/8 to 3/8
1.6	1/8 to 3/8
1.8	1/8 to 1/2
2.0	1/8 to 5/8
2.2	1/8 to 3/4
2.4	1/8 to 3/4

A number of runs were made with a block length of 1 1/4 inches to investigate non-simple flow.

Plenum pressure readings during each run were taken from the pressure gage on the Amrad Demonstrator. This gage was calibrated after

all of the runs were made and the pressure readings were corrected as necessary. A calibration curve for the pressure gage is given in Appendix B (Figure B-1).

The maximum pressure for a given Mach number was limited by "unstart" of the nozzle as explained in the DESCRIPTION OF APPARATUS section. Four to six pressures were used for each setting of Mach number and block length. The pressures for parallel (matched) flow and the maximum pressures for the various Mach numbers is given in Appendix B (Figure B-4).

Readings of deflection force resulting from turning of the mean flow were taken from the calibrated balance stand scale. The balance stand was calibrated in ounces of force at one foot of moment arm. Before each set of runs was made, the calibration of the scale was checked. A comparison of these calibration checks to the initial calibration is presented in Appendix B (Figure B-2). The reading of the balance stand scale for each run was included in the photograph taken of each run.

Mach numbers were determined by the setting of the flexible plate in the throat of the nozzle as indicated by a counter reading. A curve of Mach number versus counter reading was provided by the Amrad Corporation with their apparatus and is reproduced in Appendix B (Figure B-3). This curve took into account corrections for boundary layer growth in the nozzle.

The experimental method followed during each run was the following:

1. Record run number
2. Coat interior of Plexiglass plates with lampblack solution

3. Check Mach number counter setting
4. Set plenum chamber pressure
5. Tap balance stand several times to ensure that the deflection reading was true
6. Take photograph
7. Turn off pressure and reset variables for next run

When all of the various pressure and Mach number runs for a given block length were made, the block was removed and the next block size inserted. The negatives from the photographic data were slide mounted and each slide was projected for data reduction. The data obtained from each photograph were: run number, balance stand deflection force, and mean flow angular deflection.

IV. DISCUSSION OF RESULTS

A. DATA REDUCTION

For each run the data on deflection force and turning angle of the flow were recorded on a photograph. The information on Mach number, pressure setting and block length for each run was recorded by hand from the gages on the apparatus. Photographic data reduction was accomplished by projecting the slide mounted black and white negative of the picture taken for each run. The flow direction and a horizontal reference line (the lower surface of the Plexiglass plate) were transferred to a large sheet of paper. The flow turning angle for each run was then measured from the lines recorded on the paper. The deflection force, in ounces at one foot of moment arm, was also recorded for each run when the slide for that run was projected. After correction of the deflection data to correspond to the calibration of the balance stand (made before each set of runs), the deflection force was corrected to a force acting on the center of the particular block then in use by multiplying by the appropriate ratio of moment arms. The distance to the upstream edge of the block from the hinge was 8-9/16 inches. The appropriate moment arm length for each block was determined by adding half of the block length to the 8-9/16 inches. Plenum pressure data were corrected to correspond to the calibration curve for the Amrad pressure gage, as described in the DESCRIPTION OF APPARATUS section.

It was hypothesized that the deflection force could be predicted by calculating the force of the static pressure over the block minus the external (atmospheric) pressure acting on the block area. Because

flow throughout the nozzle was isentropic and the flow over the block was simple (except for the 1 1/4 inch block), the static pressure on the block could be calculated by multiplying the static-over-stagnation pressure ratio by the stagnation pressure, which in this case was the absolute pressure in the plenum chamber. Atmospheric pressure was 14.7 psia from a barometer reading. Force calculations on the block in use for each particular run were accomplished as follows:

$$\text{FORCE} = \left[(P/P_t)(P_p + 14.7) - 14.7\right] \quad A$$

(P/P_t) - tabulated versus Mach #

P_p - plenum pressure in psig

A - block area in sq.in.

The block width in each case was 0.25 inches. Values of static-over-total pressure ratio versus Mach number are given in Table IV-a.

It was also thought to be of interest to look at the deflection force versus pressure at various Mach numbers and block lengths when the effects of stream thrust and block area were removed from the deflection force by non-dimensionalization. The stream thrust at the

TABLE IV-a MACH NUMBER VERSUS P/P_t

Mach number	P/P_t
1.2	.4124
1.4	.3142
1.6	.2353
1.8	.1740
2.0	.1278
2.2	.09352
2.4	.0684

nozzle exit is proportional to the dynamic pressure at the exit. Using this fact, the measured deflection forces were divided by the product of dynamic pressure and block area. The calculations were as follows:

$$\frac{\text{Force}}{(q)\ (A)} = \frac{\text{Force}}{(q/P_t)(P_t)(A)}$$

q = dynamic pressure
P_t = total pressure (in plenum)
A = block area

The values of (q/P_t) versus Mach number are tabulated in Table IV-b.

TABLE IV-b MACH NUMBER VERSUS q/P_t

Mach number	q/P_t
1.2	.4157
1.4	.4311
1.6	.4216
1.8	.3947
2.0	.3579
2.2	.3169
2.4	.2758

The data for all of the runs made are presented in Appendix D.

B. GRAPHICAL RESULTS

Values of deflection force in pounds versus plenum pressure in psig for each Mach number and block length were plotted and can be found in Figures C-1 through C-7 in Appendix C. Each graph is for a separate block length. The curved lines through the data points represent the experimental results and the straight lines represent the predicted deflection force. Predicted deflection is based upon the force generated by the static pressure minus the external pressure at the nozzle exit acting on the surface area of the block.

Comparison of the experimental data with the predicted values indicates that the relationship governing the deflection force is not a simple pressure times area relationship. There are some similarities in the graphs, though, which are worthy of mention.

The trends in the slopes of the predicted and actual curves are the same for all of the figures. That is, there is a smooth decrease in the slopes of the curves as Mach number increases for both the actual and predicted curves. Both the actual and predicted curves intersect the zero deflection line at very nearly the same point. Zero deflection corresponds to matched conditions at the nozzle exit, or in other words the flow is perfectly expanded at the nozzle exit and there is no turning of the flow. Predicted plenum pressures in psig versus Mach number for matched flow at the exit are presented in Table IV-C.

The correlation between the predicted plenum pressures for matched flow and the experimentally determined values becomes increasingly accurate as the block length increases. One might expect this from the graphical results because for shorter block lengths the curves, in general, are more horizontal (i.e. slope is less) than the corresponding curves (with respect to Mach number) for greater block lengths.

TABLE IV-c MACH NUMBER VERSUS P_p

Mach number	P_p
1.2	20.9
1.4	32.0
1.6	47.8
1.8	69.7
2.0	100.3
2.2	143.3
2.4	200.3

The intercepts on the zero deflection line for lines of less slope are subject to greater error than the intercepts for lines that are more vertical (i.e. greater slope).

The predicted and experimental curves followed certain general trends. Examining just the portions of the experimental curves in the negative deflection force region, it can be seen that the curves bend back towards zero deflection as the plenum pressure becomes increasingly less than the matched pressure (i.e. as the flow becomes more over-expanded). This behavior becomes even more apparent as block length is increased. A possible explanation for this is flow separation at the AFT edge of the block and at the upper corner of the nozzle exit. Because the flow is overexpanded, the static pressure over the block is less than the external pressure, which would favor separation. By means of several diagrams, an explanation for the decrease in deflection force as the flow becomes more overexpanded can be presented.

Figure IV-a presents a typical shock interaction for overexpanded flow. If the shock originating on the lower surface were to move upstream (as in Figure IV-b) due to separation, then the pressures acting on the

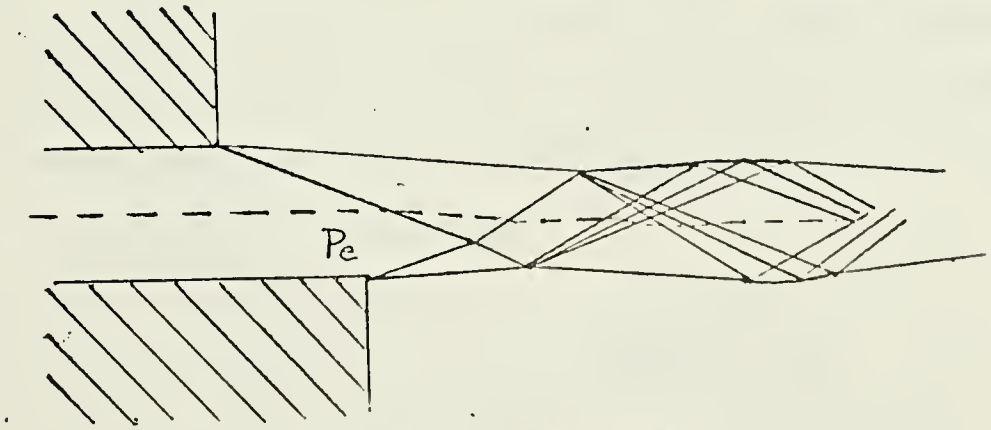

Figure IV-a. Overexpanded Flow

lower surface would be P_e and P_1 instead of just P_e. Because P_1 is greater than P_e, then P_1 would detract from the upward force generated

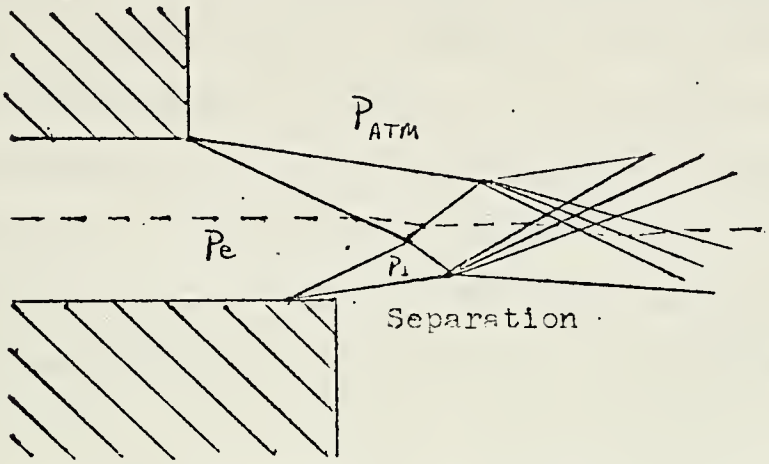

Figure IV-b. Separation on Lower Surface

by the $(P_e - P_{atm})$ difference. Also, the $(P_e - P_{atm})$ difference would be acting on a smaller area and the combination of these mechanisms would result in a smaller deflection (i.e. a smaller upward force), than the case as presented in Figure IV-a. As a result, the deflection force curve would bend up towards the zero deflection line.

The photographic data provided some justification for the hypothesis that separation occurred on the nozzle extension blocks in overexpanded flow. Examples of this appear in Figures 24, 33 and 34 in Appendix E.

If separation on the upper nozzle edge were to occur under such conditions that a situation such as presented in Figure IV-c existed, then another possible explanation could be hypothesized.

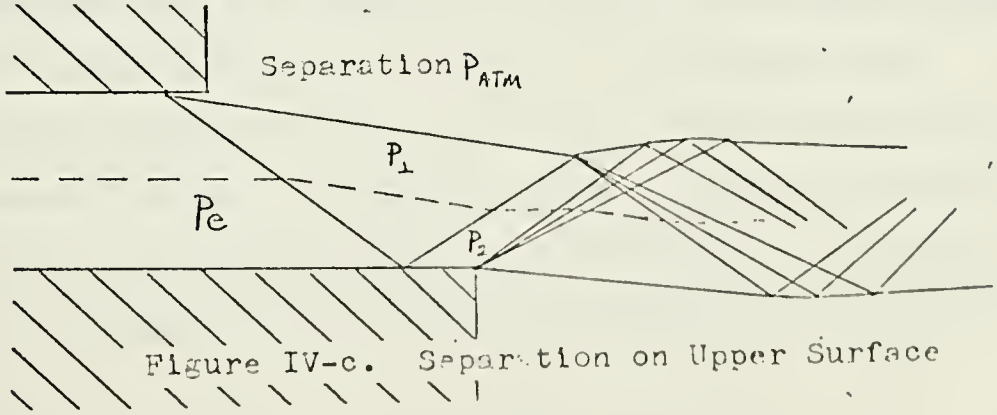

Figure IV-c. Separation on Upper Surface

For the situation presented in Figure IV-c, the shock originating from the upper surface has moved upstream a sufficient distance (and the block length of the lower surface is sufficiently long) such that it reflects from the lower surface upstream of the lower surface corner. The pressure differential ($P_e - P_{atm}$) would be acting on a smaller area than as in Figure IV-a, resulting in less upward force (i.e. less negative deflection). Also, the force resulting from ($P_2 - P_{atm}$) acting on the surface area indicated would detract from the upward force since P_2 is greater than P_e. Either the lower surface separation or the upper surface separation, or a combination of the two, would be possible explanations, then, for the upward bend in the negative deflection force portion of the curves in Figures C-1 through C-7 in Appendix C.

In the positive deflection force sector of Figures C-1 through C-7 in Appendix C the slopes of the experimental curves begin to approach the slopes of the corresponding predicted lines as the plenum pressure becomes increasingly larger than that for matched flow. This could be a result of the increasing positive static pressure at the exit, which occurs as plenum pressure is increased. This static pressure is greater than the external (atmospheric) pressure and would tend to inhibit separation. Thus the flow would approach the ideal simple flow upon which the predicted deflection force lines were based and, as a result, the experimental curves would approach the slope of the predicted lines.

Another factor was present which could have had an effect on the deflection force data. The Plexiglass plates at the nozzle exit were supported at the downstream end by small Plexiglass blocks between the plates (See Figure A-3). In certain flow conditions, the streamlines

of the flow "ran into" the blocks. This would indicate that there may have been some force generated on the support blocks which could have contributed to or detracted from the deflection force on the block at the nozzle exit.

Figure C-7 in Appendix C is for a 1-1/4 inch block. Flow over this block was not simple, in the sense described earlier. This nonsimple flow results when the Mach line from the upper nozzle corner reflects from the lower block surface. This flow situation would result in a decrease in the forces, both upward and downward on the block, that would be generated in the flow were simple over the entire block. This complex wave interaction could explain the oscillation in the deflection force curves for the 1-1/4 inch block. This oscillation also appears in the Mach 2.2 curve for the 6/8 inch block. This might indicate that nonsimple flow existed on the 6/8 inch block at Mach 2.2.

Figures C-8 through C-14 in Appendix C are graphs of plenum pressure versus the normalized deflection force (the calculation of which was described in the Data Reduction section). By dividing the deflection force by the dynamic pressure and the block area, the area dependency and stream thrust effects should have been removed from the deflection force-verses-pressure relations. If this were true, it would be expected that increasing the block length and as a result the block area, would not affect the experimental normalized curves. That is, curves for a given Mach number but different block lengths should be the same, within a reasonable amount to allow for experimental error. Looking at Figures C-8 through C-14, though, it can be seen that this is not the case. This would indicate that the earlier assumption that deflection force is simply

the result of the static pressure at the nozzle exit acting over the block area does not hold since even after the data were normalized by the block area there was still a dependency on block area in the curves.

Figures C-15 through C-21 in Appendix C are graphs of mean flow turning angle versus plenum pressure. The experimental curves follow the same general trends for all block lengths. That is, for underexpanded flow the angle is positive (up) and for overexpanded flow the angle is negative (down). The method used in measuring the angles from the photographic data gave rise to more scatter of data than for the other data measured. To comment on whether the shapes of the curves are what theory would predict would necessitate the use of some theoretical procedure such as the method of characteristics. A calculation by the method of characteristics for the first wave interactions, for both over and underexpanded flow, are presented in Figures B-6 and B-7 in Appendix B. The process involved in predicting the flow becomes more tedious as the number of interactions is increased.

The characteristic plot in Figure B-6 corresponds to the flow conditions for Figure 43 in Appendix E: PHOTOGRAPHIC DATA. In Figure 43 the measured flow deflection angle was 6.17° up. In Figure B-6 the flow is turned 3.78° up by the first expansion fan. The difference between these two values could be a result of the method used to measure the mean flow deflection angle and also might indicate that a characteristic plot of several wave interactions in the flow would be necessary to accurately predict the flow turning angle.

C. PHOTOGRAPHIC RESULTS

Figures 1 through 55 in Appendix E are prints made from the photographic data for a representative group of the total number of runs. They are for a Mach number range of 2.0 to 2.4 and block lengths of 3/8 inches to 5/8 inches. Information below each photograph is given in the following order: figure number, Mach number, block length, plenum chamber pressure in psig, deflection force in pounds with 'u' for up and 'd' for down and mean flow deflection angle in degrees with 'u' for up and 'd' for down.

The general trends for the different Mach number and block length runs are similar. For overexpanded flow the deflection angle is down and deflection force is up. Pressures for matched flow are: 101 psig for Mach 2.0, 143 psig for Mach 2.2 and 202 psig for Mach 2.4. The figures which nearly correspond to matched flow conditions are: 6, 12, 18, 24, 30, 36, 42, 48 and 54. It can be seen that the flow patterns in these figures approximate matched parallel flow. Inspection of a group of figures for a particular Mach number will yield the fact that the nearly-matched-flow photograph represents the transition between a downward flow turning angle and an upward flow turning angle. In general, for underexpanded flow the turning angles are upward and deflection forces are down. There are exceptions to the expected relation between flow turning angle and deflection force. Such exceptions are shown in Figures 12, 18, 36, and 40. All of these, but Figure 40, are for the approximately matched flow conditions. The measurement of the mean flow turning angle was subject to some error and because all of the exceptions above are for fairly small angles they do not seem too unreasonable.

These figures, again, are just a representative group of the nearly 200 data photographs taken. All of the data are presented in Appendix D and all of the photographic data, in both positive print and slide mounted negative form are also available.

V. CONCLUSIONS

Preliminary prediction of the deflection force generated by the free jet was based upon simple shock and expansion wave theory and uniform flow over the lower nozzle surface. This early model of the mechanism of the deflection force was based upon a simple linear relation between pressure and deflection force, where deflection force was considered to be the result merely of the static exit pressure of the nozzle acting on the surface area of that block which extended the lower nozzle surface and brought about asymmetric flow. The results of this investigation indicate that the early model does not adequately predict the true response of the deflection force to changes in pressure in the plenum chamber. The values of pressure for matched flow for both experimental and predicted curves are very close, but the slopes of the corresponding experimental and predicted curves were significantly different. This would indicate that the mechanism involved in generating deflection force is not as simple as was originally assumed.

If further investigations were to be made in this field, several recommendations and improvements could be made. The Plexiglass plates could be redesigned such that the support blocks would not interfere with the flow. The flexible pressure line coupling on the Amrad demonstrator could be located at the hinge point to eliminate any deflection forces due to stiffening of the pressure lines under pressure. Greater study of separation on the surfaces of the nozzle exit could be made. More sophisticated methods of measuring deflection force, such as

mounting strain gages in the lower nozzle surface extension block, could be employed. And finally, more accurate methods for measuring flow deflection angles could be devised.

Of primary importance in the experimental results were the deflection force-versus-plenum pressure curves. The slopes of these curves represent varying degrees of sensitivity of the deflection force to changes in pressure and Mach number and block length. This information could be applied to fluid logic schemes where it would be necessary for variations in the fluid flow properties to be "sensed" by some mechanism. The deflection force generated when a two-dimensional nozzle exit plane is inclined to the flow direction would provide such a mechanism.

APPENDIX A

PHOTOGRAPHS OF APPARATUS

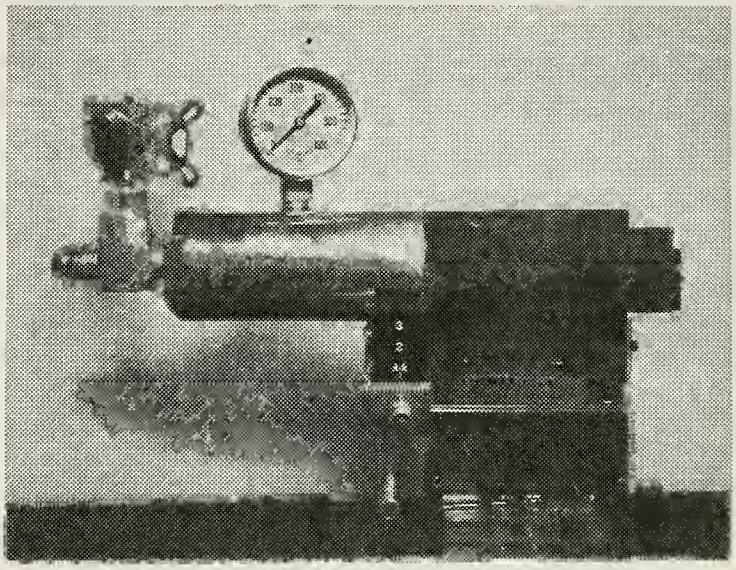

Figure A-1. Basic Amrad Supersonic Demonstrator

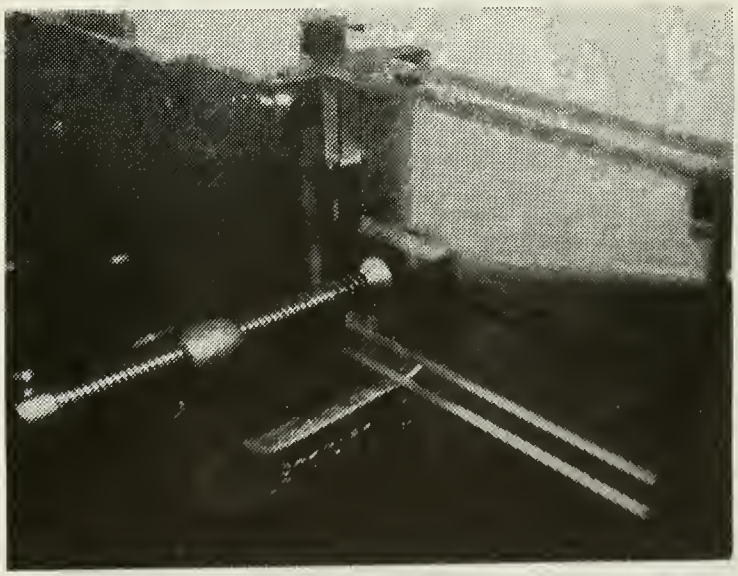

Figure A-2. Plexiglass and Block Mounting Details

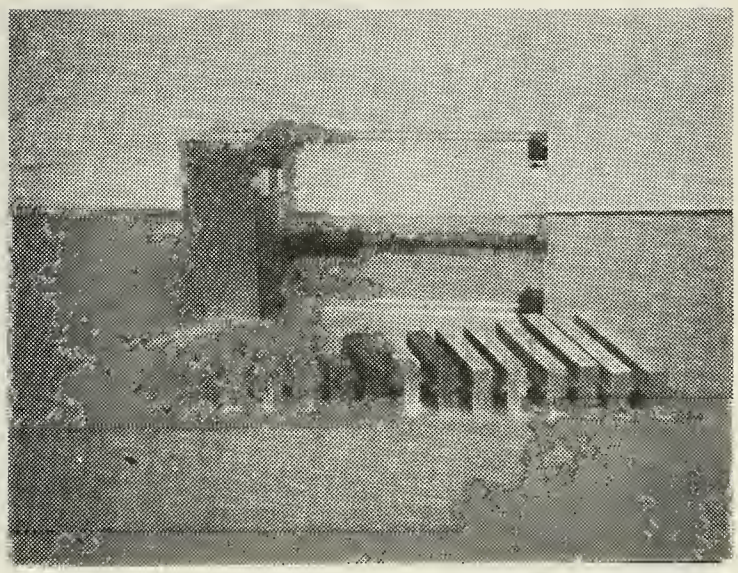

Figure A-3. Block Lengths and Plexiglass Plates

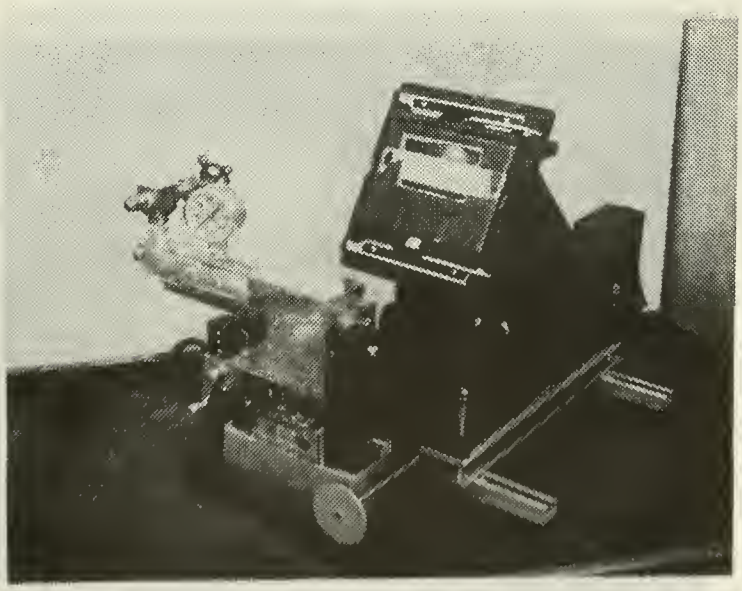

Figure A-4. Aaron Demonstrator with Schlieren

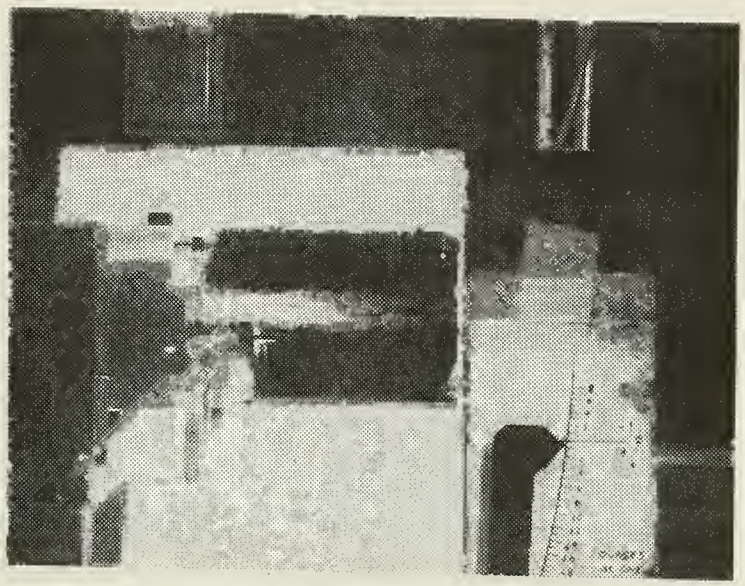

Figure A-5. Flow Visualization

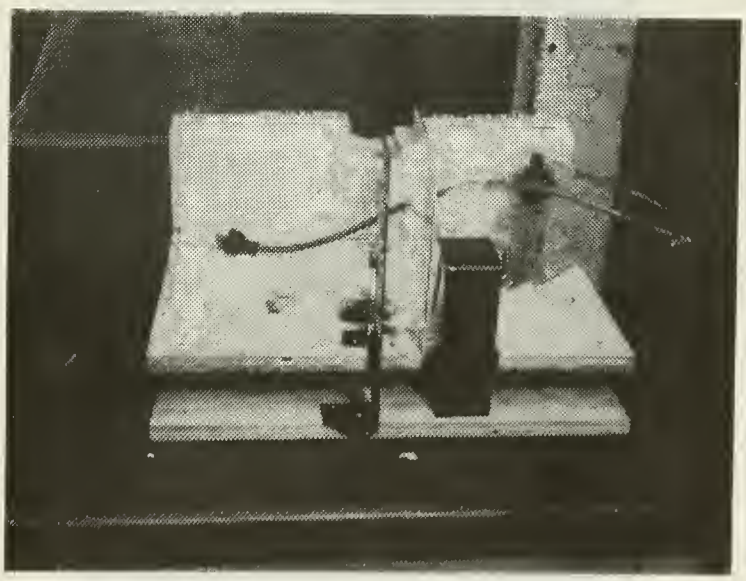

Figure A-6. Balance Stand, Downstream View

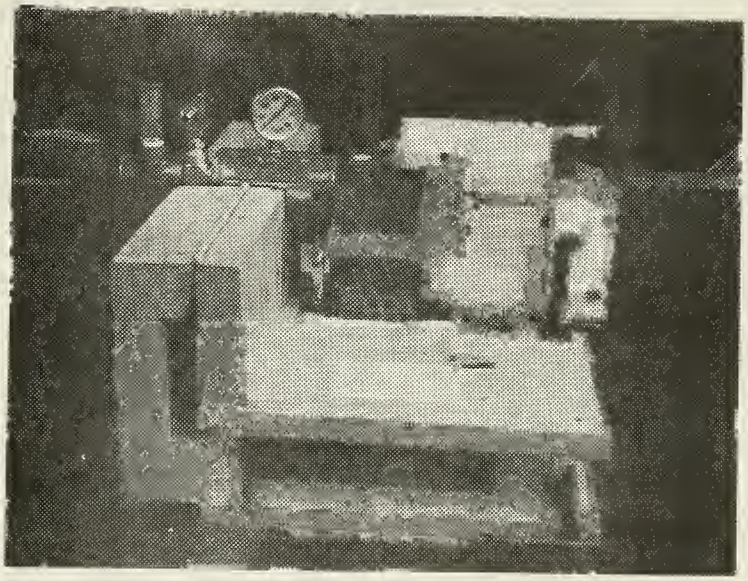

Figure A-7. Balance Stand, Side View

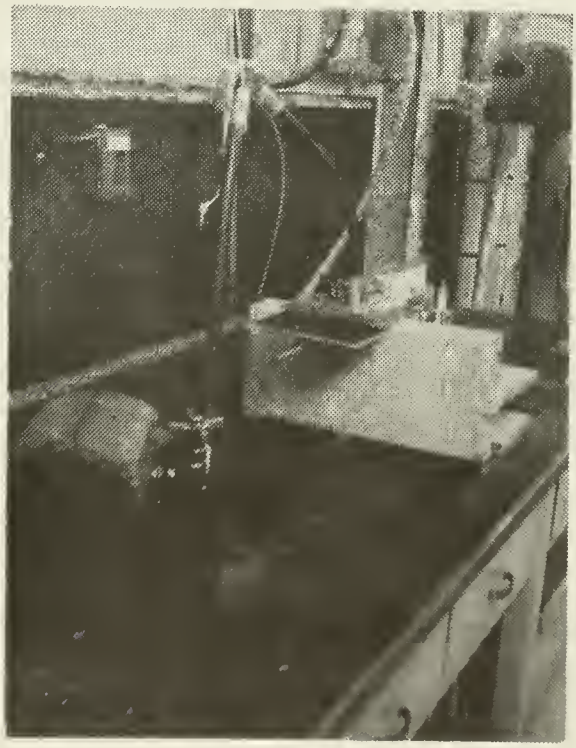

Figure A-8 Flexible Pressure Hoses

APPENDIX B

MISCELLANEOUS GRAPHS

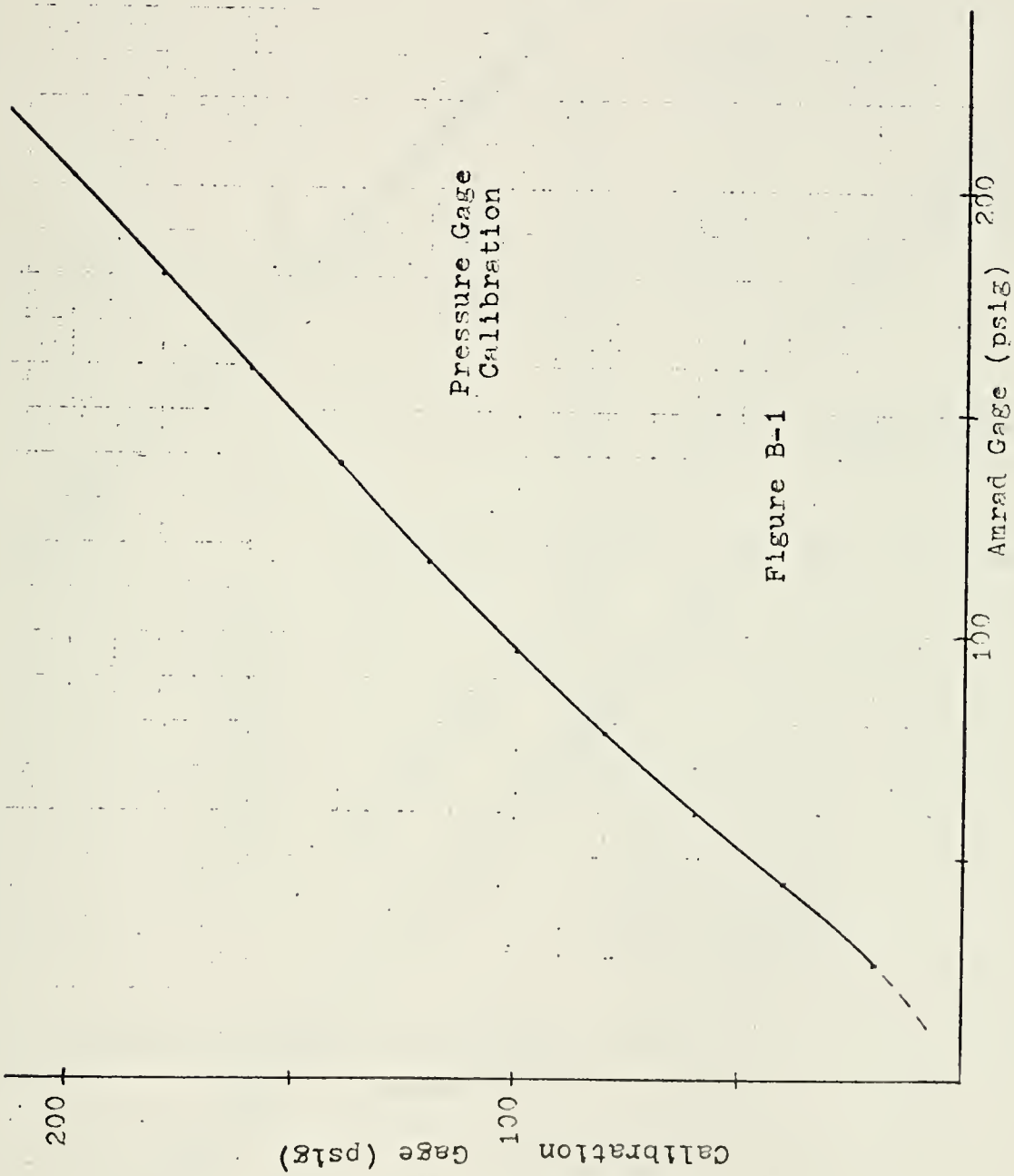

Figure B-1

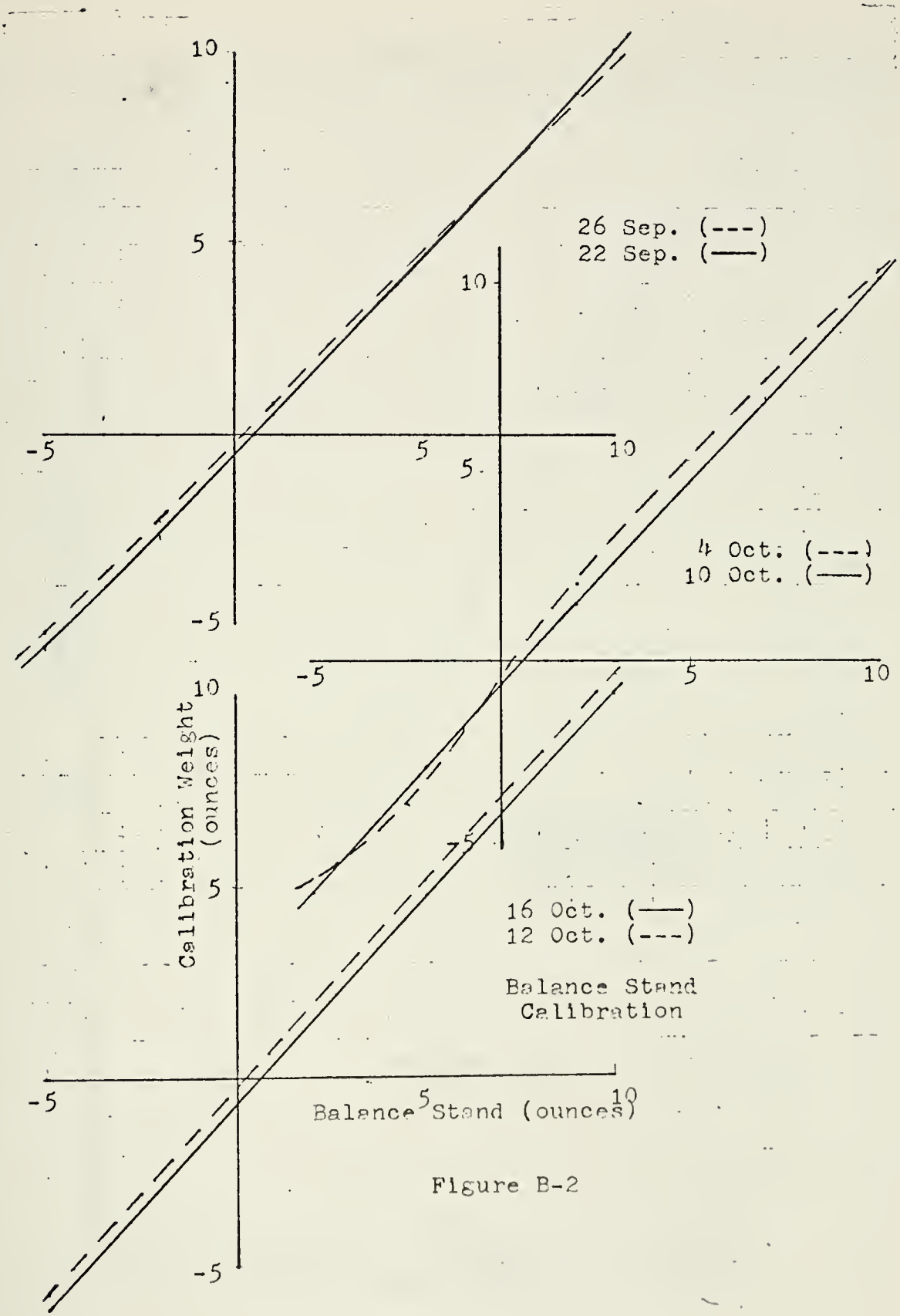
26 Sep. (---)
22 Sep. (——)
4 Oct. (---)
10 Oct. (——)
16 Oct. (——)
12 Oct. (---)
Balance Stand
Calibration
Calibration Weight (ounces)
Balance Stand (ounces)
10
5
-5
-5
5
10

Figure B-2

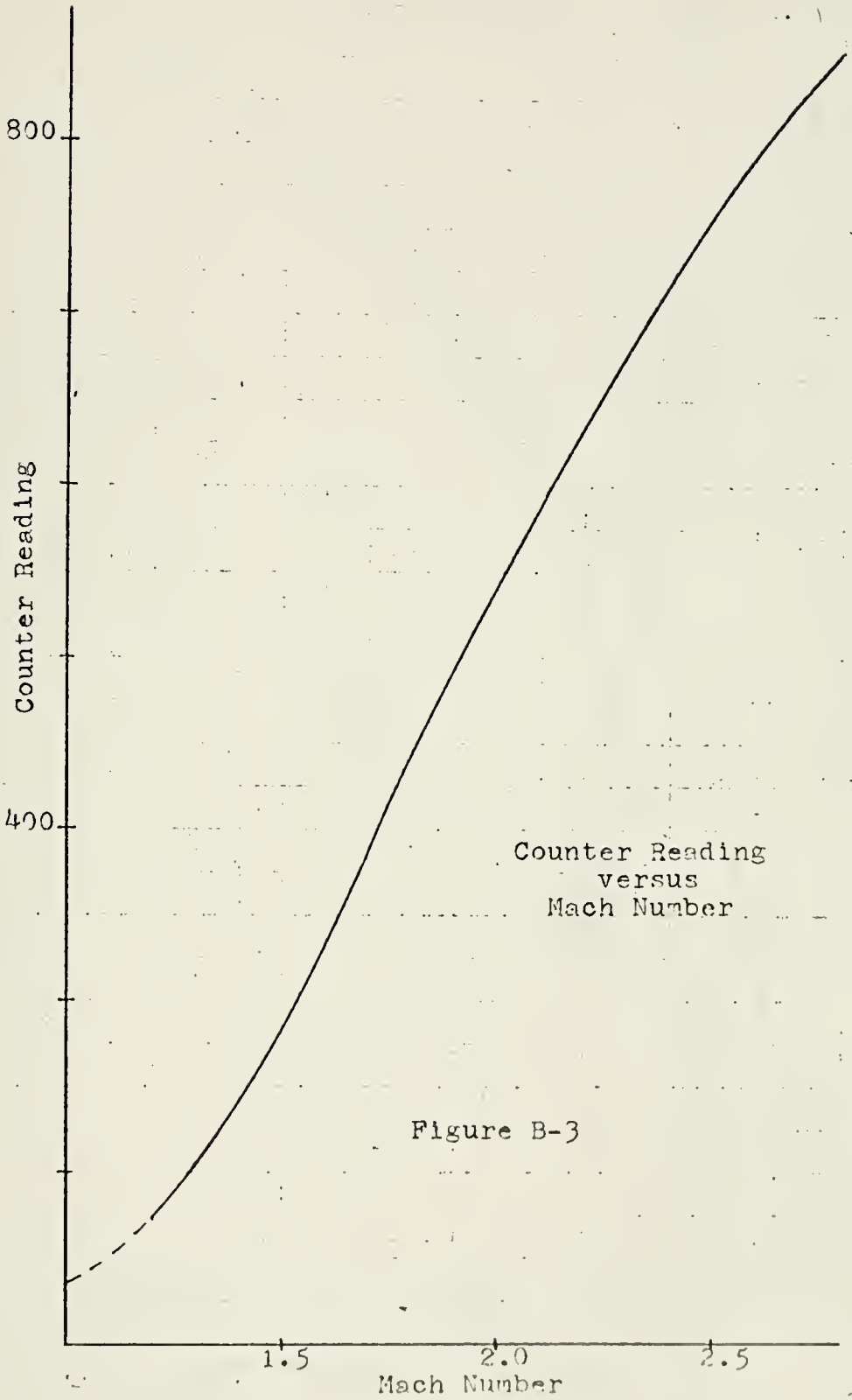
800
400
Counter Reading
1.5
2.0
2.5
Mach Number
Counter Reading
versus
Mach Number

Figure B-3

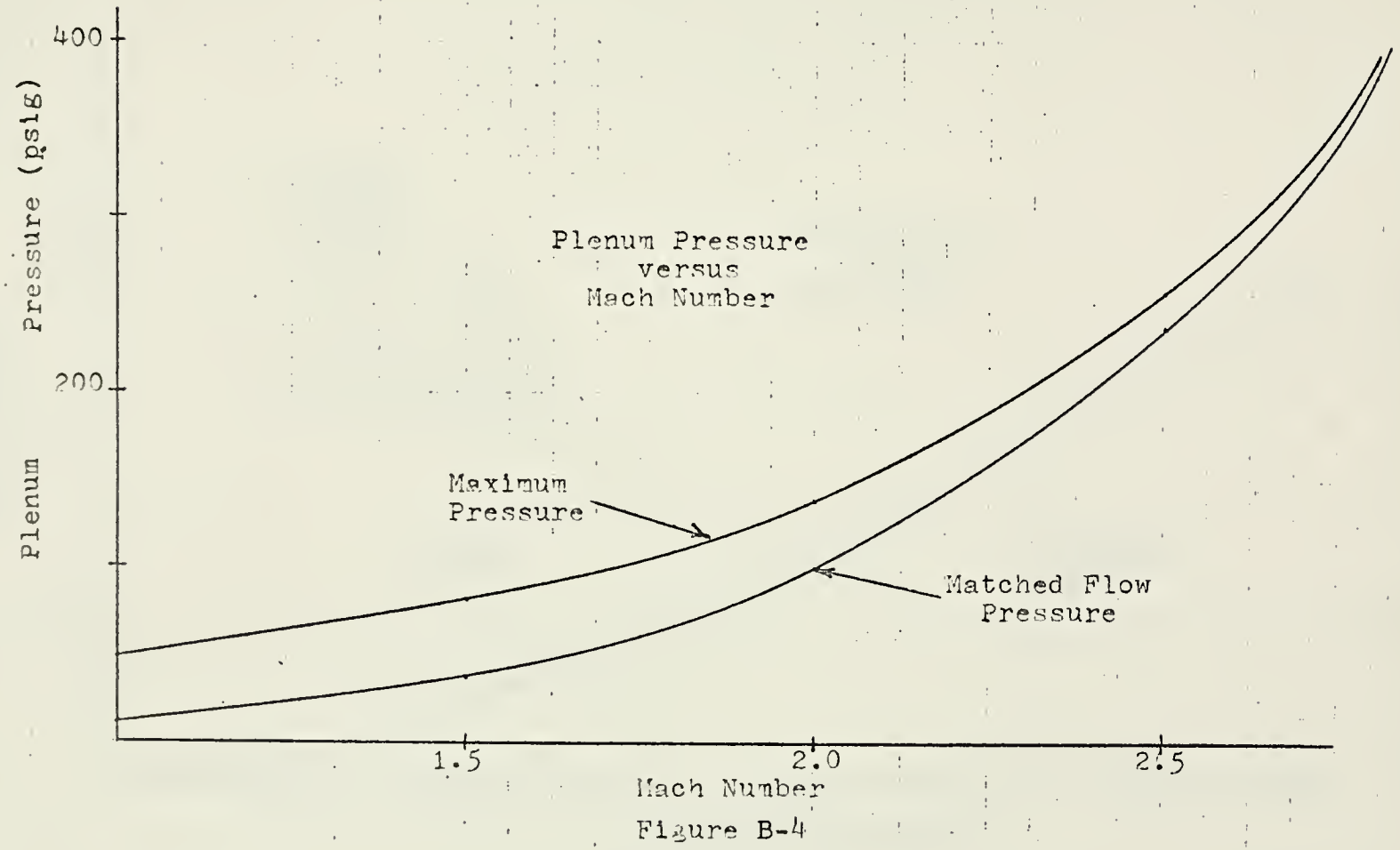
400
200
Plenum Pressure (psig)
Plenum Pressure
versus
Mach Number
Maximum
Pressure
Matched Flow
Pressure
1.5
2.0
2.5
Mach Number

Figure B-4

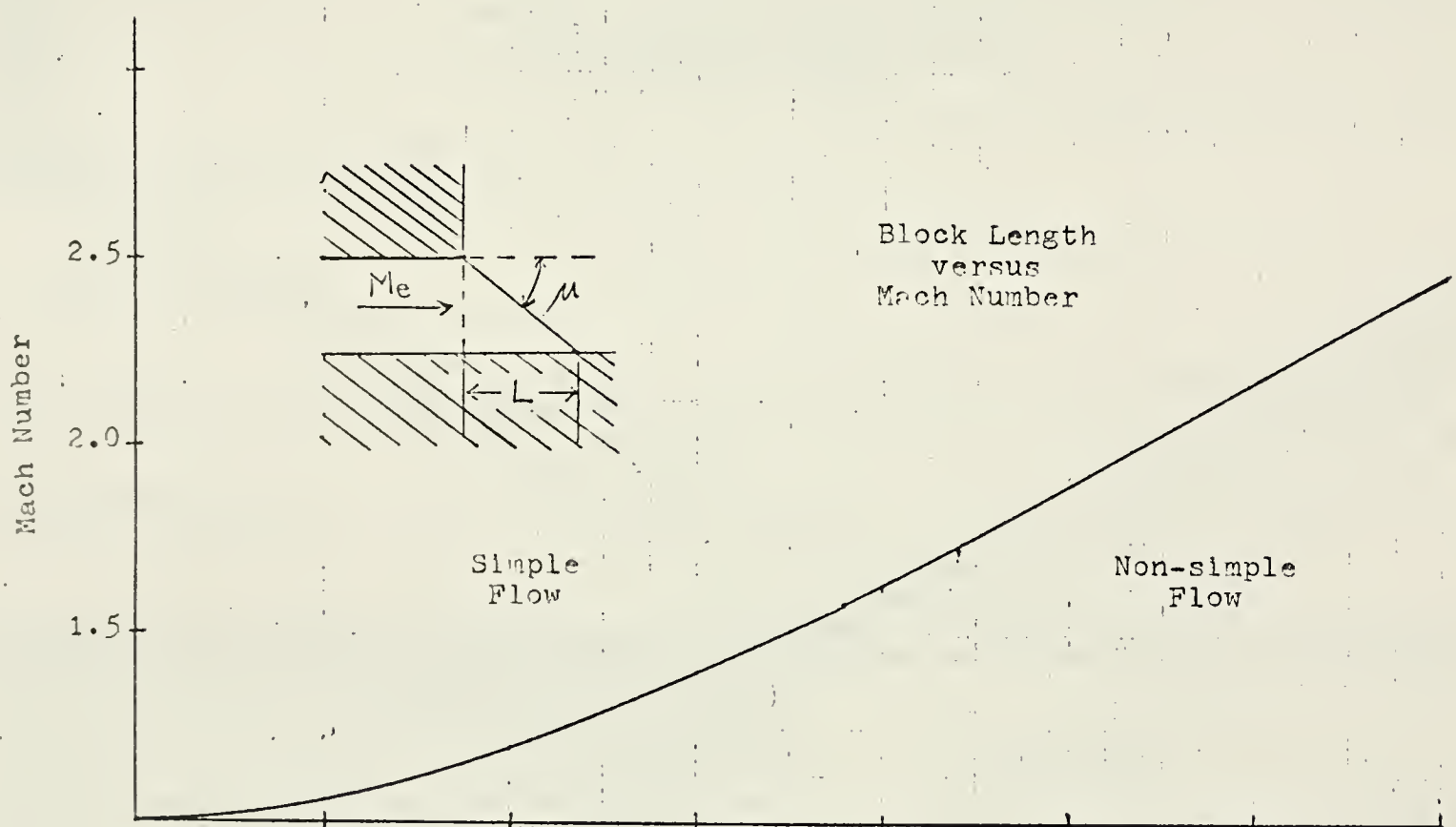
Block Length
versus
Mach Number
Me
μ
L
Mach Number
2.5
2.0
1.5
Simple
Flow
Non-simple
Flow
2/8
4/8
6/8
Block Length (inches)

Figure B-5

Method of Characteristics Plot
For Dimensions Proportional To A
5/8 Inch Block

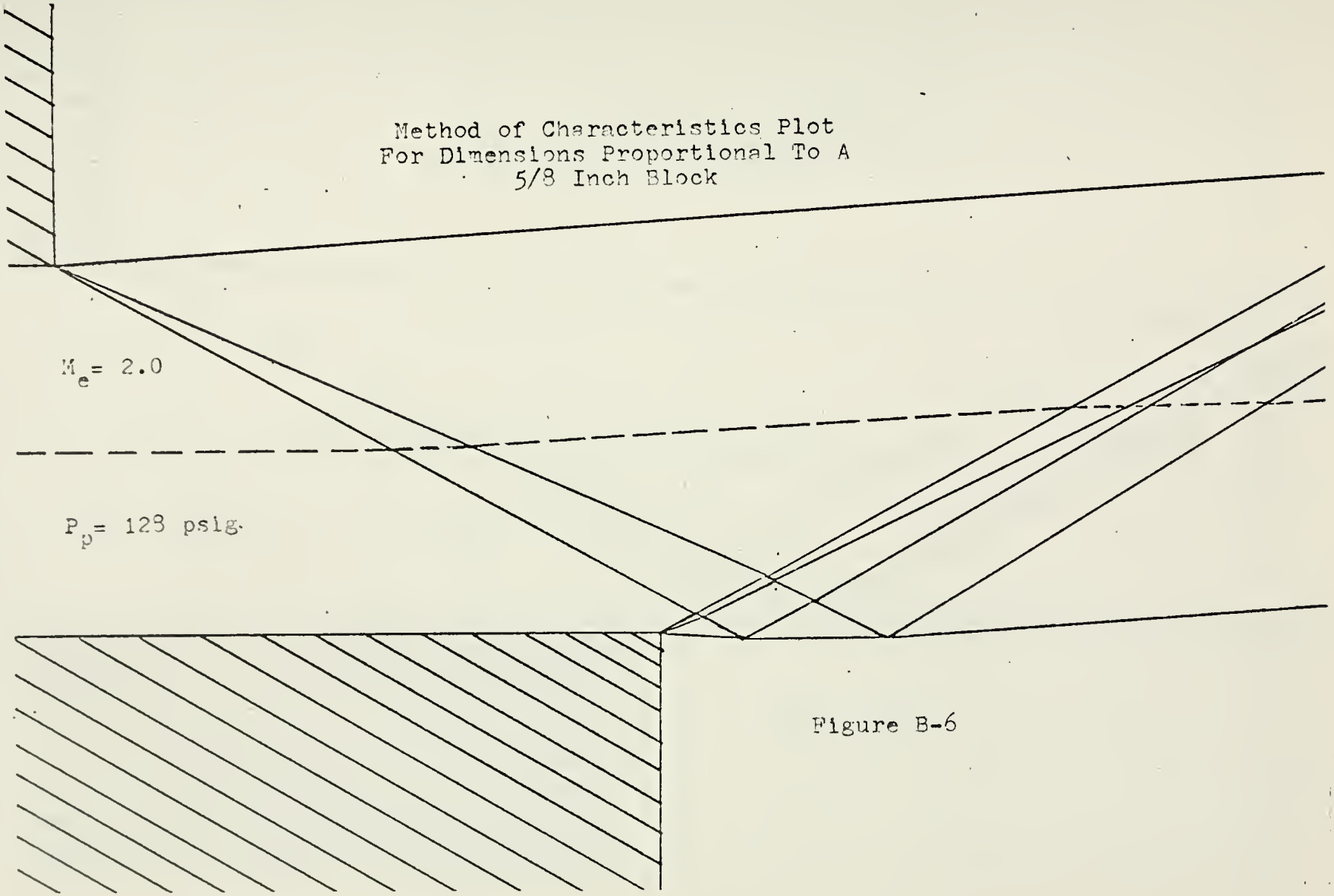

Figure B-6

Method of Characteristics Plot
For Dimensions Proportional To A
4/3 Inch Block

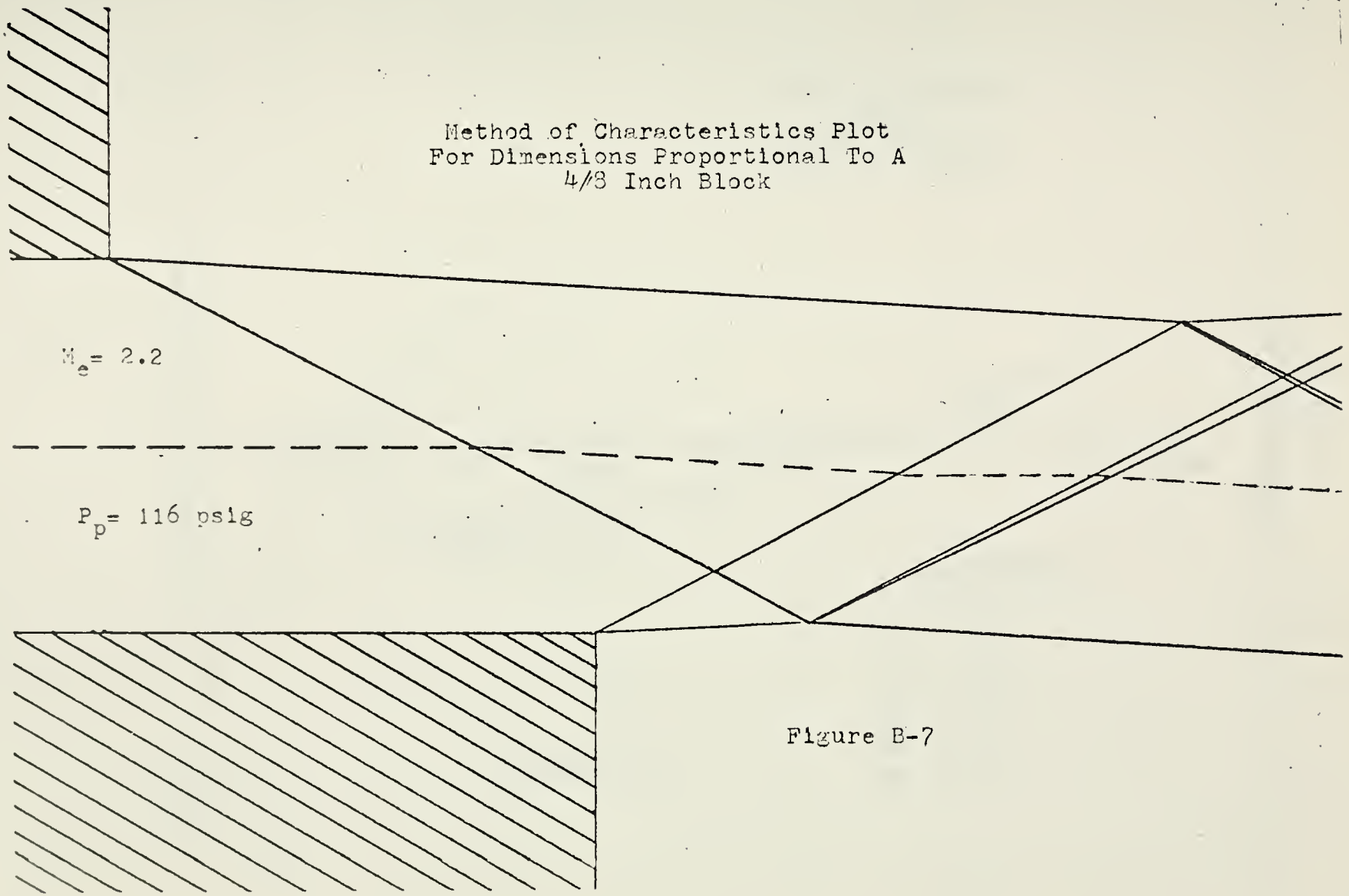

Figure B-7

APPENDIX C

GRAPHICAL RESULTS

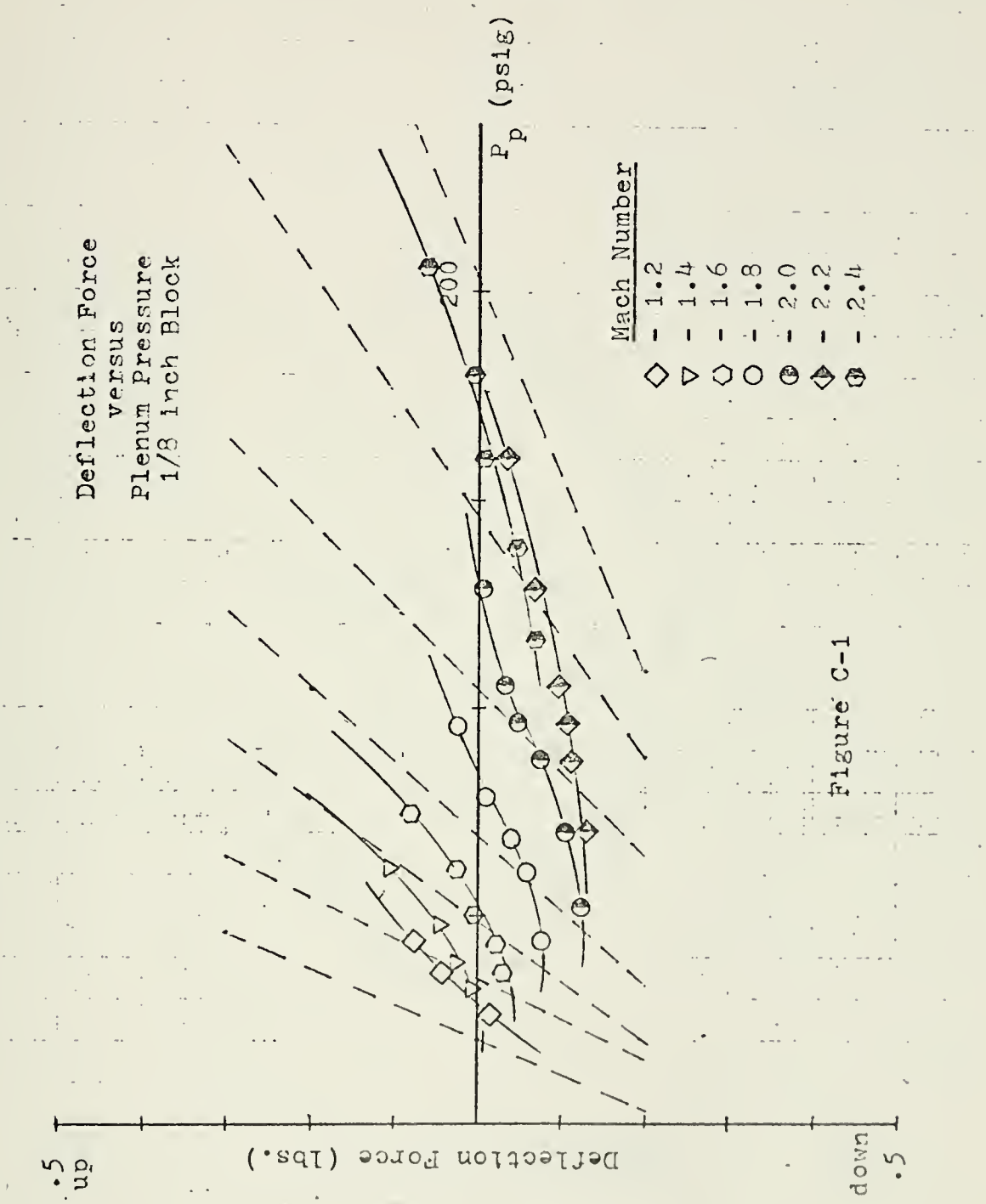

Figure C-1

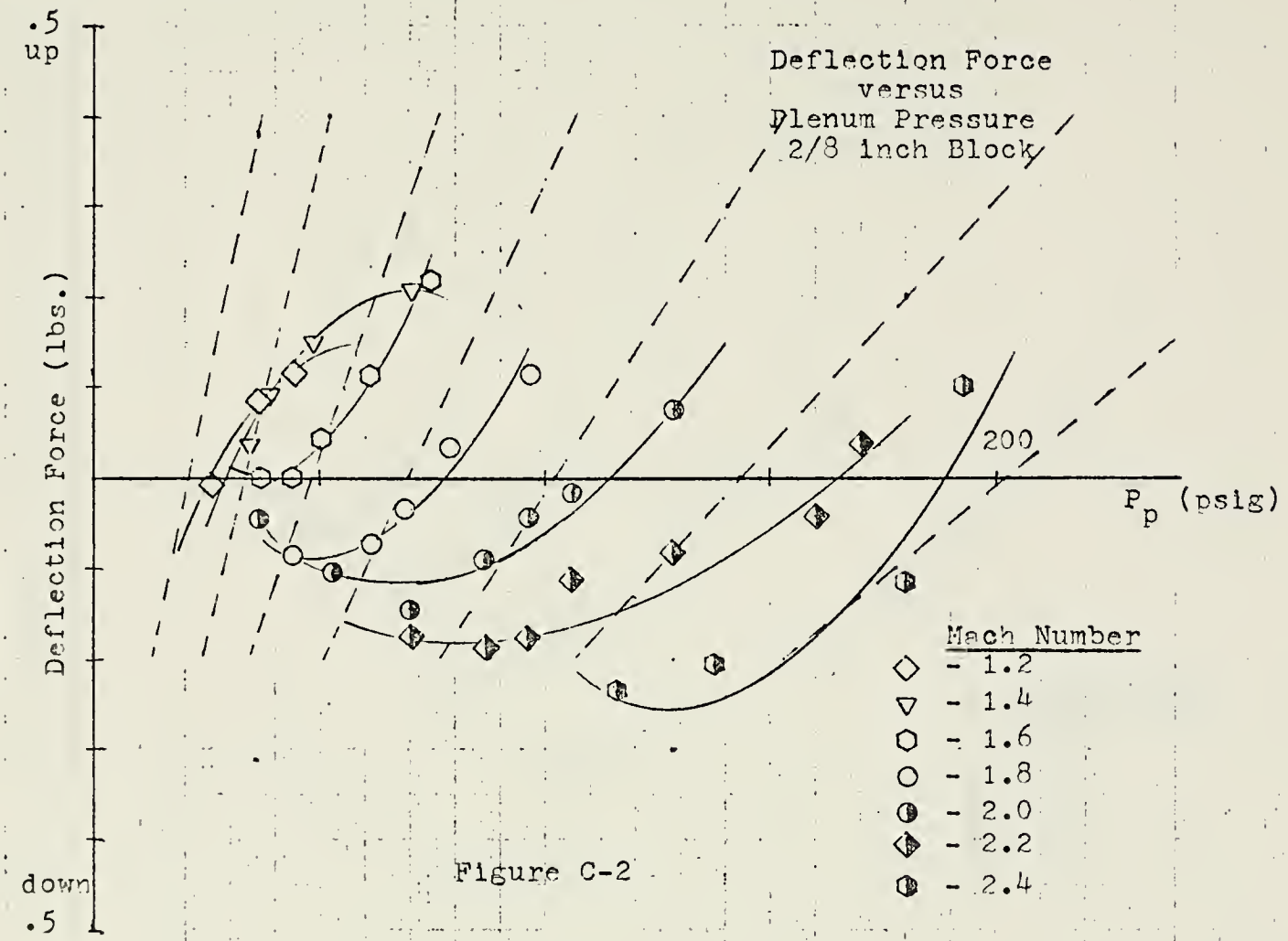
.5
up
Deflection Force
versus
Plenum Pressure
2/8 inch Block
Deflection Force (lbs.)
200
P_p (psig)
Mach Number
- 1.2
- 1.4
- 1.6
- 1.8
- 2.0
- 2.2
- 2.4
down
.5

Figure C-2

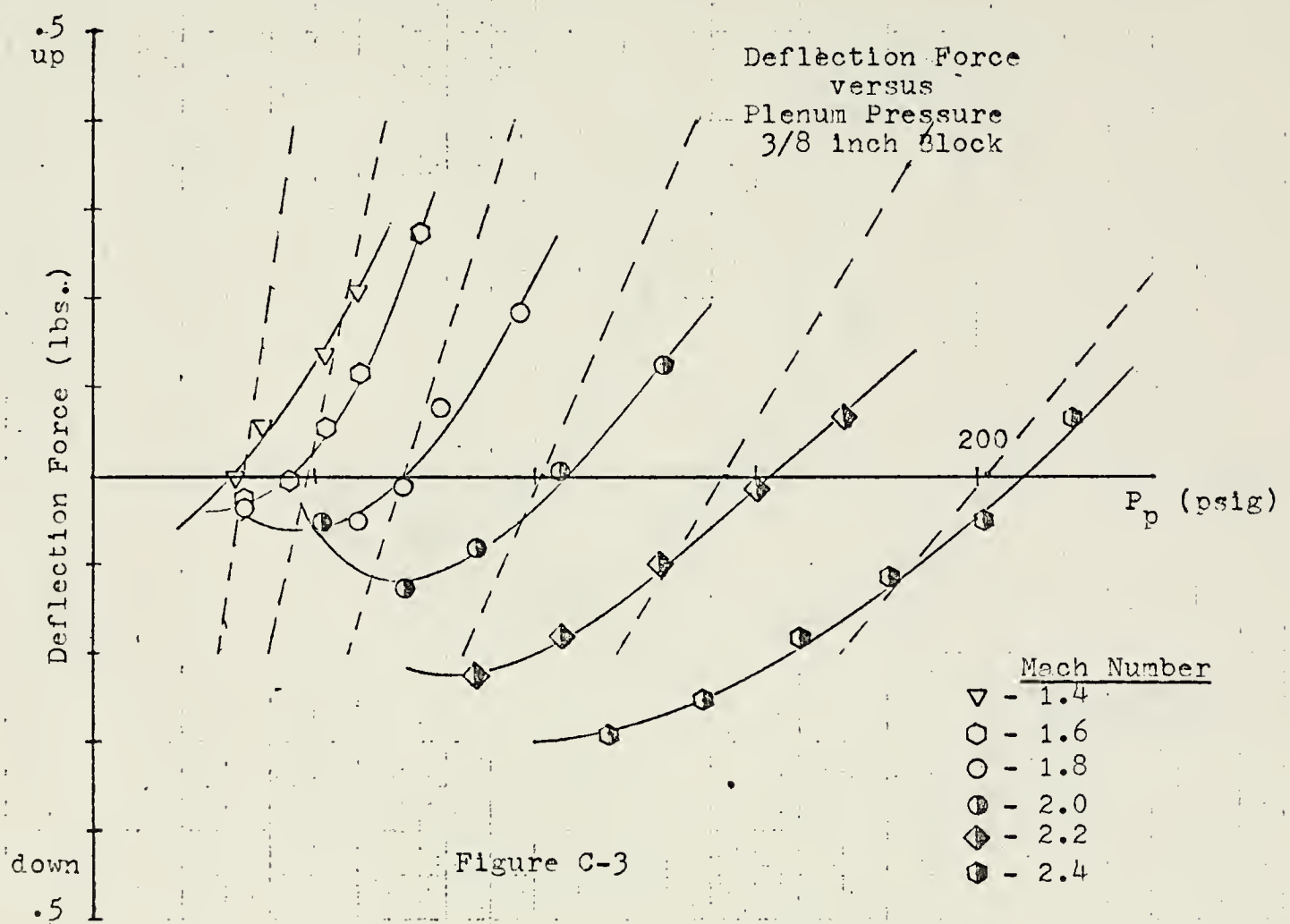
Deflection Force
versus
Plenum Pressure
3/8 inch Block
.5
up
Deflection Force (lbs.)
down
.5
200
P_p (psig)
Mach Number
▽ - 1.4
⬡ - 1.6
○ - 1.8
◑ - 2.0
◈ - 2.2
⬢ - 2.4

Figure C-3

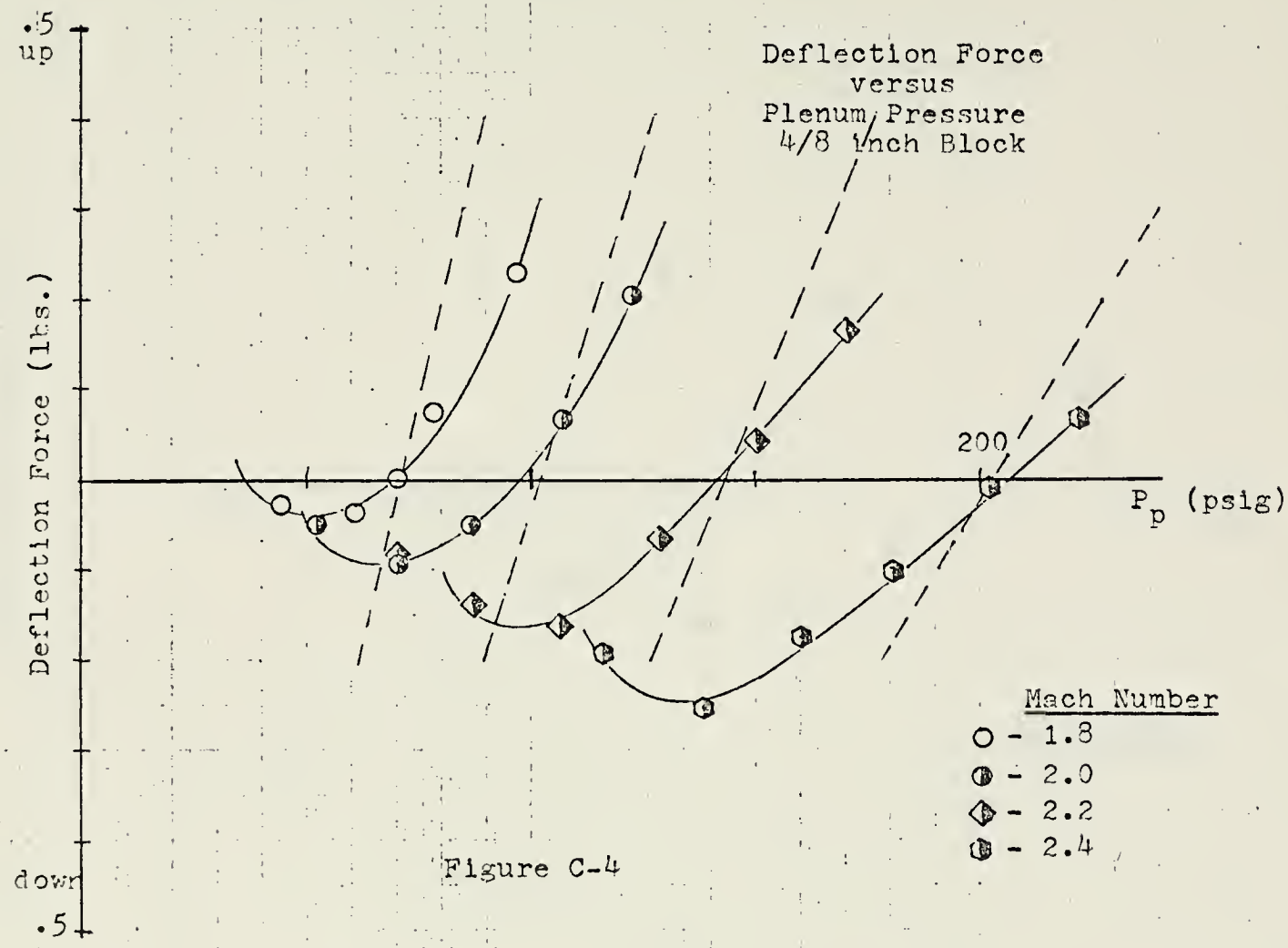
Deflection Force
versus
Plenum Pressure
4/8 inch Block
.5
up
Deflection Force (lbs.)
down
.5
200
P_p (psig)
Mach Number
- 1.8
- 2.0
- 2.2
- 2.4

Figure C-4

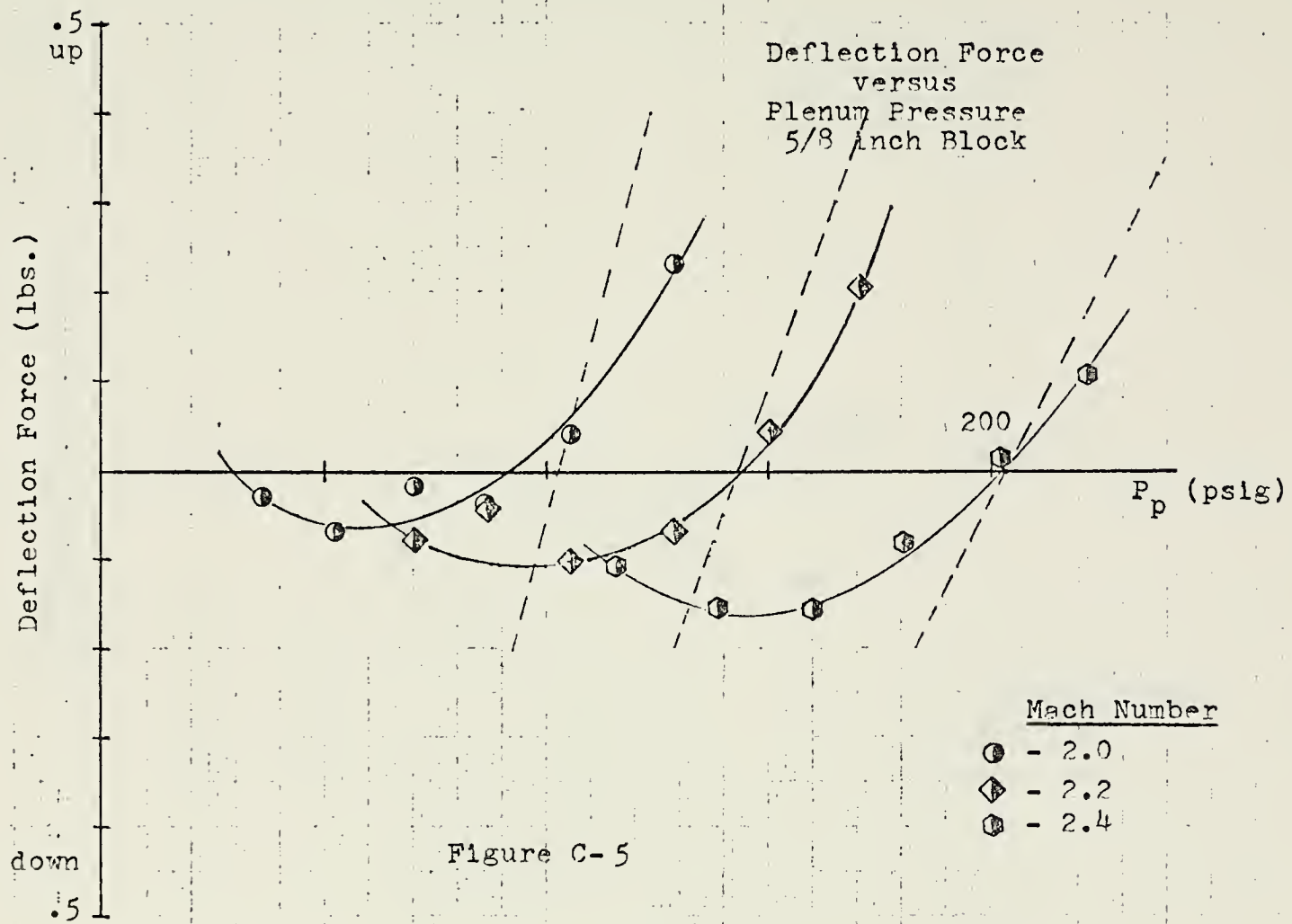
Deflection Force
versus
Plenum Pressure
5/8 inch Block
.5
up
Deflection Force (lbs.)
down
.5
200
P_p (psig)
Mach Number
- 2.0
- 2.2
- 2.4

Figure C-5

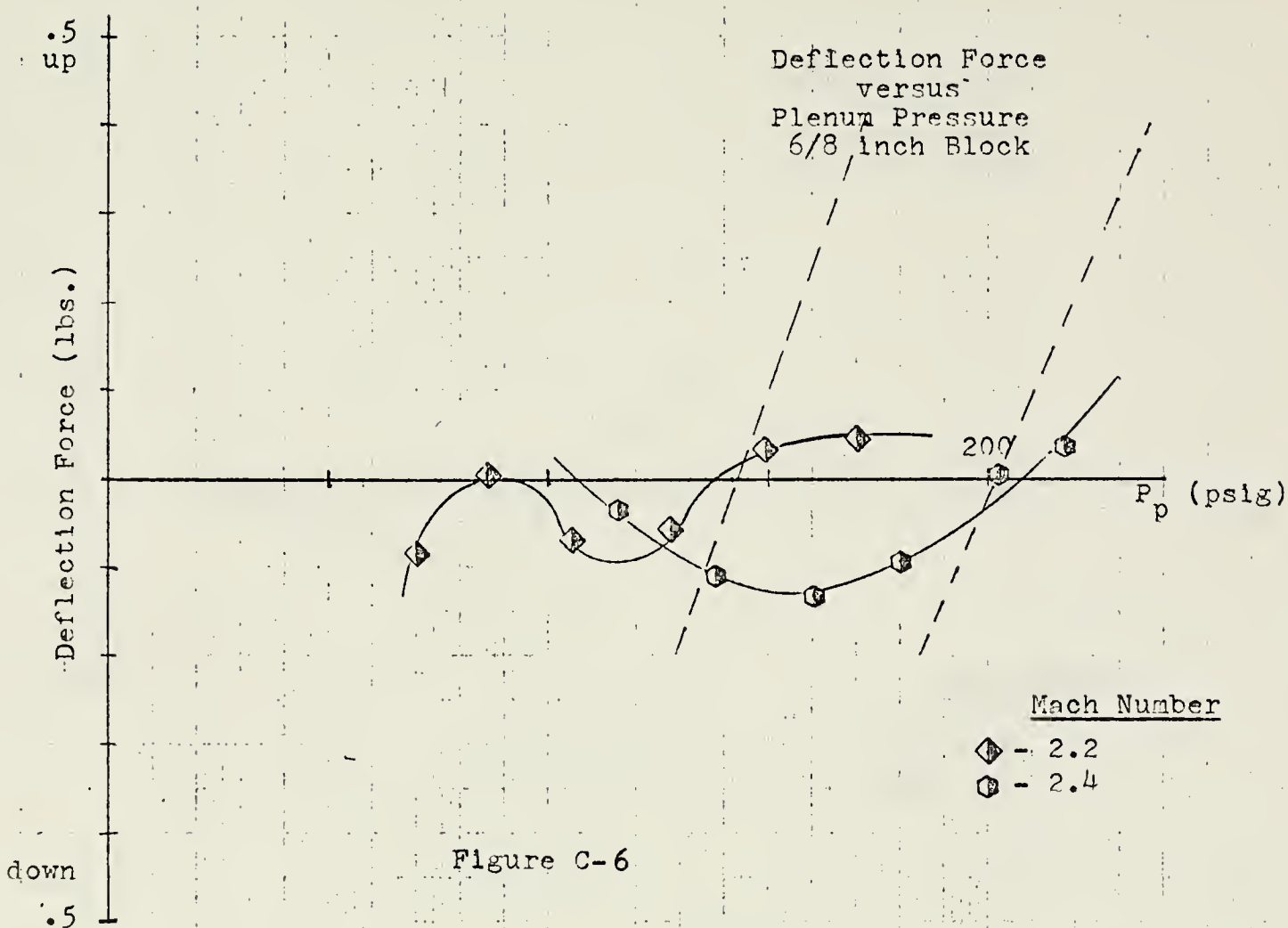
Deflection Force
versus
Plenum Pressure
6/8 inch Block
.5
up
Deflection Force (lbs.)
down
.5
200
P_p (psig)
Mach Number
- 2.2
- 2.4

Figure C-6

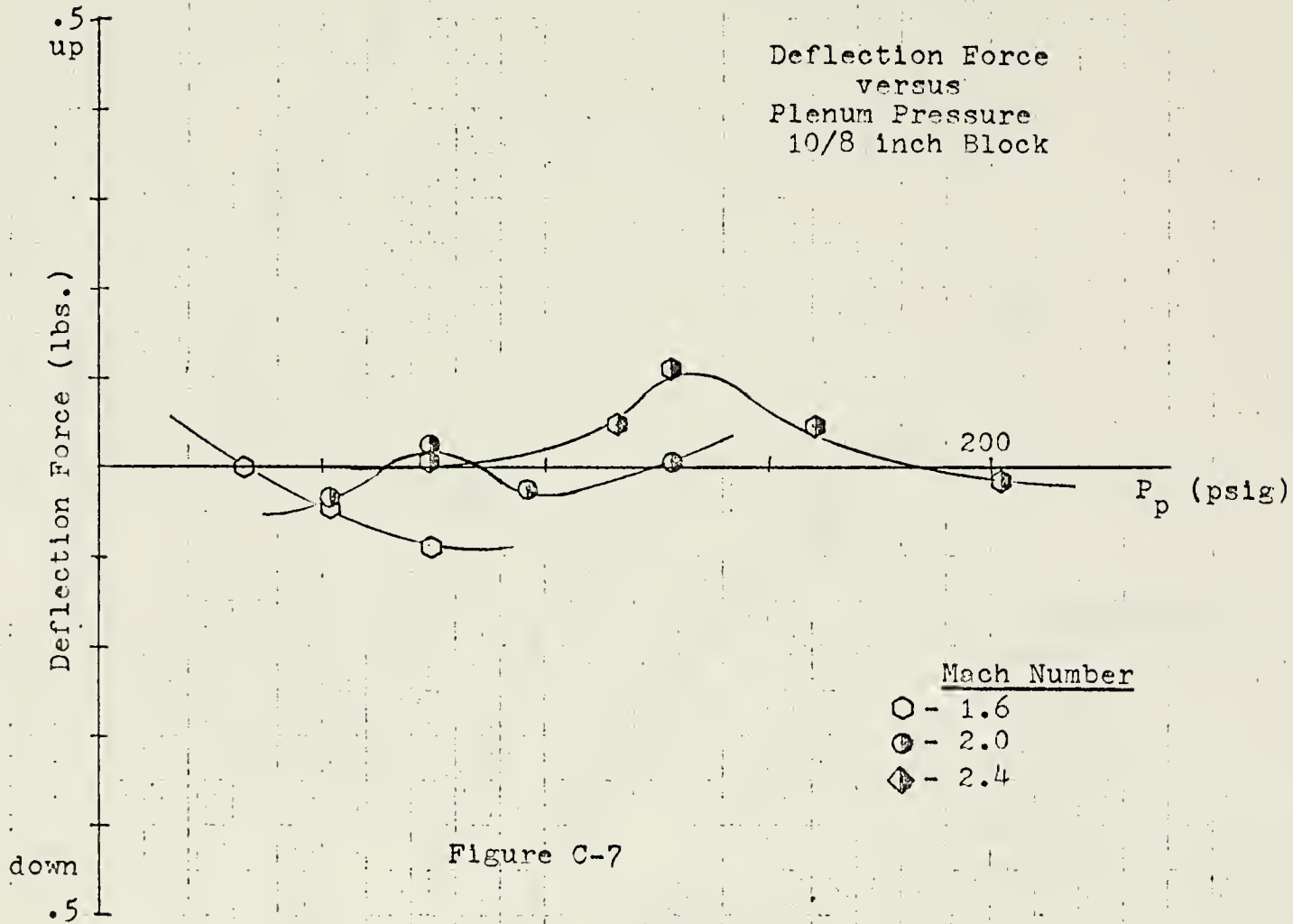
Deflection Force
versus
Plenum Pressure
10/8 inch Block
.5
up
Deflection Force (lbs.)
down
.5
200
P_p (psig)
Mach Number
- 1.6
- 2.0
- 2.4

Figure C-7

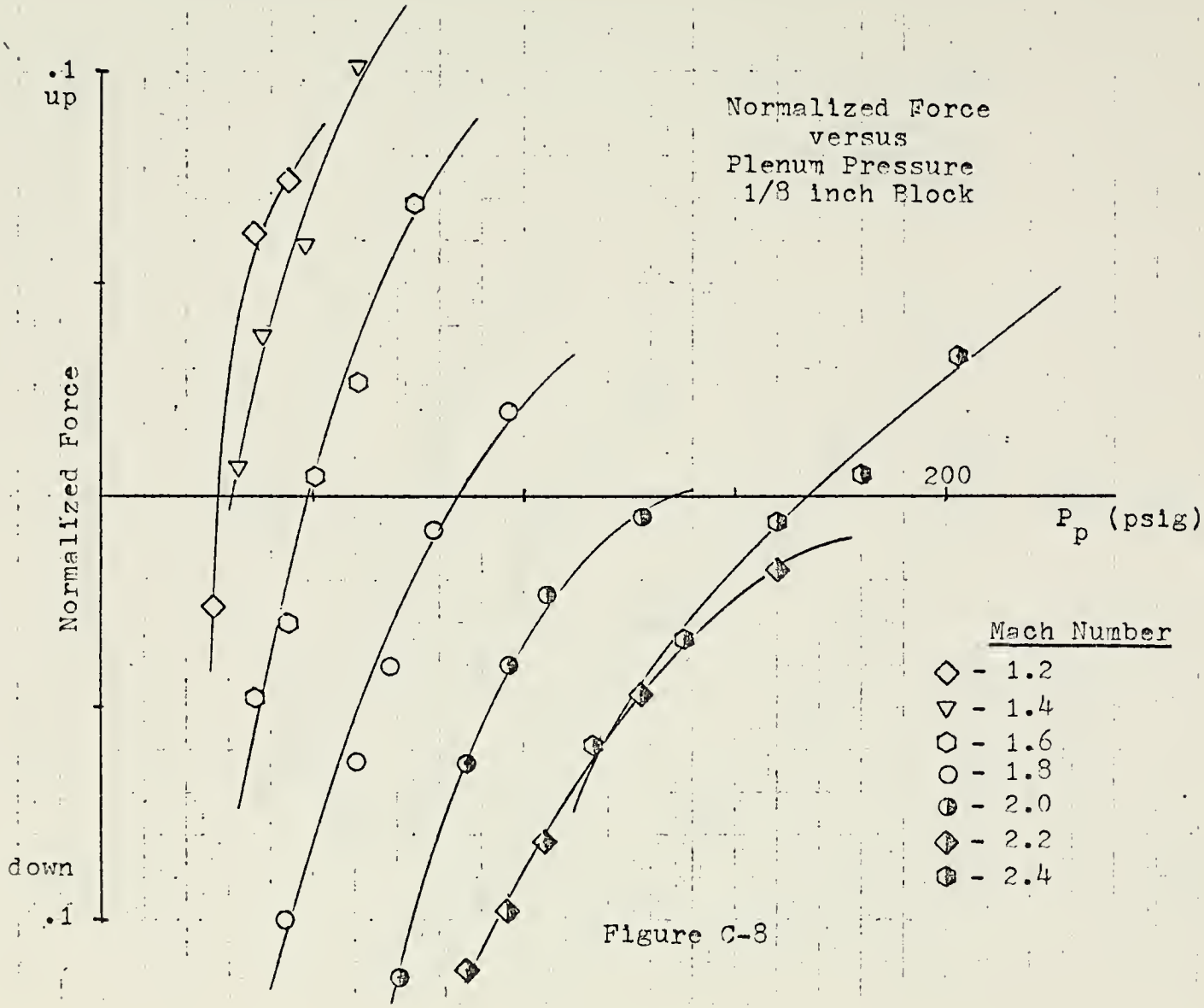
Normalized Force
versus
Plenum Pressure
1/8 inch Block
.1
up
Normalized Force
down
.1
200
P_p (psig)
Mach Number
- 1.2
- 1.4
- 1.6
- 1.8
- 2.0
- 2.2
- 2.4

Figure C-8

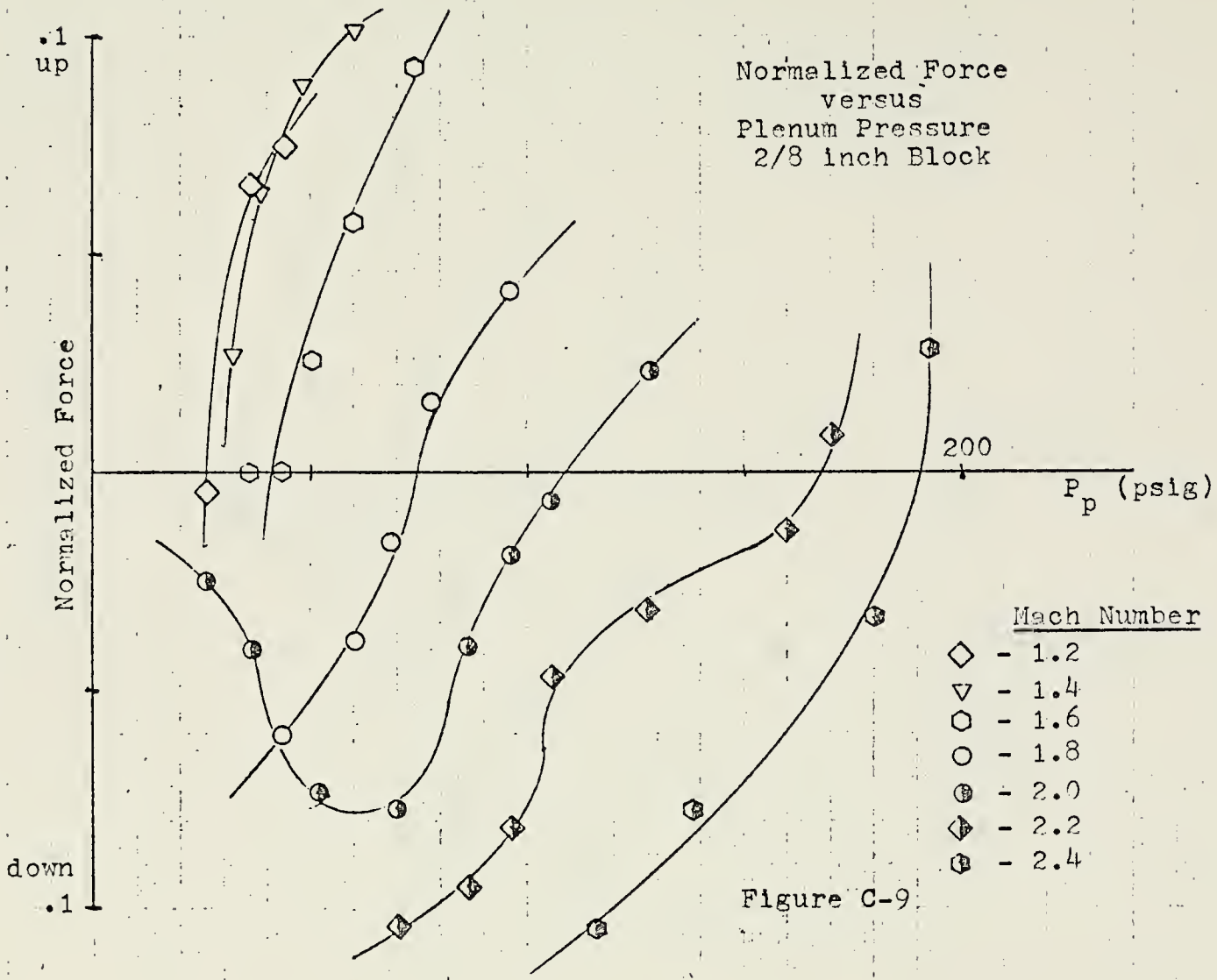
Normalized Force
versus
Plenum Pressure
2/8 inch Block
.1
up
Normalized Force
down
.1
200
P_p (psig)
Mach Number
◇ - 1.2
▽ - 1.4
⬡ - 1.6
○ - 1.8
◍ - 2.0
◈ - 2.2
⬢ - 2.4

Figure C-9

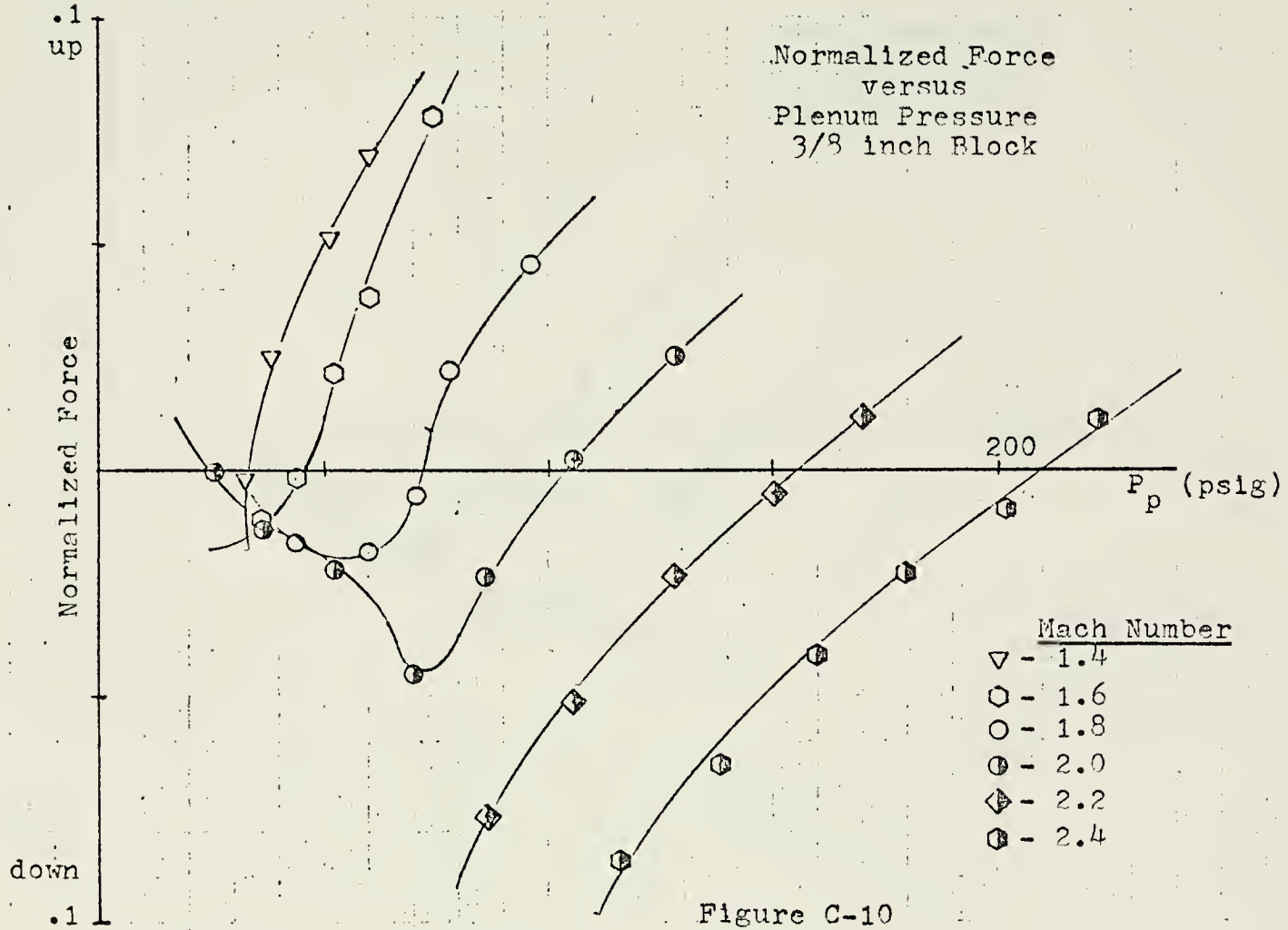
.1
up
Normalized Force
versus
Plenum Pressure
3/8 inch Block
Normalized Force
200
P_p (psig)
Mach Number
▽ - 1.4
⬡ - 1.6
○ - 1.8
◑ - 2.0
◈ - 2.2
⬢ - 2.4
down
.1

Figure C-10

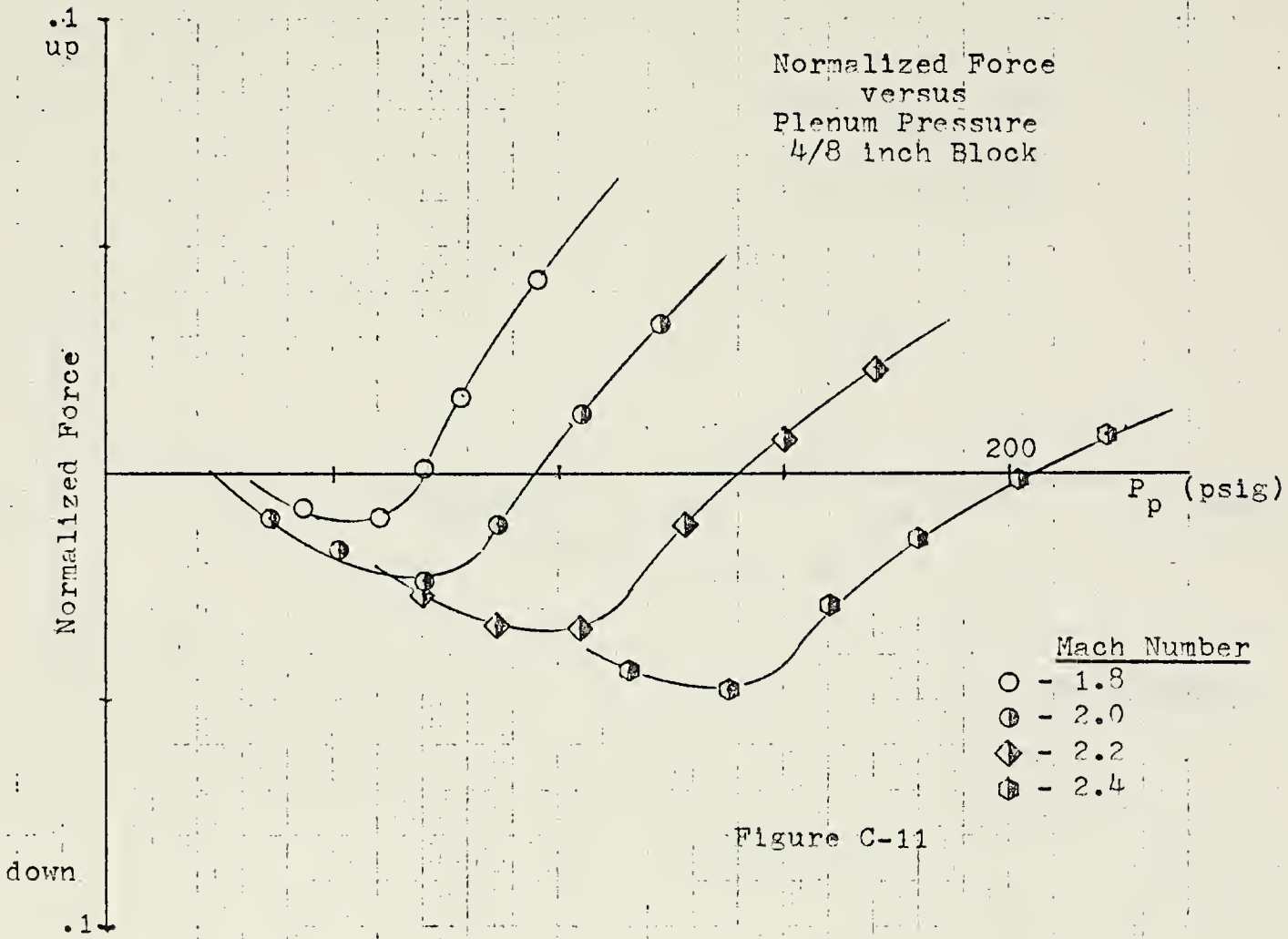
Normalized Force
versus
Plenum Pressure
4/8 inch Block
.1
up
Normalized Force
down
.1
200
P_p (psig)
Mach Number
○ - 1.8
◑ - 2.0
◈ - 2.2
⬢ - 2.4

Figure C-11

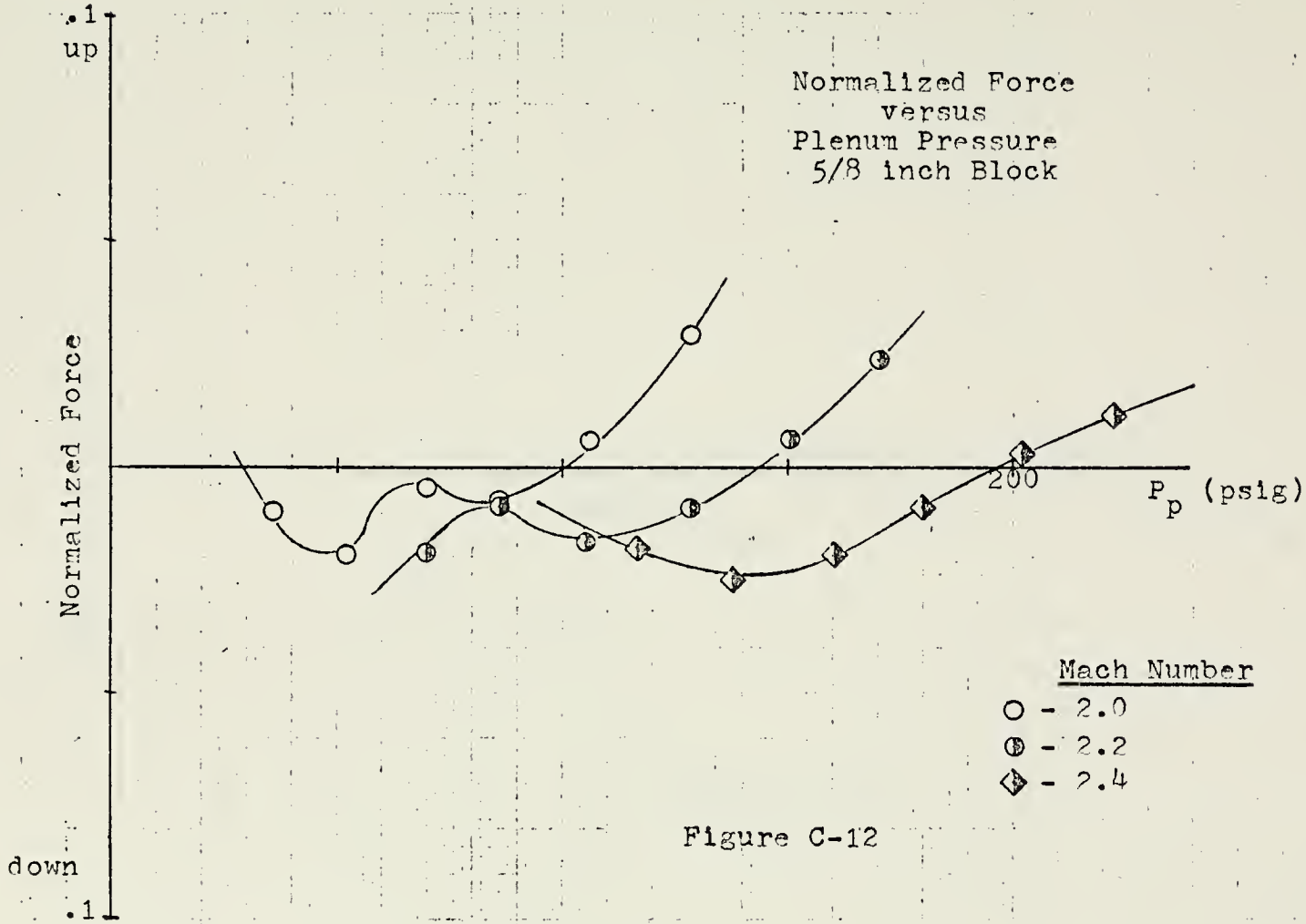
.1
up
Normalized Force
versus
Plenum Pressure
5/8 inch Block
Normalized Force
200
P_p (psig)
Mach Number
○ - 2.0
◑ - 2.2
◇ - 2.4
down
.1

Figure C-12

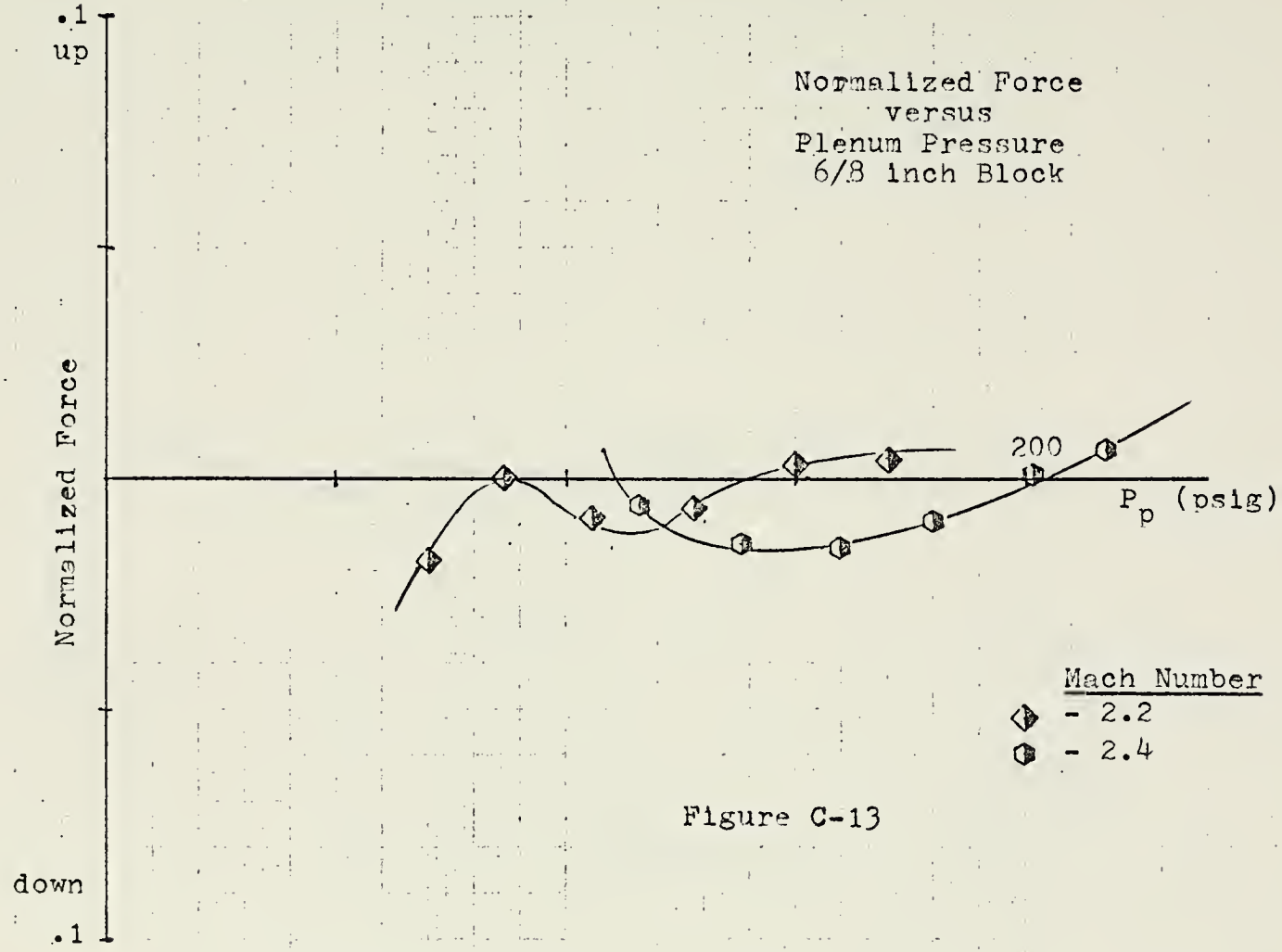
Normalized Force
versus
Plenum Pressure
6/8 inch Block
.1
up
Normalized Force
down
.1
200
P_p (psig)
Mach Number
- 2.2
- 2.4

Figure C-13

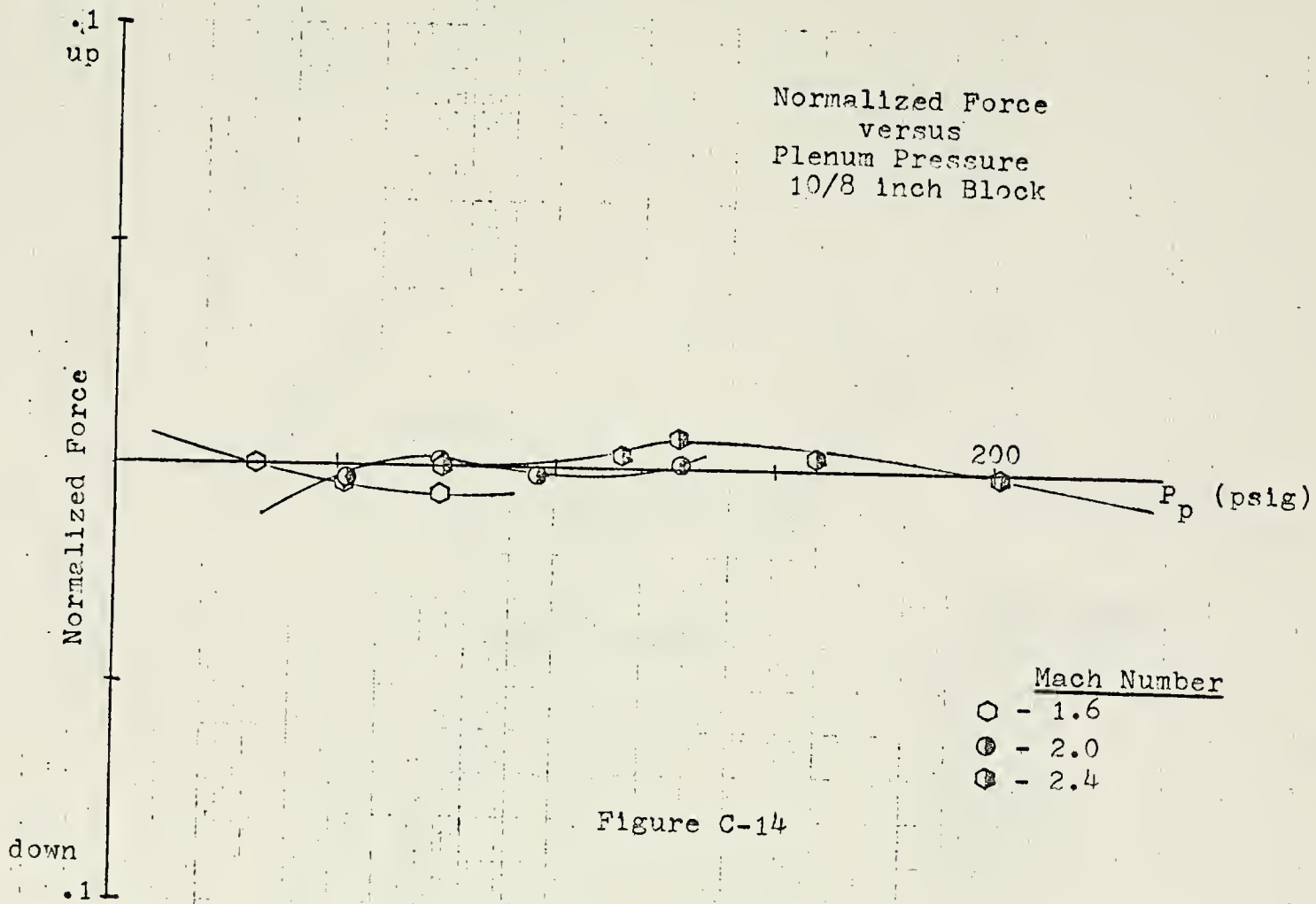
.1
up
Normalized Force
versus
Plenum Pressure
10/8 inch Block
Normalized Force
200
P_p (psig)
Mach Number
- 1.6
- 2.0
- 2.4
down
.1

Figure C-14

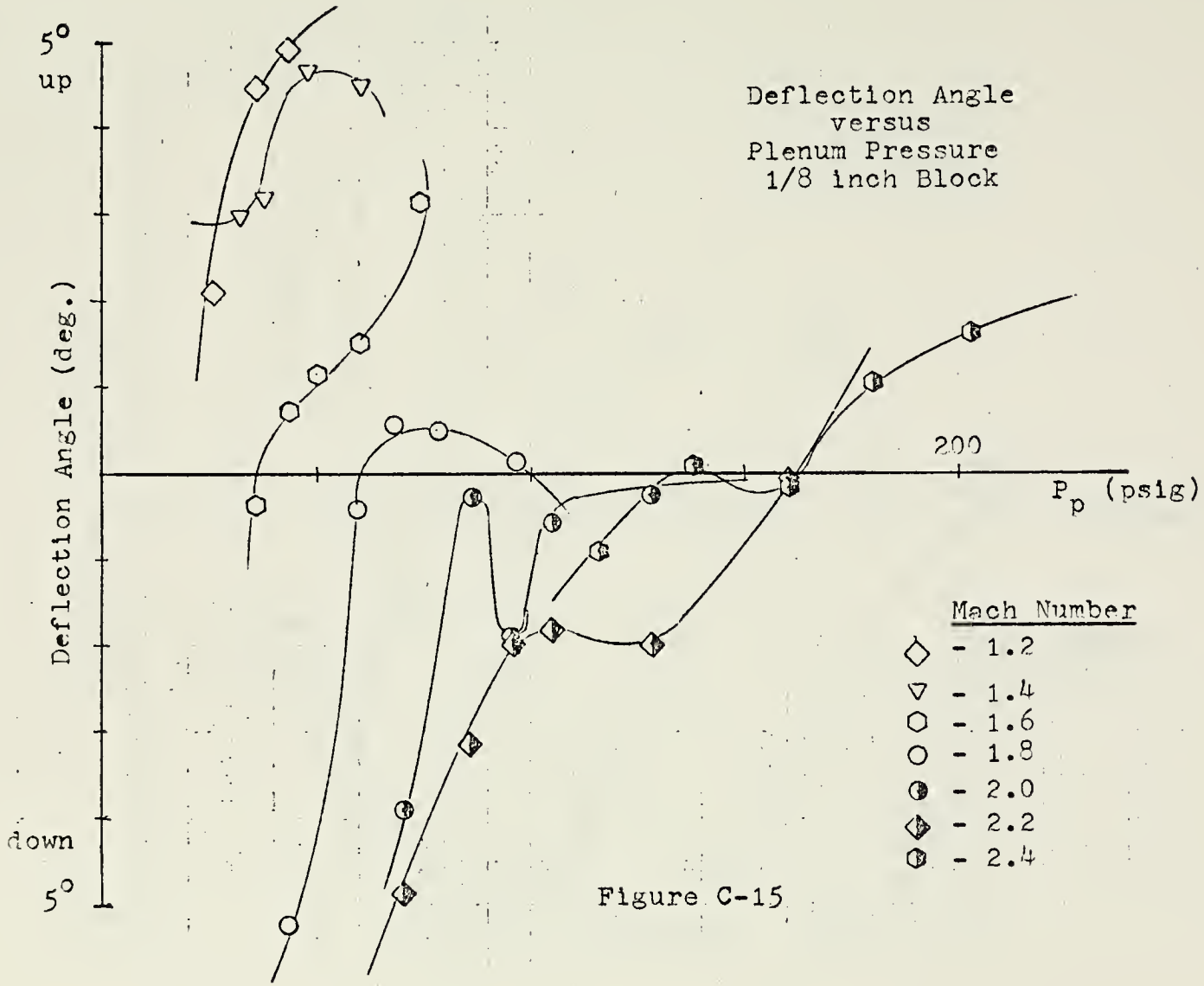
Deflection Angle
versus
Plenum Pressure
1/8 inch Block
5° up
Deflection Angle (deg.)
down 5°
200
P_p (psig)
Mach Number
- 1.2
- 1.4
- 1.6
- 1.8
- 2.0
- 2.2
- 2.4

Figure C-15

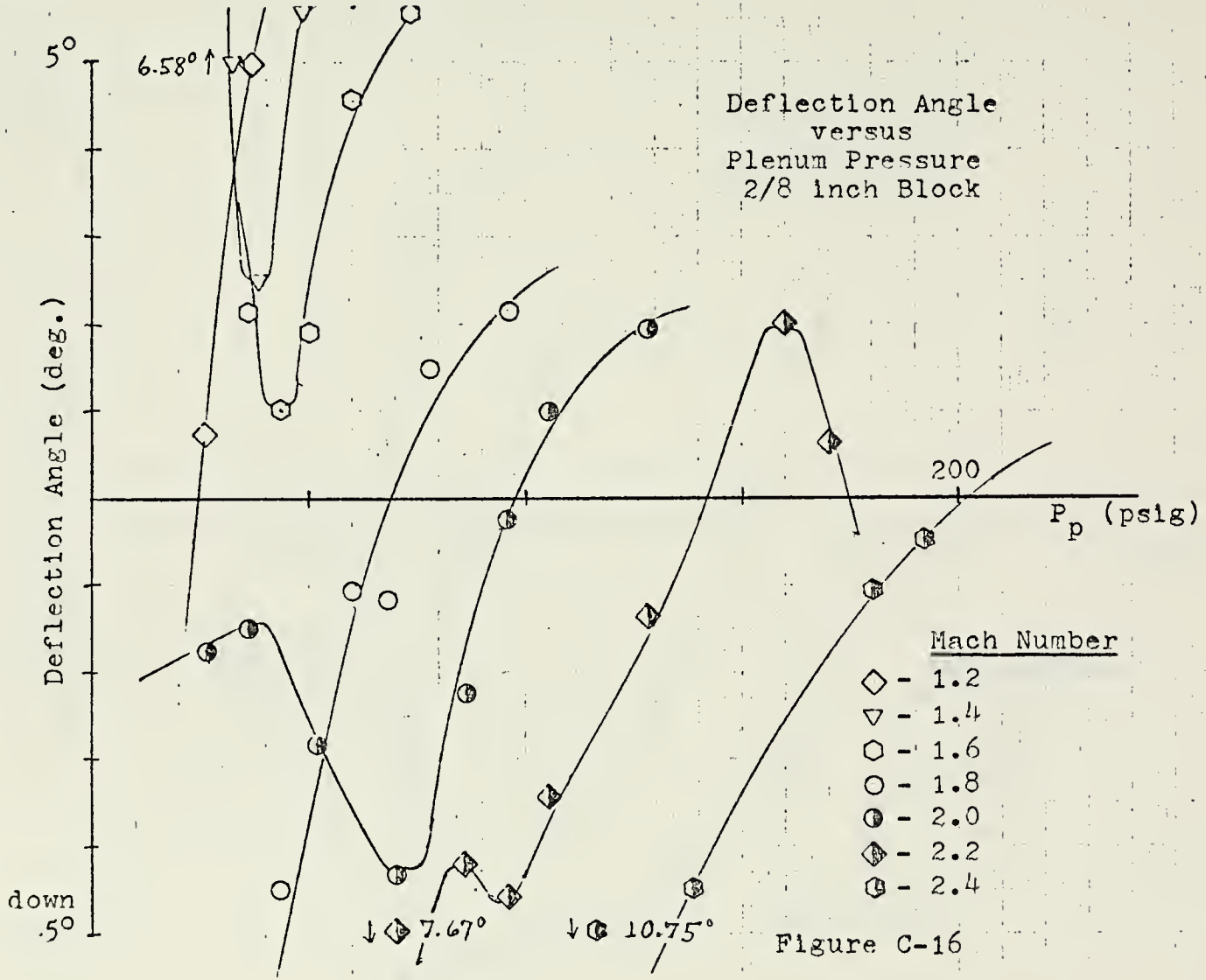
Deflection Angle
versus
Plenum Pressure
2/8 inch Block
5°
6.58°
Deflection Angle (deg.)
200
P_p (psig)
Mach Number
◇ - 1.2
▽ - 1.4
⬡ - 1.6
○ - 1.8
◐ - 2.0
◈ - 2.2
◍ - 2.4
down
.5°
7.67°
10.75°

Figure C-16

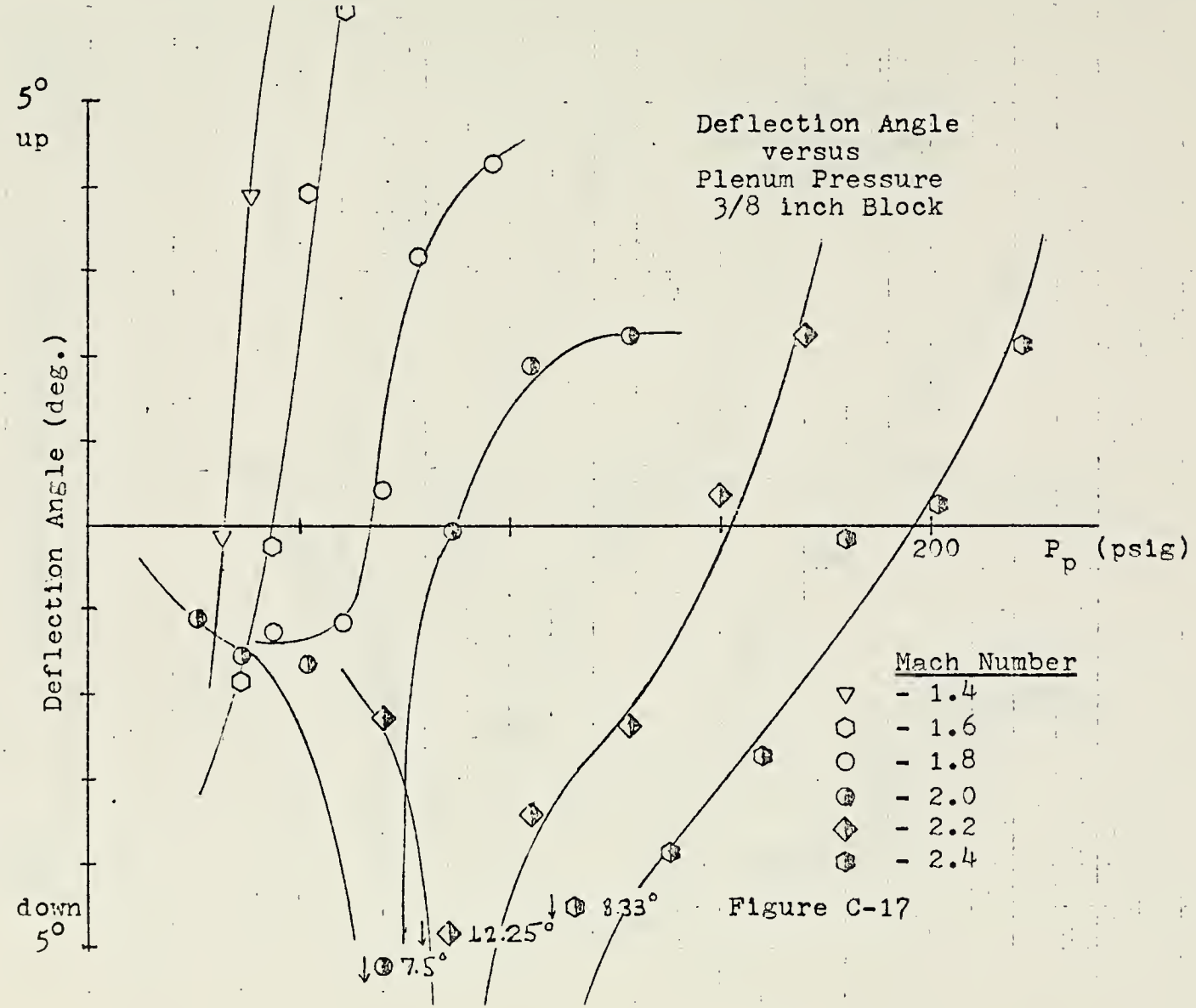
Deflection Angle
versus
Plenum Pressure
3/8 inch Block
5°
up
Deflection Angle (deg.)
down
5°
200
P_p (psig)
Mach Number
- 1.4
- 1.6
- 1.8
- 2.0
- 2.2
- 2.4
7.5°
12.25°
8.33°

Figure C-17

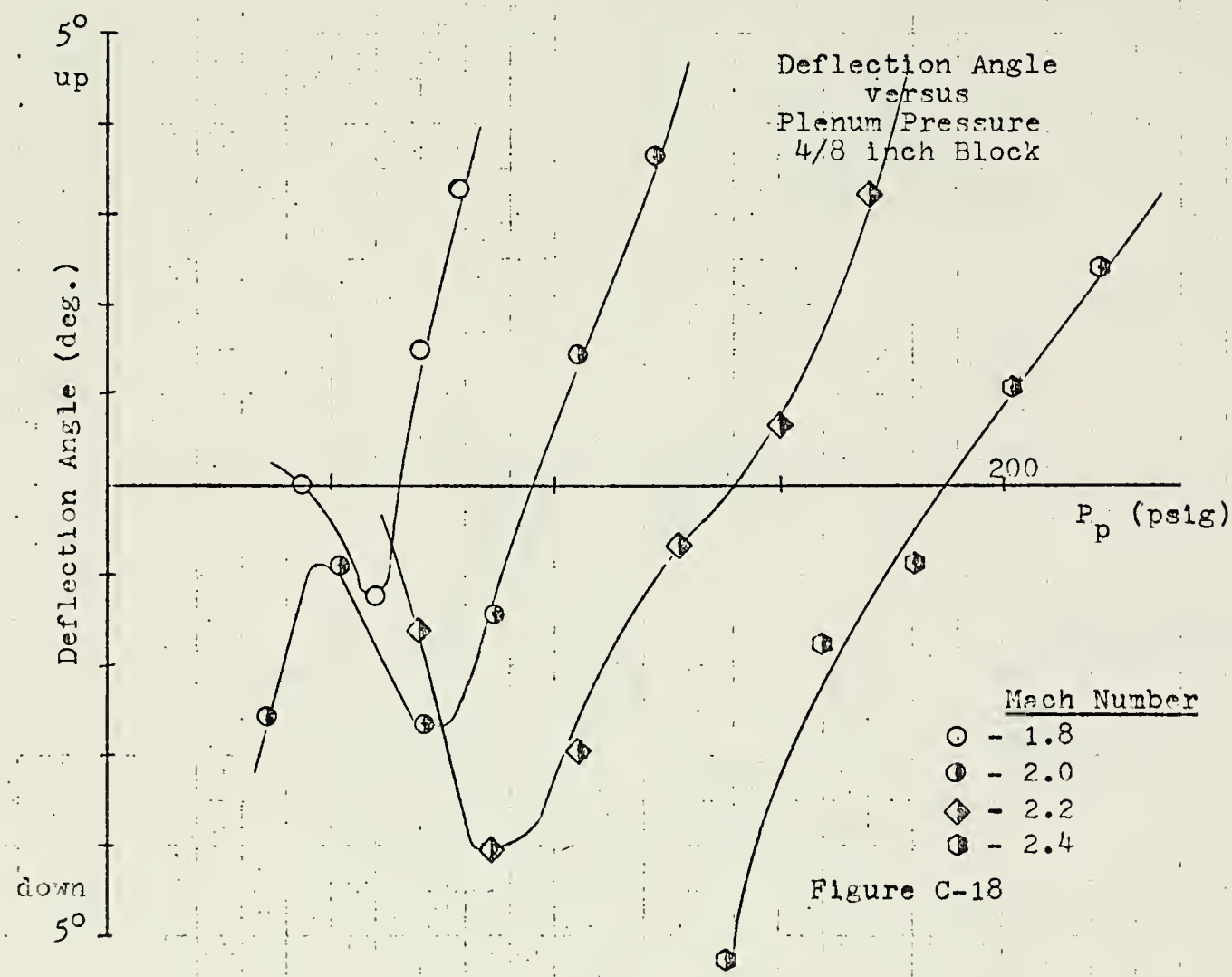
Deflection Angle
versus
Plenum Pressure
4/8 inch Block
5°
up
Deflection Angle (deg.)
down
5°
200
P_p (psig)
Mach Number
○ - 1.8
◑ - 2.0
◈ - 2.2
◑ - 2.4

Figure C-18

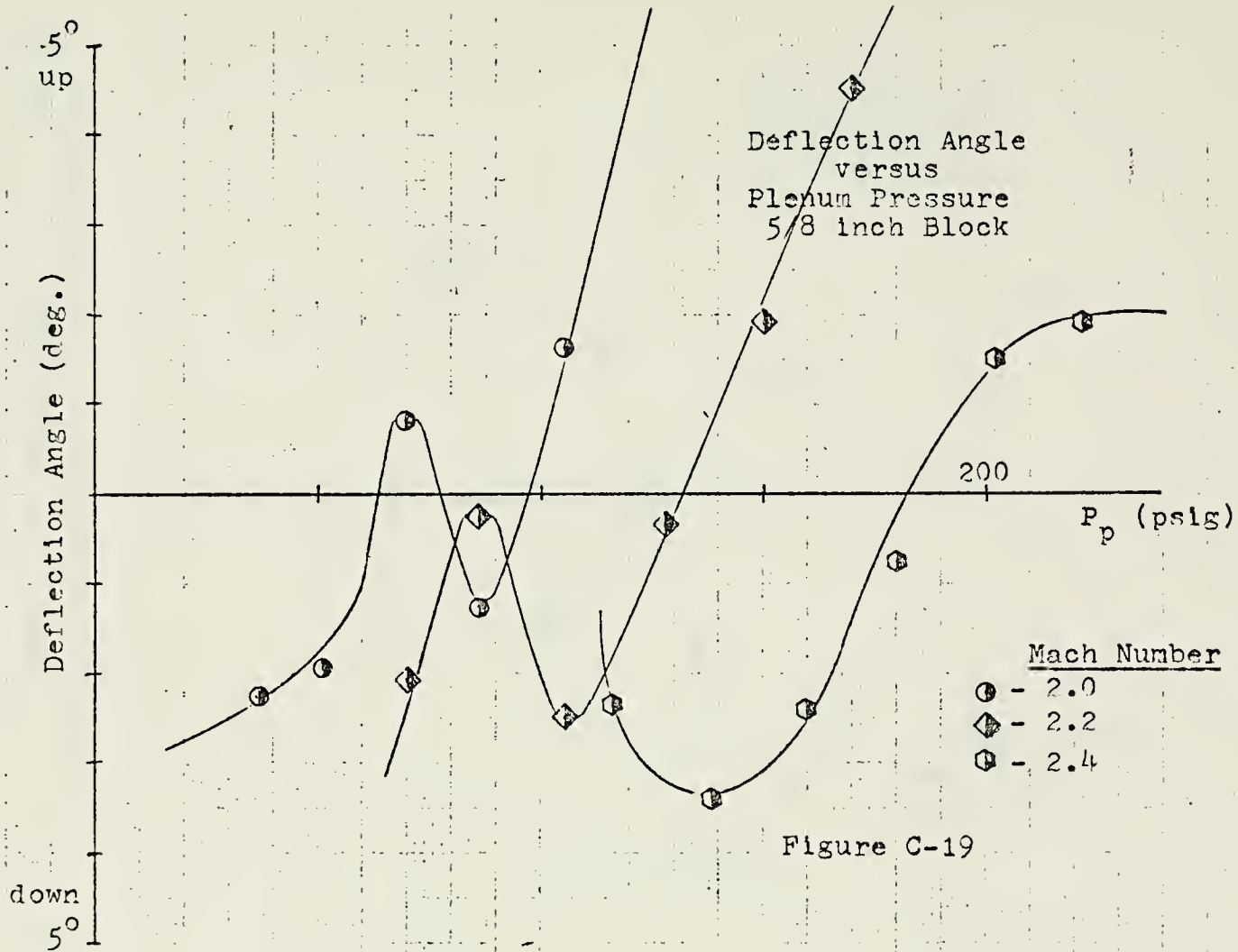
5°
up
Deflection Angle (deg.)
down
5°
Deflection Angle
versus
Plenum Pressure
5/8 inch Block
200
P_p (psig)
Mach Number
- 2.0
- 2.2
- 2.4

Figure C-19

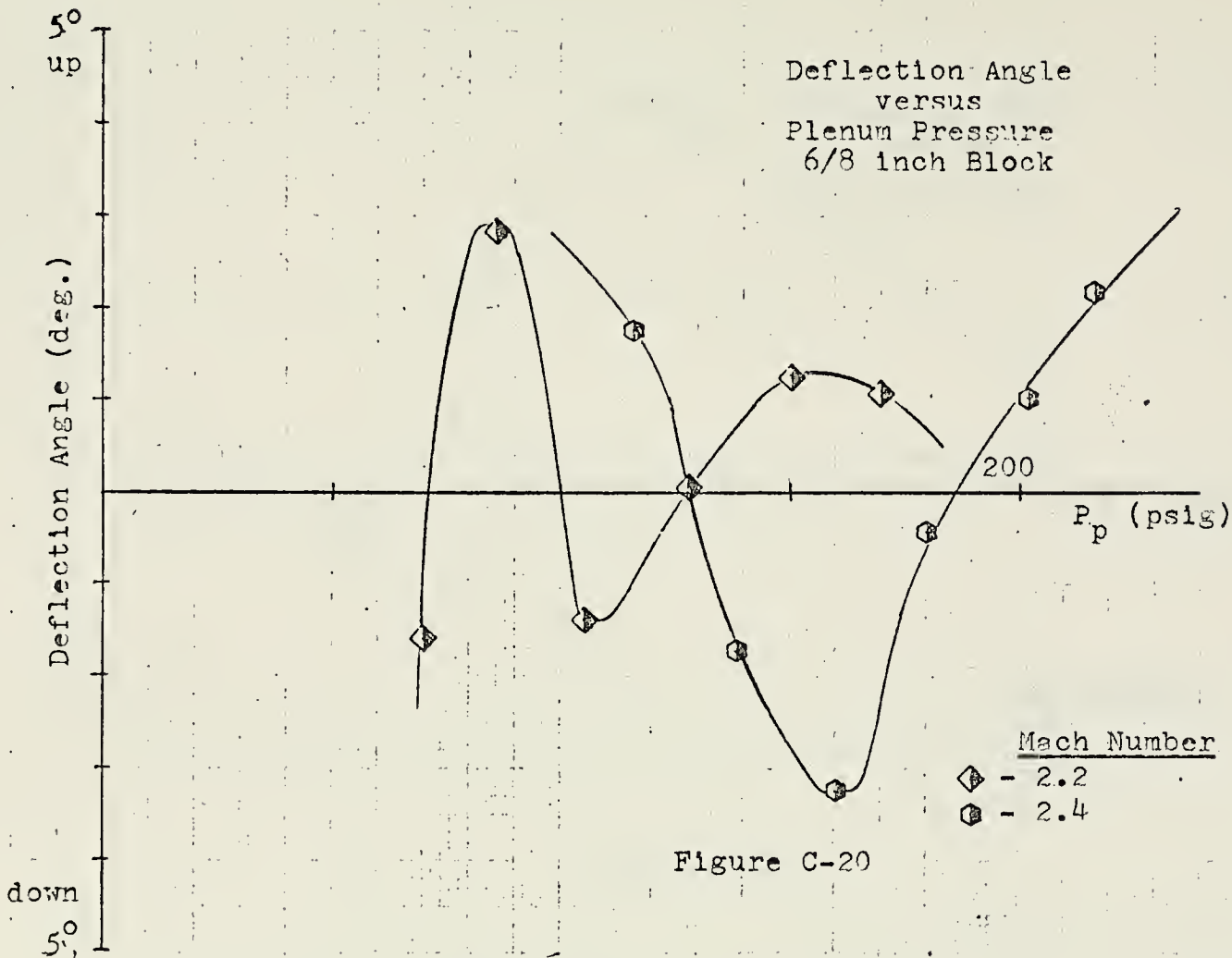
Deflection Angle
versus
Plenum Pressure
6/8 inch Block
5° up
down 5°
Deflection Angle (deg.)
200
P_p (psig)
Mach Number
- 2.2
- 2.4

Figure C-20

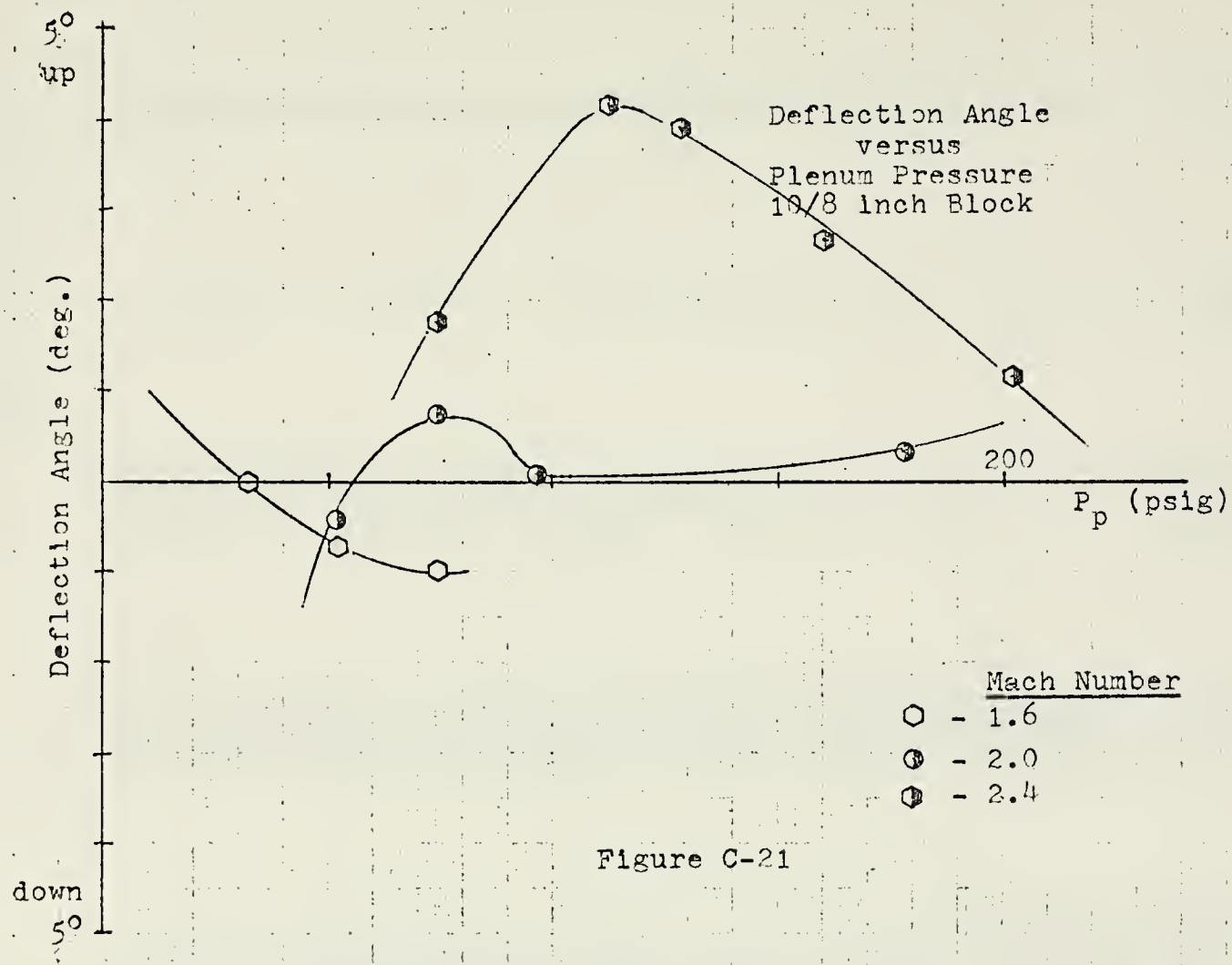
5°
up
Deflection Angle (deg.)
down
5°
Deflection Angle
versus
Plenum Pressure
10/8 inch Block
200
P_p (psig)
Mach Number
- 1.6
- 2.0
- 2.4

Figure C-21

APPENDIX D
DATA
1/8 INCH BLOCK

Run Number	Mach Number	Plenum Pressure (psig)	Defl. Force (lbs.)	Defl. Angle (Degrees)
14	1.2	26	.014u*	2.08u*
15	"	36	.041d	4.5u
16	"	43.5	.0719d	4.92u
18	1.4	32	.0045d	3.0u
19	"	38	.027d	3.17u
20	"	47.5	.0495d	4.67
21	"	60.5	.103d	4.5u
22	1.6	36	.032u	.42d
23	"	43.5	.023u	.75u
24	"	50	.0045d	1.17u
25	"	60.5	.027d	1.5u
26	"	74	.081d	3.17u
27	1.8	43.5	.0718u	5.25d
28	"	60.5	.058u	.42d
29	"	68	.041u	.58u
30	"	78	.009u	.5u
31	"	95.5	.027d	.16u
32	2.0	69.5	.107u	3.92d
33	"	86.5	.0718u	.25d
34	"	96	.0495u	1.92d
35	"	105.5	.032u	.58d
36	"	128	.009u	.25d
37	"	51.5	.121u	6.58d
40	2.2	69.5	.130u	4.92d
41	"	86.5	.112u	3.17d
42	"	96	.108u	2.0d
43	"	105.5	.098u	1.83d
44	"	128	.067u	2.0d
45	"	159.5	.032u	.08d
46	2.4	138	.045u	.08u
47	"	180.5	.009d	1.08u
48	"	203.7	.063d	1.67u
49	"	116.5	.067u	.92d
50	"	159.5	.009u	.16d

* 'u' - up, 'd' - down

2/8 INCH BLOCK

Run Number	Mach Number	Plenum Pressure (psig)	Defl. Force (lbs.)	Defl. Angle (Degrees)
52	1.2	26	.0045u	.75u
53	"	36	.087d	5.0u
54	"	43.5	.114d	6.5u
56a	1.4	32	.036d	6.58u
57a	"	38	.091d	2.5u
58a	"	48	.150d	5.66u
59a	"	60.5	.205d	5.75u
60a	1.6	43.5	0.0	1.0u
61a	"	36	0.0	2.08u
62a	"	50	.045d	1.92u
63a	"	60.5	.114d	4.6u
64a	"	74	.219d	5.58u
65	1.8	43.5	.087u	4.5d
66	"	60.5	.073u	1.08d
67	"	68	.032u	1.16d
68	"	78	.036d	1.5u
69	"	95.5	.114d	2.16u
70	2.0	26	.023u	1.75d
71	"	36	.046u	1.5d
72	"	51.5	.109u	3.83d
73	"	69.5	.146u	4.33d
74	"	86.5	.091u	2.25d
75	"	96	.046u	.25d
76	"	105.5	.019u	1.0u
77	"	128	.073d	1.92u
78	2.2	69.5	.173u	7.67d
79	"	86.5	.191u	4.16d
80	"	96	.178u	4.58d
81	"	105.5	.114u	3.42d
82	"	128	.091u	1.33d
83	"	159.5	.046u	2.0u
84	"	170	.032d	.67u
85	2.4	138	.205u	4.5d
86	"	180.5	.114u	1.08d
87	"	192.5	.1d	.5d
88	"	116.5	.237u	10.75d

3/8 INCH BLOCK

Run Number	Mach Number	Plenum Pressure (psig)	Defl. Force (lbs.)	Defl. Angle (Degrees)
89	2.4	116.5	.292u	8.33d
90	"	138	.256u	3.83d
91	"	159.5	.183u	2.75d
92	"	180.5	.114u	.17d
93	"	202	.05u	.25u
94	"	222	.068d	2.17u
95	2.2	69.5	.073u	2.25d
96	"	86.5	.228u	12.25d
97	"	105.5	.183u	3.42d
98	"	128	.1u	2.33d
99	"	149	.023u	.33u
100	"	170	.068d	2.25u
101	2.0	26	0.0	1.08d
102	"	36	.023u	1.58d
103	"	51.5	.05u	1.67d
104	"	69.5	.128u	7.5d
105	"	86.5	.082u	.08d
106	"	105.5	.009d	1.92u
107	"	128	.123d	2.25u
108	1.8	43.5	.036u	1.25d
109	"	60.5	.050u	1.17d
110	"	69.5	.018u	.42u
111	"	78	.077d	3.17u
112	"	95.5	.182d	4.25u
118	1.6	36	.023u	1.83d
119	"	43.5	.0045u	.25d
120	"	51.5	.059d	3.92u
121	"	60.5	.114d	6.08u
122	"	74	.273d	7.08u
123	1.4	32	.0045u	.17d
124	"	38	.055d	3.92u
125	"	51.5	.137d	7.75u
126	"	60.5	.209d	9.58u

4/8 INCH BLOCK

Run Number	Mach Number	Plenum Pressure (psig)	Defl. Force (lbs.)	Defl. Angle (Degrees)
127	1.8	43.5	.023u	0.0
128	"	60.5	.037u	1.25d
129	"	69.5	.0046d	1.5u
130	"	78	.078d	3.33u
131	"	95.5	.229d	6.75u
132	2.0	36	.023u	2.58d
133	"	51.5	.05u	.92d
134	"	69.5	.092u	2.67d
135	"	86.5	.05u	1.42d
136	"	105.5	.069d	1.42u
137	"	122.5	.202d	3.67u
138	2.2	69.5	.069u	1.58d
139	"	86.5	.138u	4.08d
140	"	105.5	.161u	2.92d
141	"	128	.064u	.67d
142	"	149	.046d	.67u
143	"	170	.169d	3.25u
144	2.4	116.5	.193u	6.75d
145	"	138	.252u	5.25d
146	"	159.5	.174u	1.75d
147	"	180.5	.1u	.83d
148	"	202	.009u	1.08u
149	"	222	.069d	2.42u

5/8 INCH BLOCK

Run Number	Mach Number	Plenum Pressure (psig)	Defl. Force (lbs.)	Defl. Angle (Degrees)
150	2.4	116.5	.102u	2.33d
151	"	138	.152u	3.42d
152	"	159.5	.152u	2.42d
153	"	180.5	.079u	.75d
154	"	202	.014d	1.5u
155	"	222	.111d	1.92u
156	2.2	69.5	.079u	2.08d
157	"	86.5	.042u	.25d
158	"	105.5	.102u	2.5d
159	"	128	.069u	.33d
160	"	149	.046d	1.92u
161	"	170	.208d	4.5u
162	2.0	36	.028u	2.25d
163	"	51.5	.069u	1.92d
164	"	69.5	.018u	.83u
165	"	86.5	.042u	1.33d
166	"	105.5	.042d	1.67u
167	"	128	.231d	6.17u

6/8 INCH BLOCK

Run Number	Mach Number	Plenum Pressure (psig)	Defl. Force (lbs.)	Defl. Angle (Degrees)
168	2.2	69.5	.088u	1.58d
169	"	86.5	.0047d	2.83u
170	"	105.5	.07u	1.42d
171	"	128	.056u	.08u
172	"	149	.033d	1.25u
173	"	170	.042d	1.08u
174.	2.4	116.5	.037u	1.75u
175	"	138	.112u	1.75d
176	"	159.5	.135u	3.25d
177	"	180.5	.093u	.42d
178	"	202	.0046d	1.0u
179	"	217	.07d	2.17u

10/8 INCH BLOCK

Run Number	Mach Number	Plenum Pressure (psig)	Defl. Force (lbs.)	Defl. Angle (Degrees)
180	2.4	74	.0048d	1.75u
181	"	116.5	.048d	4.17u
182	"	159.5	.048d	2.67u
183	"	202	.014u	1.17u
183a	"	128	.11d	3.92u
184	2.0	51.5	.033u	.42d
185	"	74	.029d	.75u
186	"	95.5	.024u	.08u
187	"	128	.0048d	.33u
188	1.6	32	0.0	0.0
189	"	51.5	.048u	.75d
190	"	74	.091u	1.0u

APPENDIX E

PHOTOGRAPHIC RESULTS

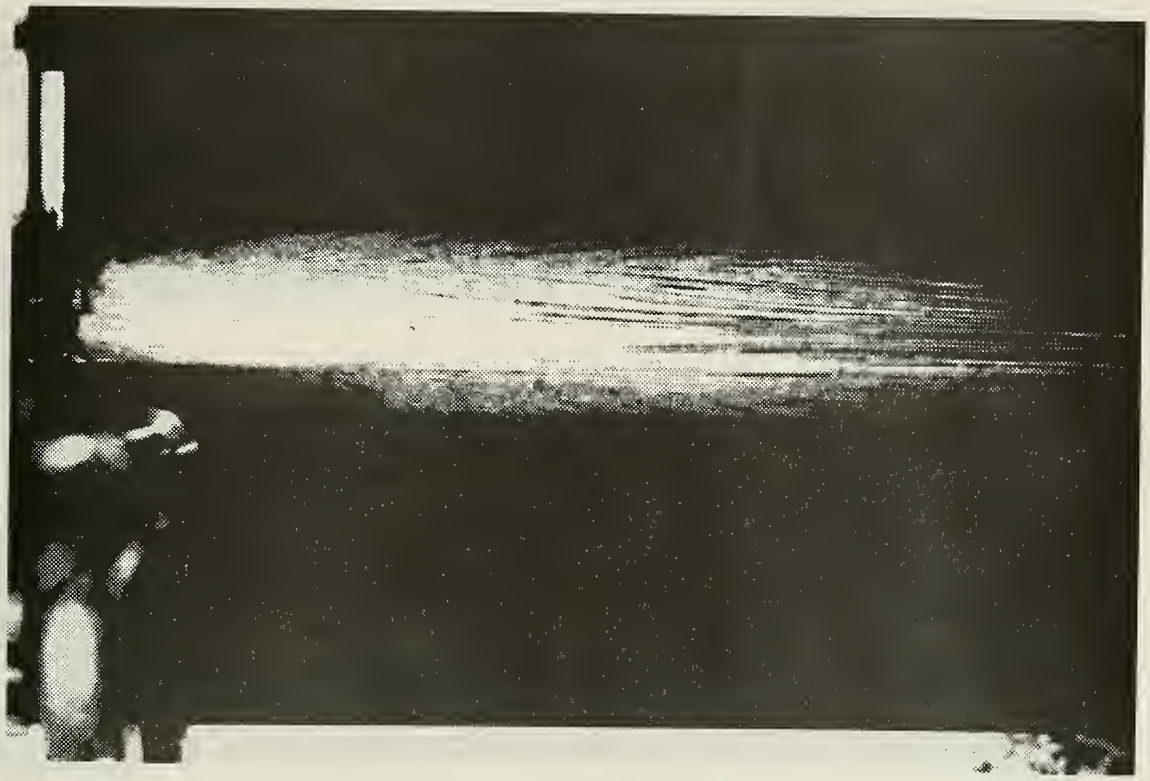

Figure 1, Mach 2.0, 3/8", 26 psig, 0.0 lbs., 1.08° up

Figure 2, Mach 2.0, 3/8", 36 psig, .023 lbs. up, 1.58° dn

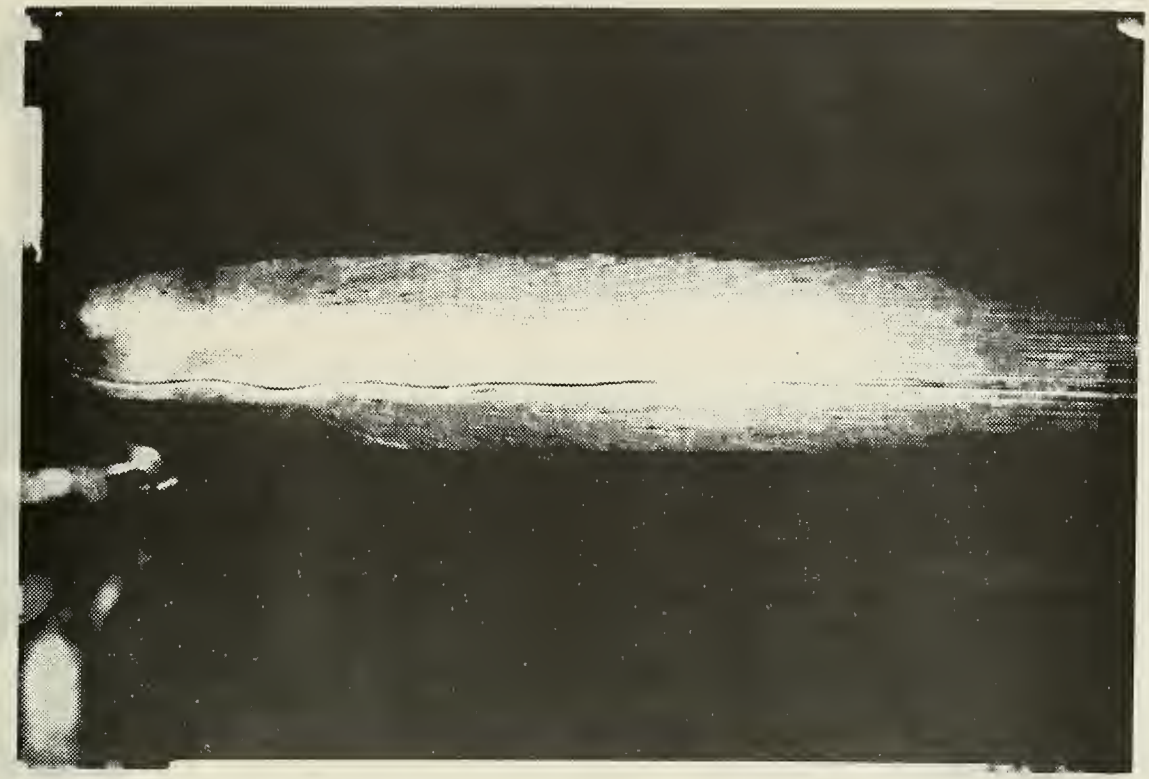

Figure 3, Mach 2.0, 3/8", 51 psig, .05 lbs. up, 1.67° dn

Figure 4, Mach 2.0, 3/8", 69 psig, .128 lbs. up, 7.5° dn

Figure 5, Mach 2.0, 3/8", 86 psig, .082 lbs. up, .08° dn

Figure 6, Mach 2.0, 3/8", 105 psig, .009 lbs. dn, 1.92° up

Figure 7, Mach 2.0, 3/8", 128 psig, .123 lbs. dn, 2.25° up

Figure 8, Mach 2.2, 3/8", 69 psig, .073 lbs. up, 2.25° dn

Figure 9, Mach 2.2, 3/8", 86 psig, .228 lbs. up, 12.25° dn

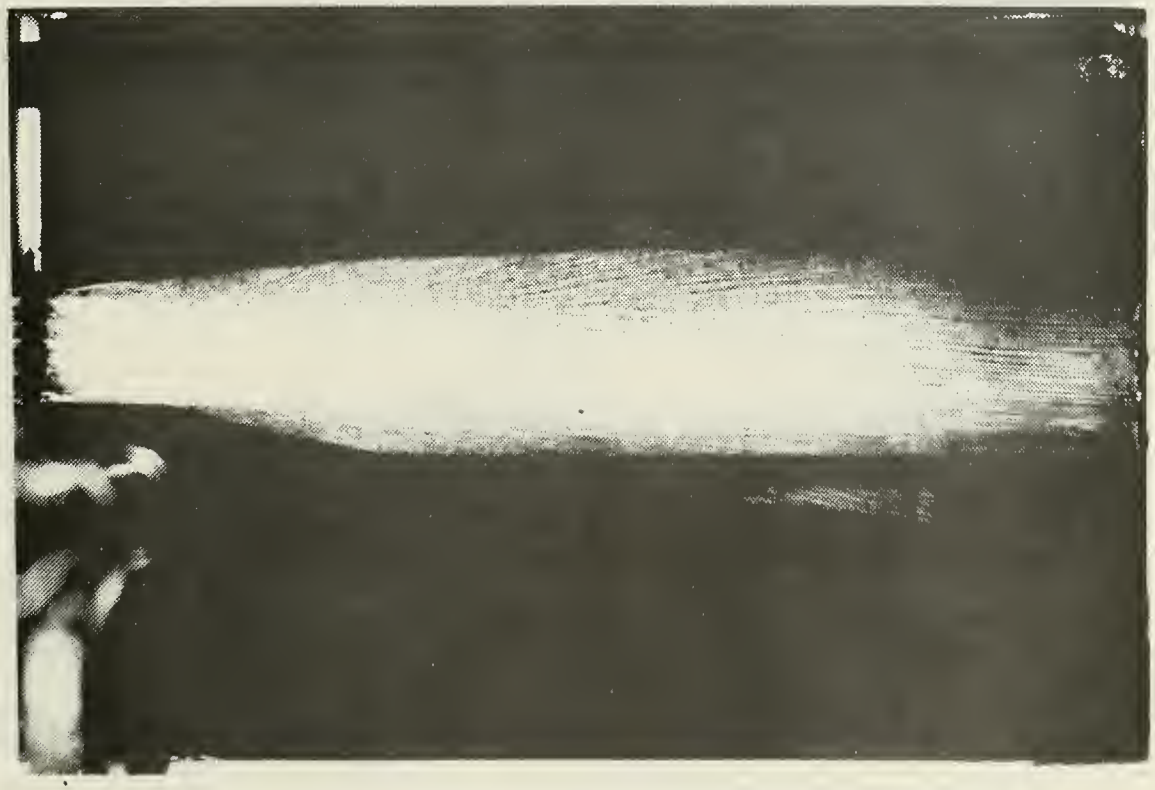

Figure 10, Mach 2.2, 3/8", 105 psig, .183 lbs. up, 3.42° dn

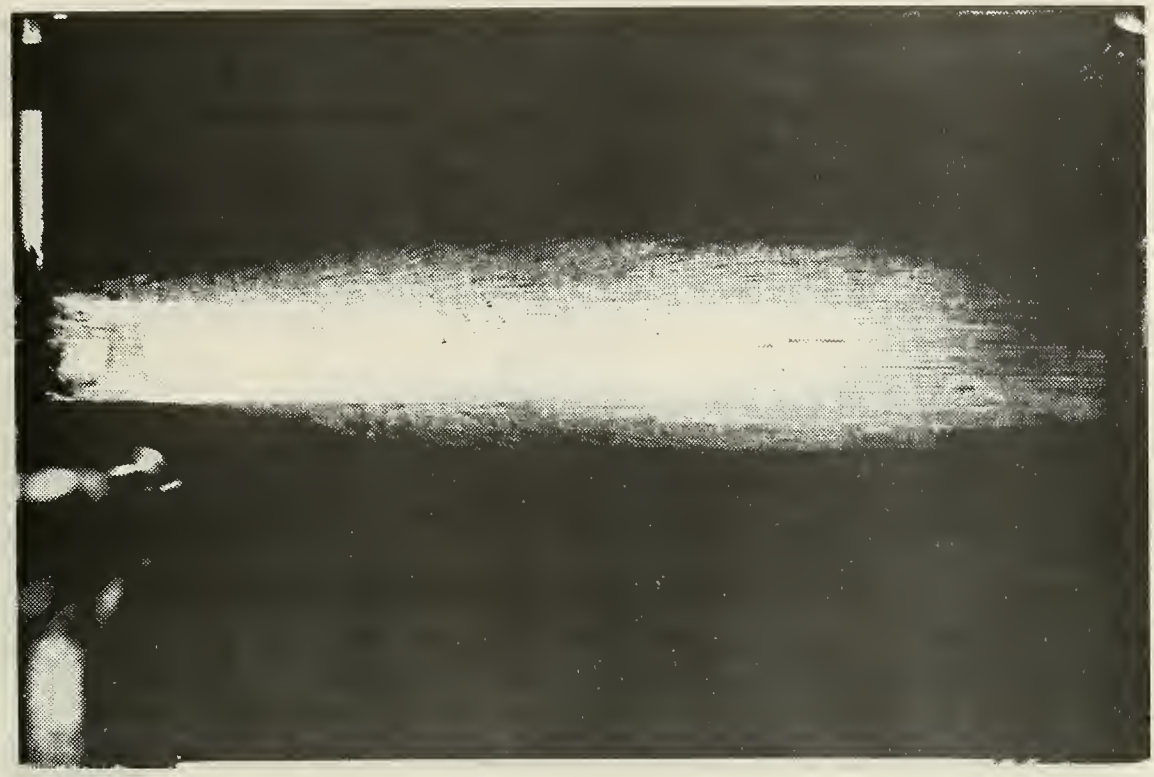

Figure 11, Mach 2.2, 3/8", 128 psig, .1 lbs. up, 2.33° dn

Figure 12, Mach 2.2, 3/8", 149 psig, .023 lbs up, .33° up

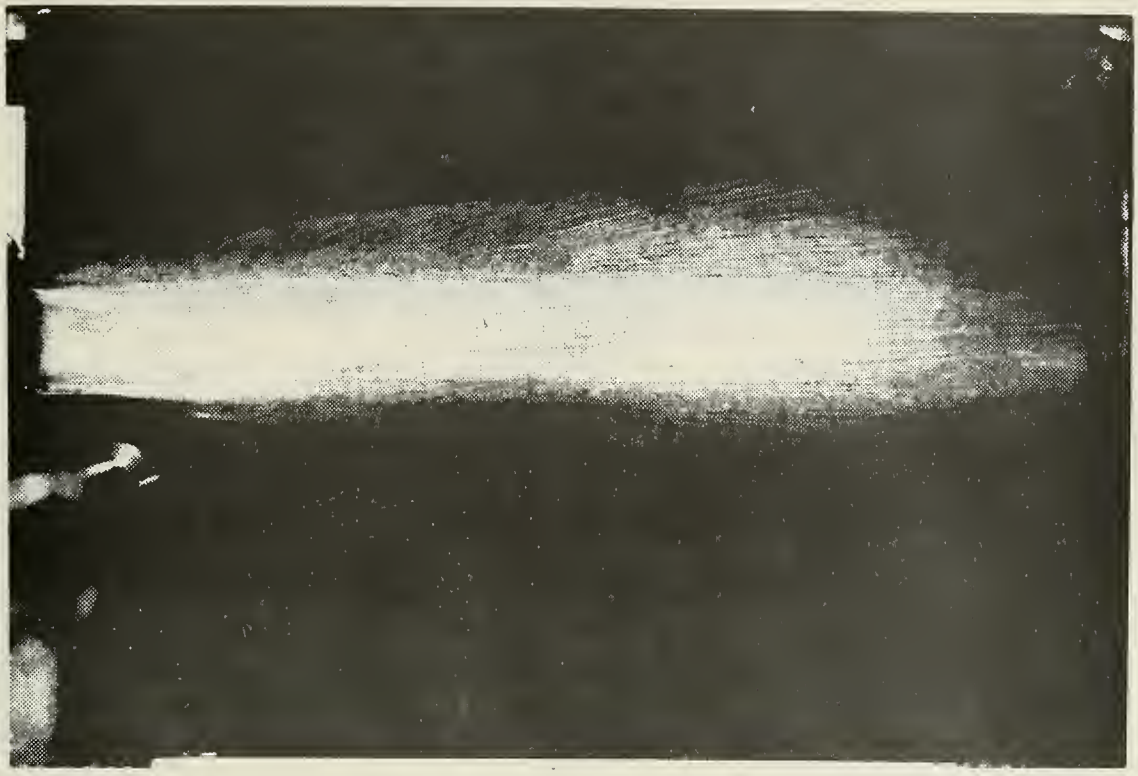

Figure 13, Mach 2.2, 3/8", 170 psig, .068 lbs. dn, 2.25° up

Figure 14, Mach 2.4, 3/8", 116 psig, .292 lbs. up, 8.33° dn

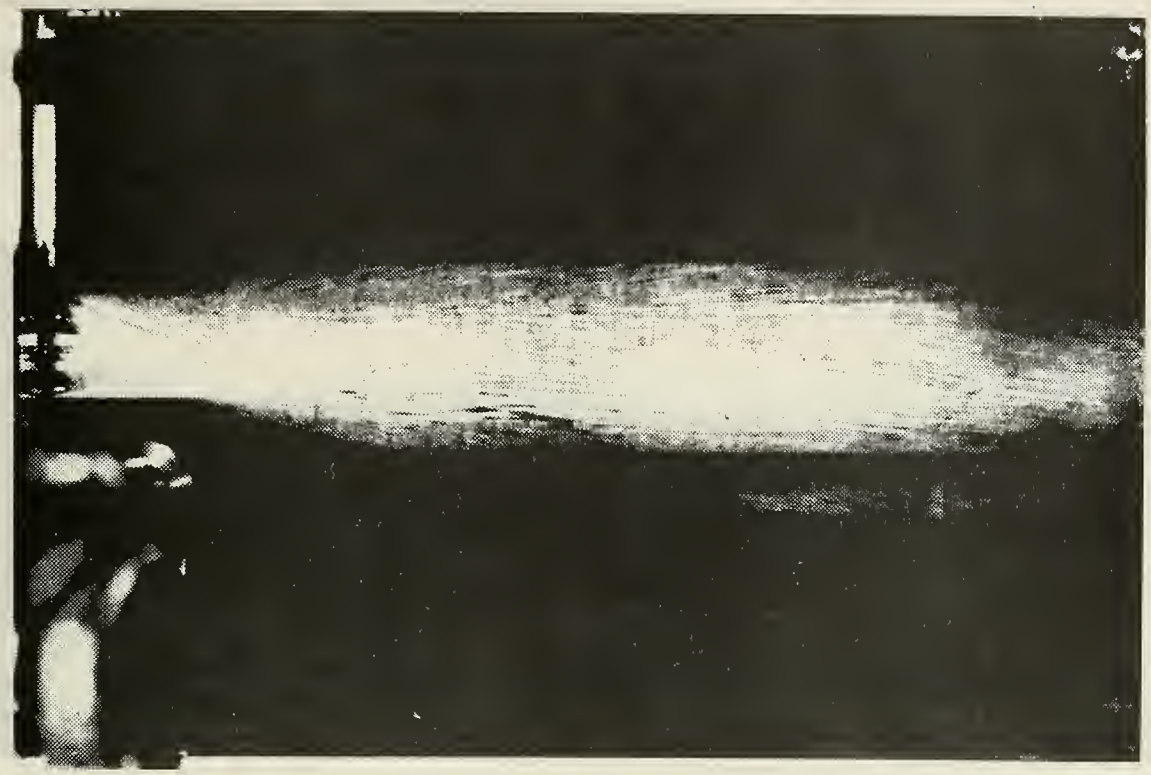

Figure 15, Mach 2.4, 3/8", 138 psig, .256 lbs. up, 3.83° dn

Figure 16, Mach 2.4, 3/8", 159 psig, .183 lbs. up, 2.8° dn

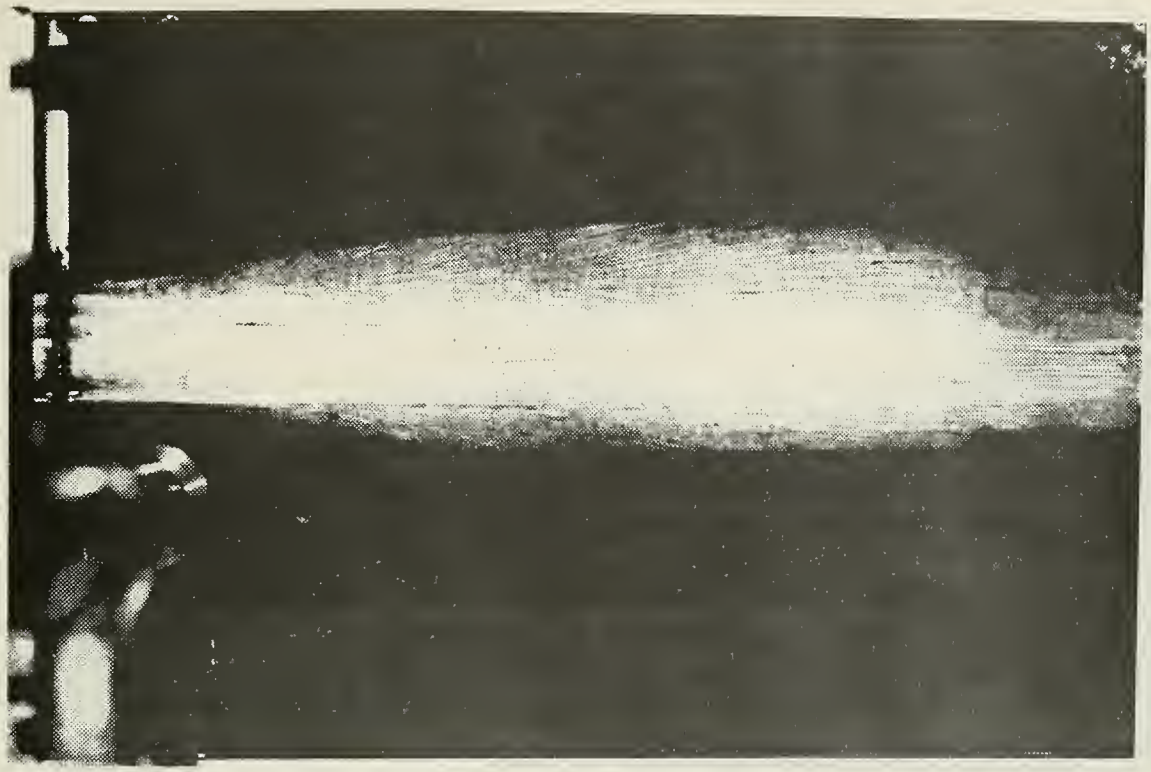

Figure 17, Mach 2.4, 3/8", 180 psig, .114 lbs. up, .17° dn

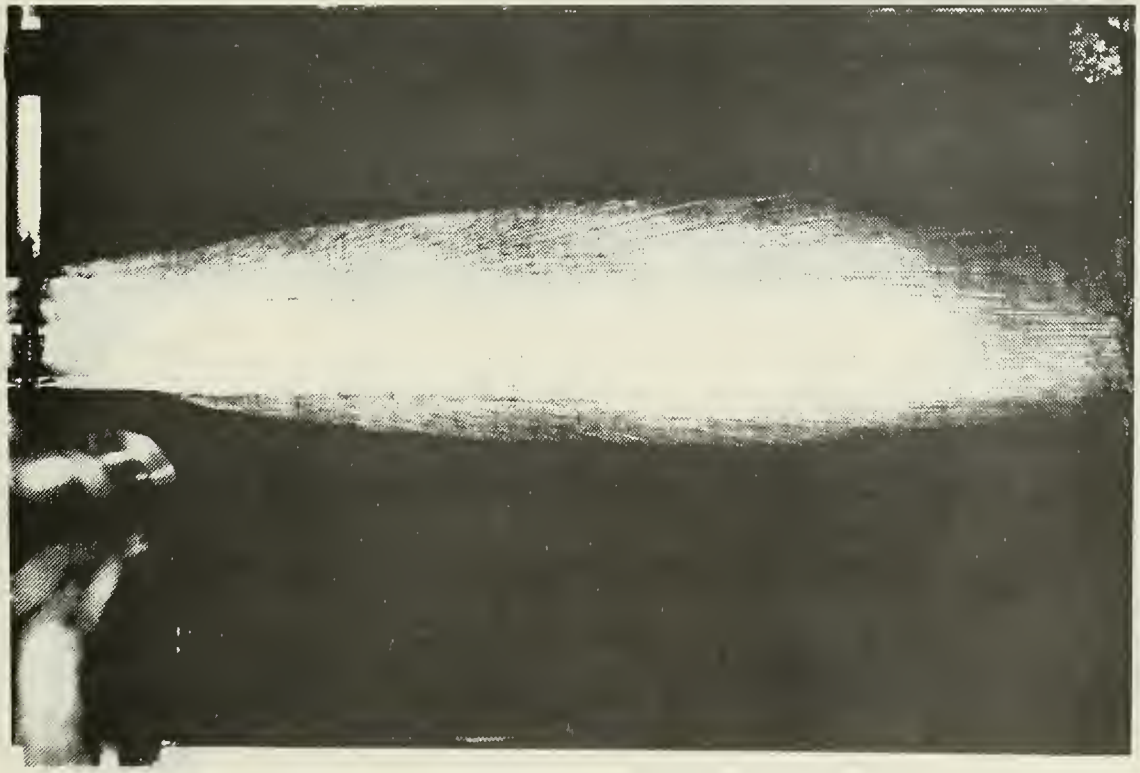

Figure 18, Mach 2.4, 3/8", 202 psig, .05 lbs. up, .25° up

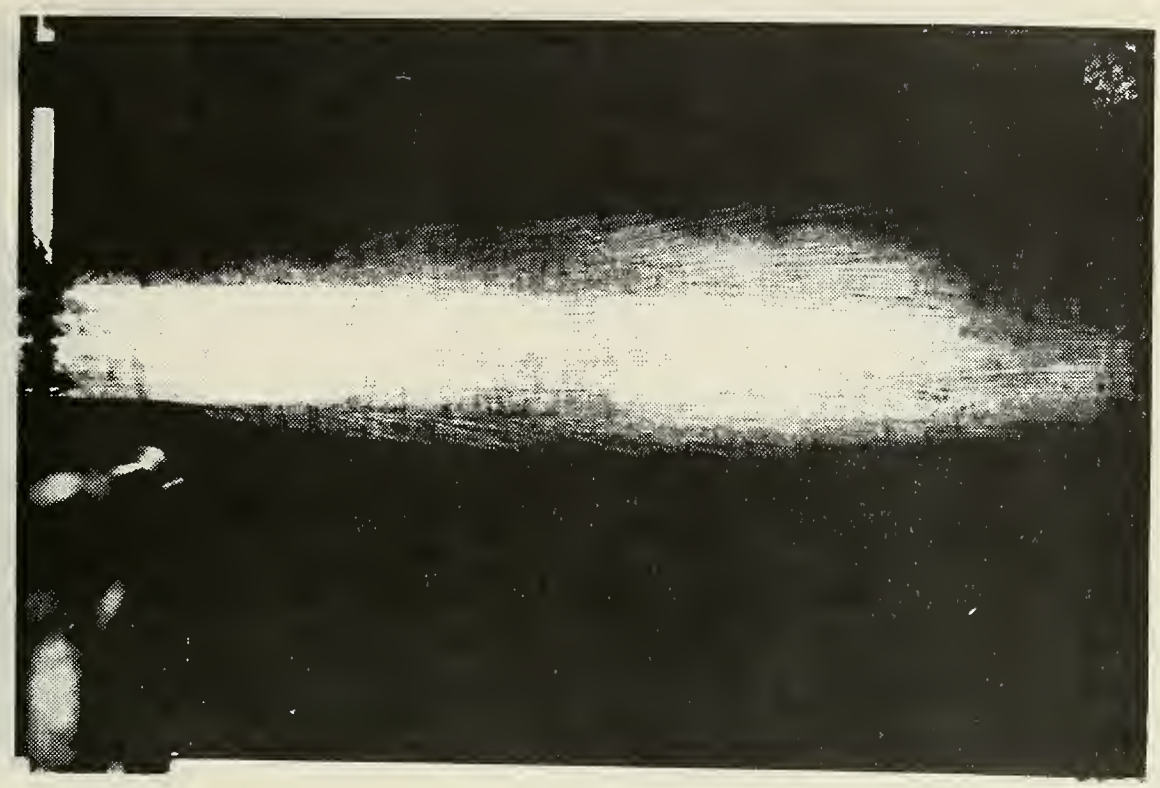

Figure 19, Mach 2.4, 3/8", 222 psig, .068 lbs. dn, 2.2° up

Figure 20, Mach 2.0, 1/2", 43 psig, .023 lbs. up, 0.0°

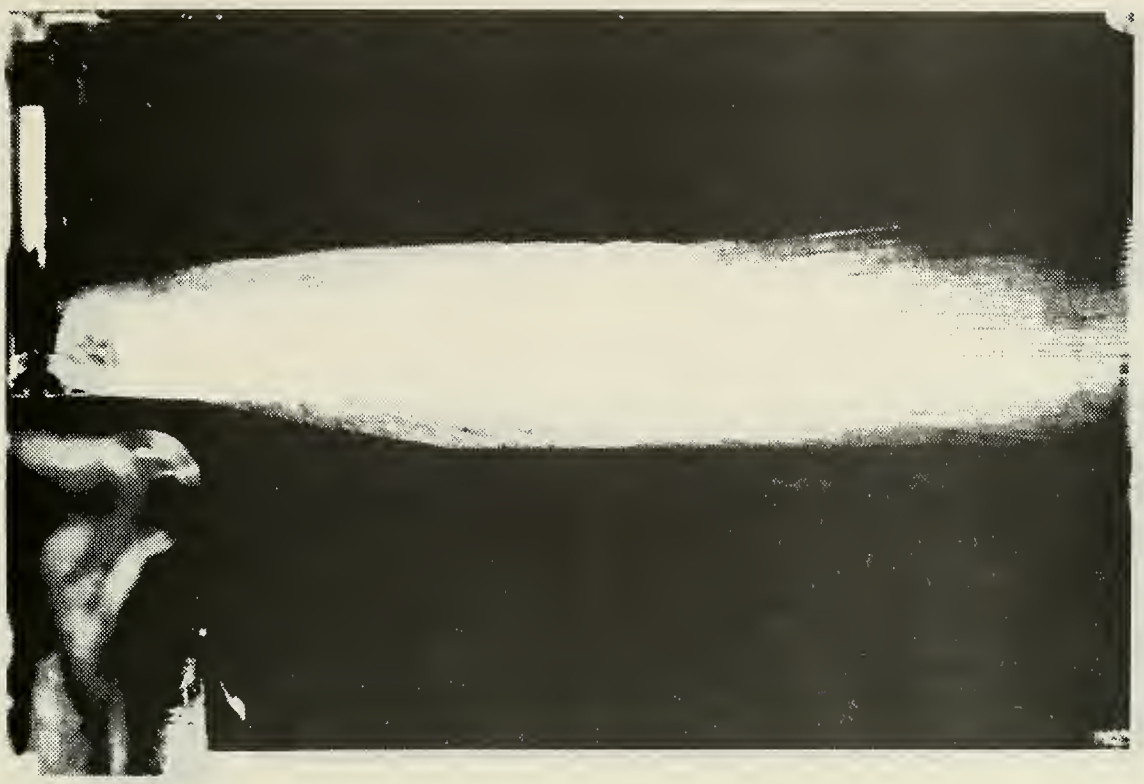

Figure 21, Mach 2.0, 1/2", 51 psig, .05 lbs. up, .92° dn

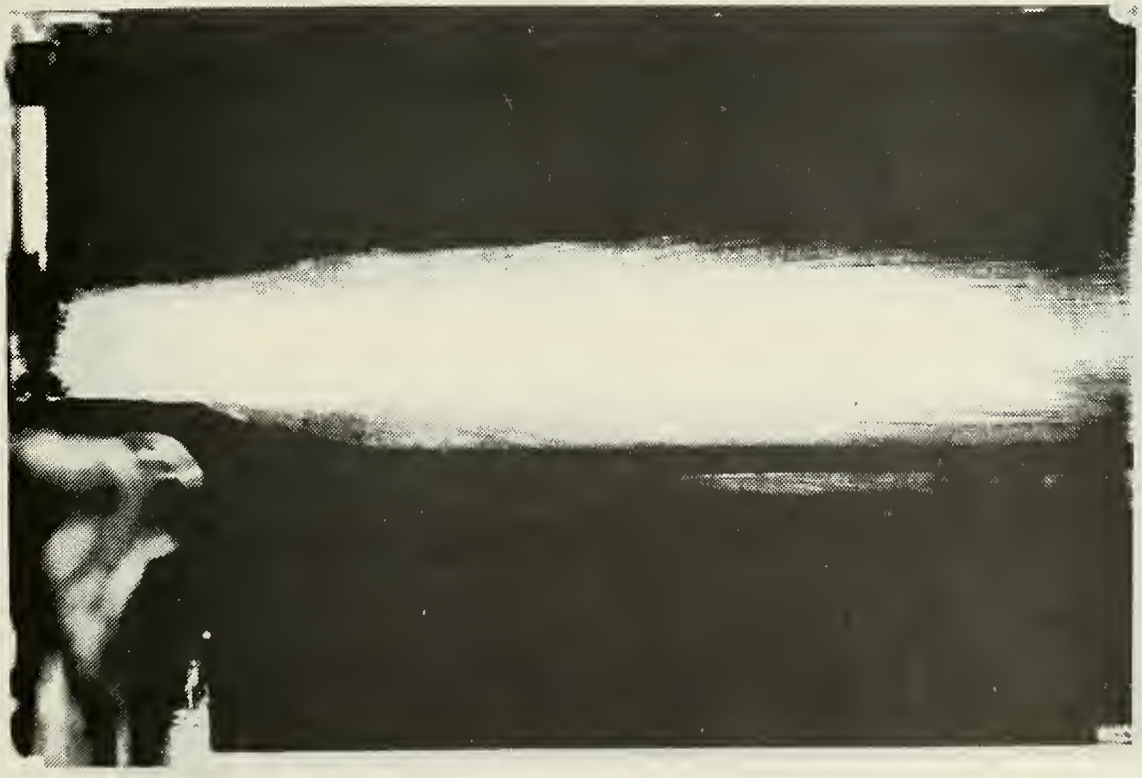

Figure 22, Mach 2.0, 1/2", 69 psig, .092 lbs. up, 2.7° dn

Figure 23, Mach 2.0, 1/2", 86 psig, .05 lbs. up, 1.42° dn

Figure 24, Mach 2.0, 1/2", 105 psig, .069 lbs. dn, 1.42° dn

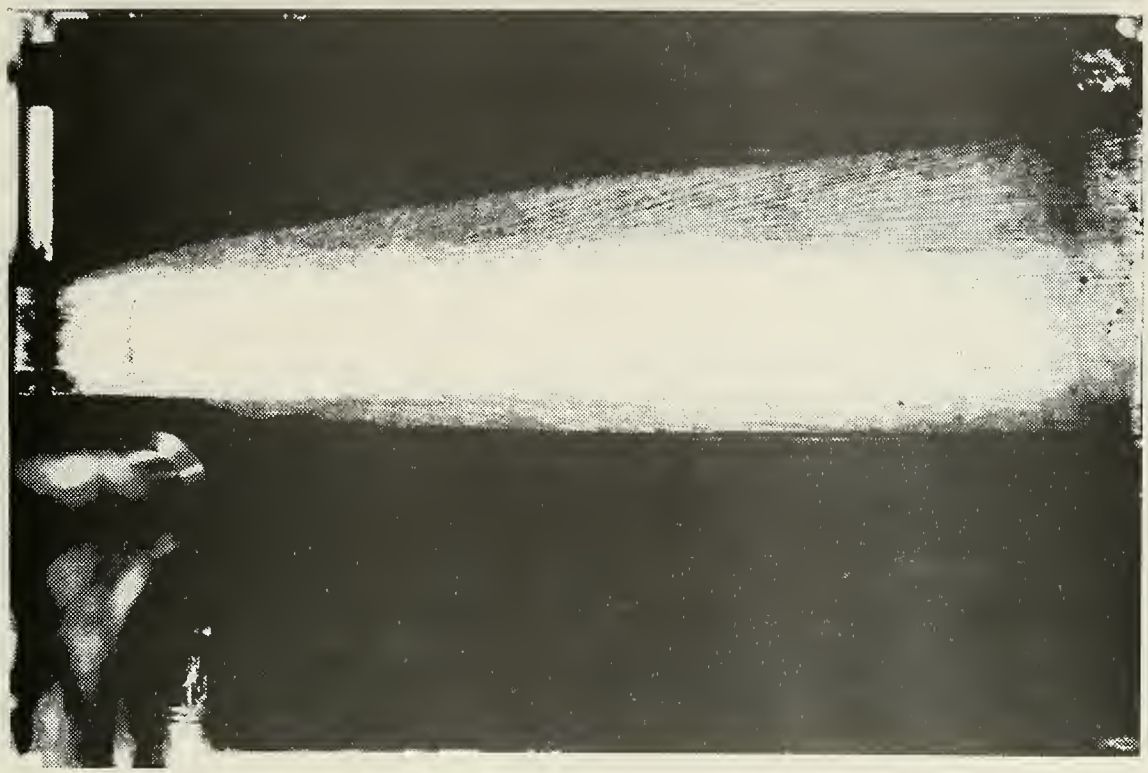

Figure 25, Mach 2.0, 1/2", 122 psig, .202 lbs. dn, 3.67° up

Figure 26, Mach 2.2, 1/2", 69 psig, .069 lbs. up, 1.58° dn

Figure 27, Mach 2.2, 1/2", 86 psig, .138 lbs. up, 4.08° dn

Figure 28, Mach 2.2, 1/2", 105 psig, .161 lbs. up, 2.92° dn

Figure 29, Mach 2.2, 1/2", 128 psig, .064 lbs. up, .67° dn

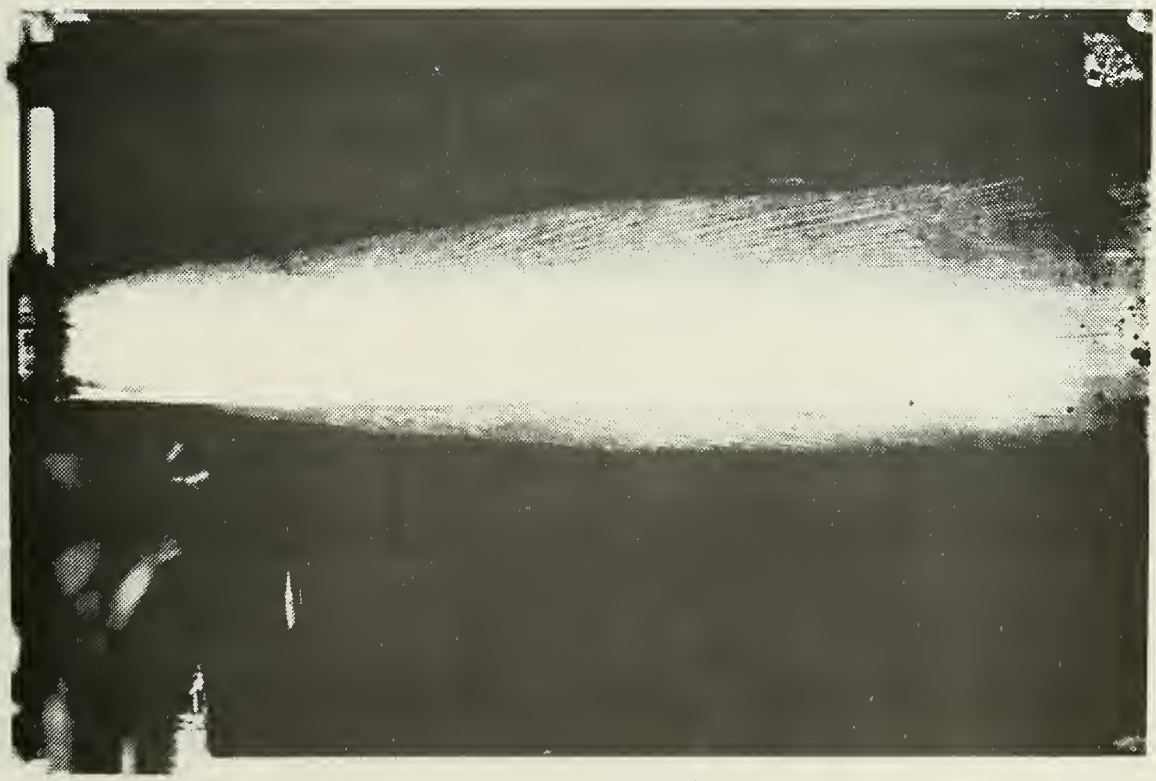

Figure 30, Mach 2.2, 1/2", 149 psig, .049 lbs. dn, .67° up

Figure 31, Mach 2.2, 1/2", 170 psig, .169 lbs. dn, 3.25° up

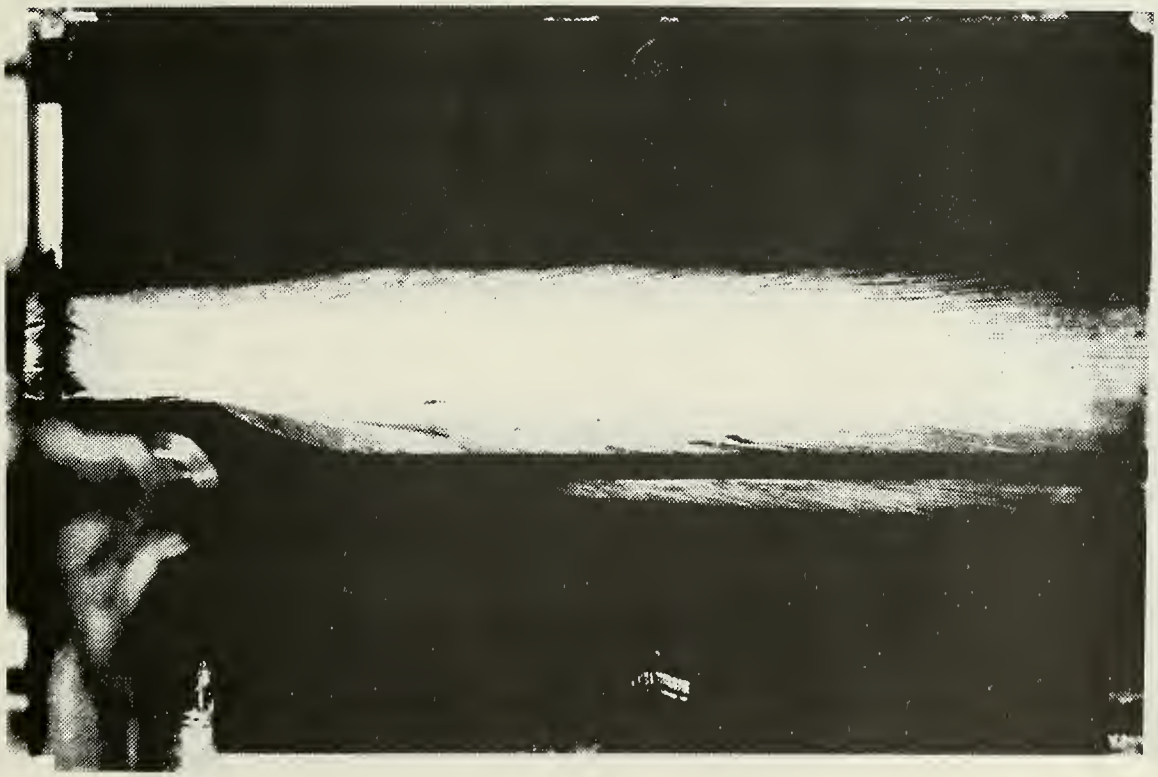

Figure 32, Mach 2.4, 1/2", 116 psig, .193 lbs. up, 6.75° dn

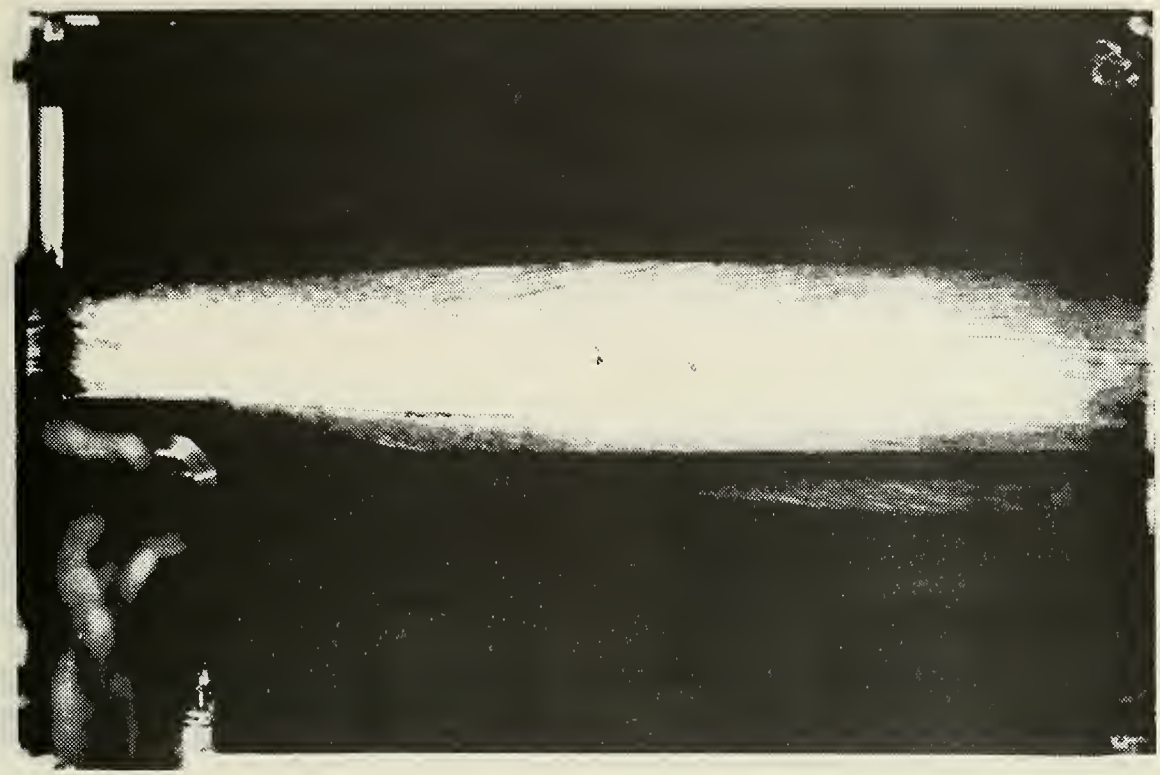

Figure 33, Mach 2.4, 1/2", 138 psig, .252 lbs. up, 5.3° dn

Figure 34, Mach 2.4, 1/2", 159 psig, .174 lbs. up, 1.75° dn

Figure 35, Mach 2.4, 1/2", 180 psig, .1 lbs. up, .83° dn

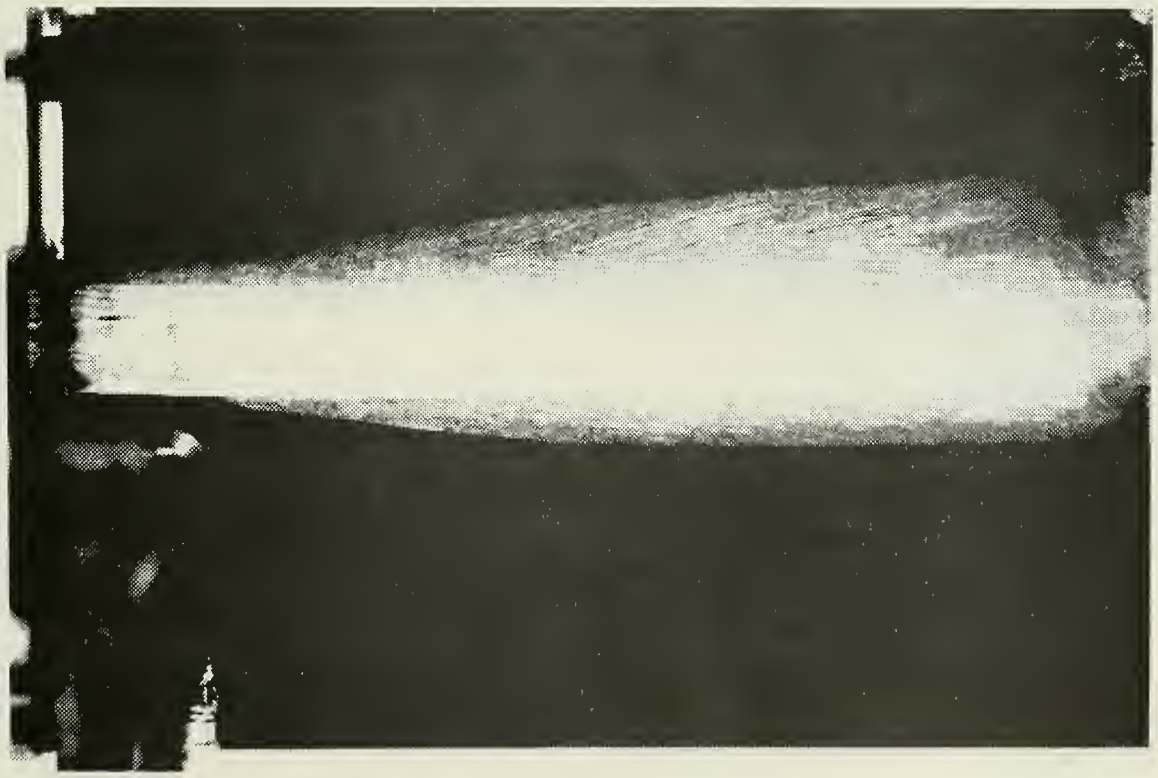

Figure 36, Mach 2.4, 1/2", 202 psig, .009 lbs. up, 1.08° up

Figure 37, Mach 2.4, 1/2", 222 psig, .069 lbs. dn, 2.42° up

Figure 38, Mach 2.0, 5/8", 36 psig, .028 lbs. up, 2.25° dn

Figure 39, Mach 2.0, 5/8", 51 psig, .069 lbs. up, 1.92° dn

Figure 40, Mach 2.0, 5/8", 69 psig, .018 lbs. up, .83° up

Figure 41, Mach 2.0, 5/8", 86 psig, .042 lbs. up, 1.33° dn

Figure 42, Mach 2.0, 5/8", 105 psig, .042 lbs. dn, 1.67° up

Figure 43, Mach 2.0, 5/8", 128 psig, .231 lbs. dn, 6.17° up

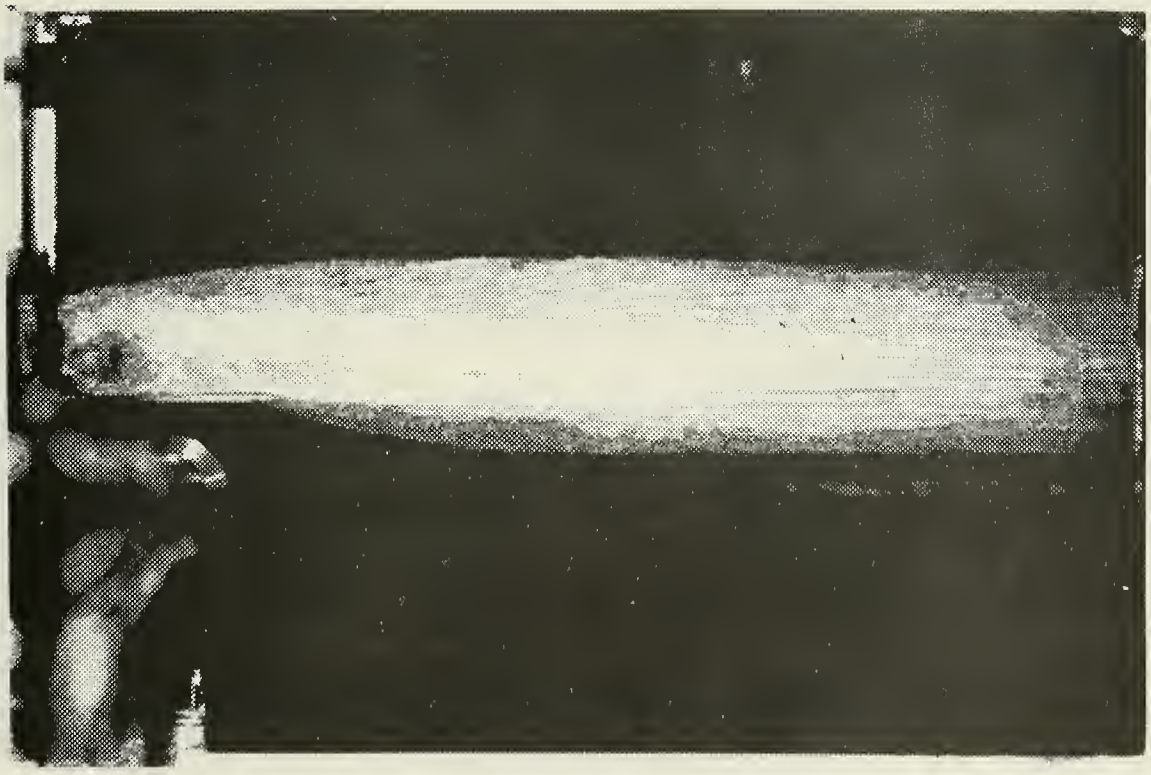

Figure 44, Mach 2.2, 5/8", 69 psig, .079 lbs. up, 2.08° dn

Figure 45, Mach 2.2, 5/8", 86 psig, .042 lbs. up, .25° dn

Figure 46, Mach 2.2, 5/8", 105 psig, .102 lbs. up, 2.5° dn

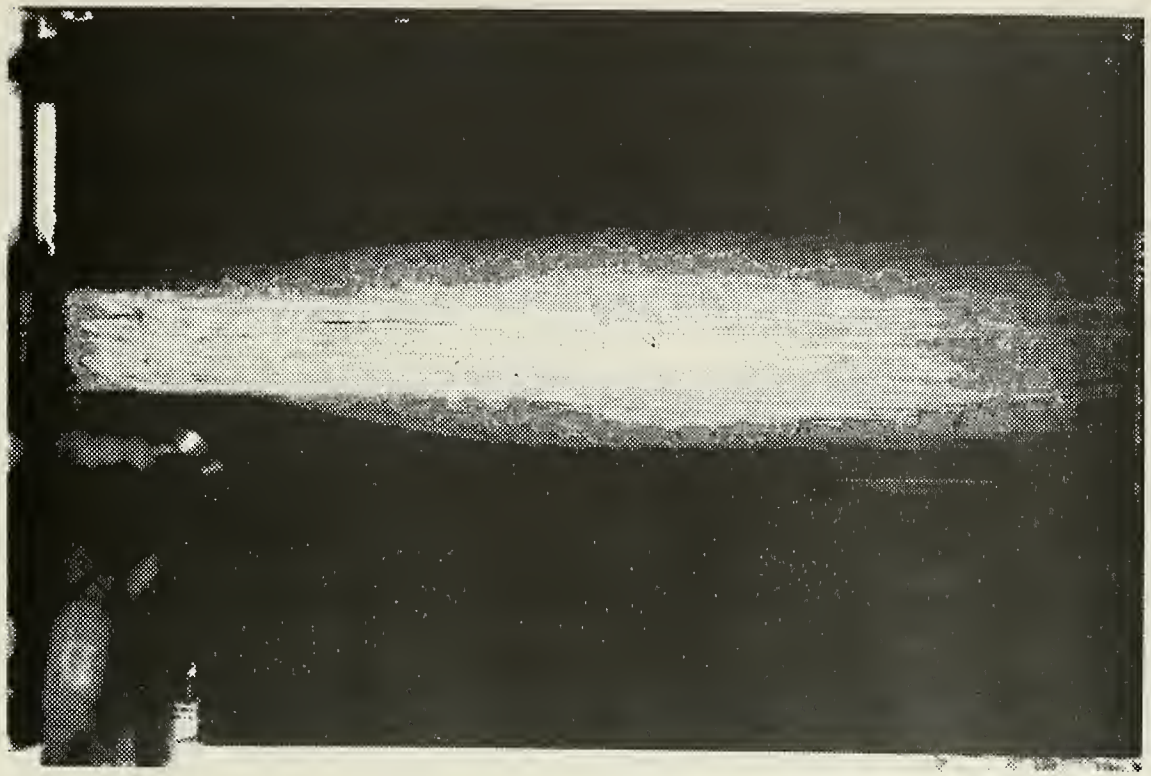

Figure 47, Mach 2.2, 5/8", 128 psig, .069 lbs. up, .33° dn

Figure 48, Mach 2.2, 5/8", 149 psig, .046 lbs. dn, 1.92° up

Figure 49, Mach 2.2, 5/8", 170 psig, .208 lbs. dn, 4.5° up

Figure 50, Mach 2.4, 5/8", 116 psig, .102 lbs. up, 2.33° dn

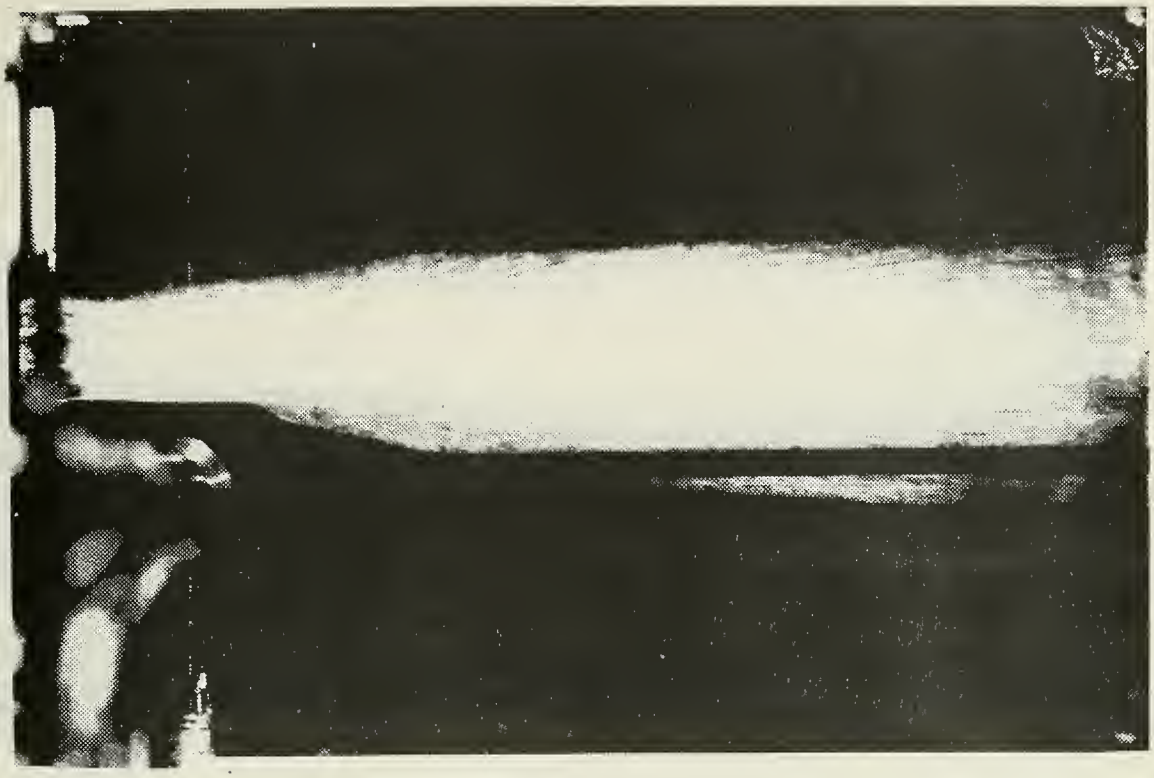

Figure 51, Mach 2.4, 5/8", 138 psig, .152 lbs. up, 3.42° dn

Figure 52, Mach 2.4, 5/8", 159 psig, .152 lbs. up, 2.42° dn

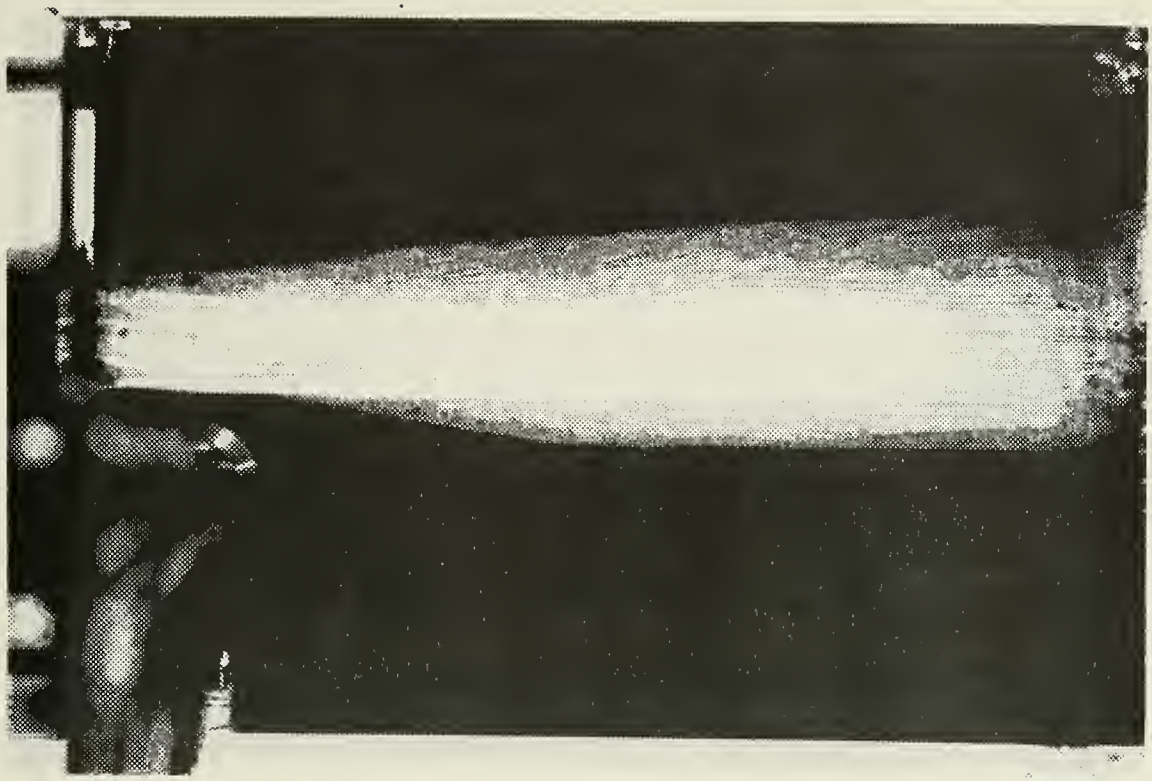

Figure 53, Mach 2.4, 5/8", 180 psig, .079 lbs. up, .75° dn

Figure 54, Mach 2.4, 5/8", 202 psig, .014 lbs. dn, 1.5° up

Figure 55, Mach 2.4, 5/8", 222 psig, .111 lbs. dn, 1.92° up

BIBLIOGRAPHY

Ferri, A., Elements of Aerodynamics of Supersonic Flows, p. 170-172, The Maxmillan Company, 1949.

Liepman, H. W., and Roshko, A., Elements of Gasdynamics, p. 284-304, John Wiley & Sons, Inc., 1957.

NACA Report 1135, Equations, Tables, and Charts For Compressible Flow, Ames Research Staff, p. 21-23, 1953.

INITIAL DISTRIBUTION LIST

		No. Copies
1.	Defense Documentation Center Cameron Station Alexandria, Virginia 22314	2
2.	Library, Code 0212 Naval Postgraduate School Monterey, California 93940	2
3.	Professor R. W. Bell, Code 57 BE Department of Aeronautical Engineering Naval Postgraduate School Monterey, California 93940	1
4.	Asst. Professor G. J. Hokenson, Code 57 Hw Department of Aeronautical Engineering Naval Postgraduate School Monterey, California 93940	2
5.	Brian J. Horais 8664 Sturbridge Dr. Cincinnati, Ohio 45236	1

Security Classification

DOCUMENT CONTROL DATA - R & D

(Security classification of title, body of abstract and indexing annotation must be entered when the overall report is classified)

ORIGINATING ACTIVITY *(Corporate author)*

Naval Postgraduate School
Monterey, California 93940

2a. REPORT SECURITY CLASSIFICATION

Unclassified

2b. GROUP

REPORT TITLE

Vectored Thrust Control

DESCRIPTIVE NOTES *(Type of report and inclusive dates)*

Master's Thesis; December 1972

AUTHOR(S) *(First name, middle initial, last name)*

Brian J. Horais

REPORT DATE	7a. TOTAL NO. OF PAGES	7b. NO. OF REFS
December, 1972	100	3

8a. CONTRACT OR GRANT NO.	9a. ORIGINATOR'S REPORT NUMBER(S)
b. PROJECT NO.	
c.	9b. OTHER REPORT NO(S) *(Any other numbers that may be assigned this report)*
d.	

10. DISTRIBUTION STATEMENT

Approved for public release; Distribution Unlimited.

11. SUPPLEMENTARY NOTES	12. SPONSORING MILITARY ACTIVITY
	Naval Postgraduate School Monterey, California 93940

13. ABSTRACT

Supersonic two-dimensional flow from a nozzle with the exit plane inclined to the central axis of the nozzle will be turned if the exit pressure of the nozzle is not matched to the external pressure. The direction and magnitude of the flow deflection angle and the resulting deflection force is a function of the exit pressure of the nozzle, the exit Mach number and the amount the exit plane is inclined to the central axis of the nozzle. A study of the deflection forces and deflection angles generated for a Mach number range of 1.2 to 2.4 and for a wide range of exit pressures is presented in this paper.

DD FORM 1 NOV 68 1473 (PAGE 1)

S/N 0101-807-6811

Security Classification

A-31408

4. KEY WORDS	LINK A		LINK B		LINK C	
	ROLE	WT	ROLE	WT	ROLE	WT
Vectored Thrust Control						